이학박사 학위논문

Non-perturbative Approaches to Conformal Field Theory

등각장론의 비섭동적인 접근 방법

2015년 8월

서울대학교 대학원
물리천문학부
배진범

Non-perturbative Approaches to Conformal Field Theory

등각장론의 비섭동적인 접근 방법

지도교수 이 수 종

이 논문을 이학박사 학위논문으로 제출함
2015년 5월

서울대학교 대학원
물리천문학부
배진범

배진범의 박사 학위논문을 인준함
2015년 6월

위 원 장 _____ (인)
부위원장 _____ (인)
위 원 _____ (인)
위 원 _____ (인)
위 원 _____ (인)

Abstract

Non-perturbative Approaches to Conformal Field Theory

Jinbeom Bae
School of Physics & Astronomy
The Graduate School
Seoul National University

The goal of this thesis is suggesting diverse method of analysing conformal field theory which related to string theory/higher spin theory via AdS/CFT correspondence. In this thesis, we focus on two specific objects in conformal field theory : 4-point correlation function in $O(N)$ vector model and polygonal Wilson loop expectation value in 3D $\mathcal{N}=6$ superconformal field theory.

The first part of this thesis devoted to non-perturbative analysis of conformal field theory. Based on unitarity and crossing symmetry of 4-point correlation function, conformal bootstrap program enables pick up UV and IR fixed point of $O(N)$ symmetric theory for $2<D<4$. We showed conformal bootstrap program can be successfully applied to specify interacting fixed point even for the 5-dimensional $O(N)$ symmetric theory.

The polygonal Wilson loop expectation value is intensively discussed in second part of this thesis. We computed hexagonal two-loop Polygonal Wilson loop expectation value in 3D $\mathcal{N}=6$ superconformal field theory and showed structurewise similiarity with that of $\mathcal{N}=4$ super Yang-Mills theory. Also, we focused on its universal behavior under collinear-soft limit. Based on this observation, we constructed structure of polygonal Wilson loop for arbitrary number of edges at two-loop order. At circular limit, the result agrees to circular Wilson loop expectation value.

Keywords : String theory, Conformal Field Theory, Conformal Bootstrap, Polygonal Wilson loop, AdS/CFT
Student Number : 2008-20435

Table of Contents

Chapter 1

Intro - Symmetries in Relativistic Quantum Physics

The discovery of standard model is one of the greatest triumph of theoretical physics during the 20th century. Now we have a successful model for describing the phenomena of electromagnetism, weak interaction and strong interaction based on *relativistic quantum field theory*.

The most basic building block in QFT is a field, which expected to describe elementary particles. In the group theoretical viewpoint, therefore field should lies on irreducible representation of given spacetime symmetry. Typically we impose Lorentz group $SO(3,1)$ as a spacetime symmetry in relativistic quantum field theory. $SO(3,1)$ is outranged from typical Lie group, therefore it requires infinite dimensional object to have unitary irreducible representation of Lorentz group. This is the reason of why we introduce infinite dimensional object in field theory.

Combining with translation invariance, this Lorentz group is extends to Poincare group, which is semi-product combination of Lorentz rotation and translation. Elementary particles will thus be associated with unitary representations of the Poincare group. The infinitesimal generators of Poincare group are translation(P_μ) and rotation($M_{\mu\nu}$). There algebra is given by

$$[P_\mu, P_\nu] = 0, \quad [M_{\mu\nu}, P_\rho] = i(\eta_{\mu\rho}P_\nu - \eta_{\nu\rho}P_\mu)$$
$$[M_{\mu\nu}, M_{\rho\sigma}] = i(\eta_{\mu\rho}M_{\nu\sigma} - \eta_{\mu\sigma}M_{\nu\rho} - \eta_{\nu\rho}M_{\nu\sigma} + \eta_{\nu\sigma}M_{\mu\rho})$$

In unitary representation of Poincare group, Massive 1-particle states are labeled by mass and spin. These quantum numbers are also realized by quadratic Casimir of Poincare group.

We can also make several assumptions of our field theory. First, we can introduce internal global symmetries, defining other conserved quantum numbers like isospin or electric charge. The generator of these global symmetries are not correlated with Poincare symmetry. That is, generator of such global symmetry obey Lie algebra by themselves

$$[R_i, R_j] = f_{ij}^k R_k \tag{1.1}$$

and they are commute with other Poincare generator. Second, we assumes our theory is invariant under *CPT* transformation.

Remarkable point of the above symmetries is that all the generators are Lorentz scalars except Poincare generators. That is, given these symmetries, the most general group of invariance is always the *direct product* of the Poincare group with another internal symmetry group. Coleman and Mandular suggested above no-go theorem, based on S-matrix defined in larger than 1+1 dimension [1].

The Coleman-Mandula no-go theorem is bypassed by introducing fermionic conserved charges, that is, introducing anti-commuting generators. Such an algebra is called by a graded Lie algebra, or superalgebra. This graded Lie algebra is summarized by

$$\begin{gathered}
[Q_\alpha, M^{\mu\nu}] = (\sigma^{\mu\nu})_\alpha^\beta Q_\beta, \quad [Q_\alpha, P^\mu] = [\bar{Q}^{\dot{\alpha}}, P^\mu] = 0 \\
\{Q_\alpha, Q_\beta\} = 0, \quad \{Q_\alpha, \bar{Q}_{\dot{\beta}}\} = 2(\sigma^\mu)_{\alpha\dot{\beta}} P_\mu \\
[Q_\alpha, R] = Q_\alpha, \quad [\bar{Q}_{\dot{\alpha}}, R] = -\bar{Q}_{\dot{\alpha}}
\end{gathered} \tag{1.2}$$

Therefore, supersymmetric quantum field theory do not conflict to no-go theorem.

By the way, we can consider a different kind of peculiar extension of Poincare group, often called by conformal group. This system can be considered as extension of Poincare symmetry by adding dilatation generator D and special conformal generator K_μ. There algebra is given by,

$$\begin{gathered}
[D, P_\mu] = iP_\mu, \quad [D, K_\mu] = -iK_\mu \\
[K_\mu, P_\nu] = 2i(\eta_{\mu\nu} D - M_{\mu\nu}), \quad [K_\mu, M_{\rho\sigma}] = i(\eta_{\mu\rho} K_\sigma - \eta_{\mu\sigma} K_\rho)
\end{gathered}$$

Manifestly, dilatation and special conformal generators are not commute with Poincare generators. Then how can we consider such kind of system? Is it not conflict to Coleman-Mandular no-go theorem?

Actually, conformal field theory is outranged from Coleman-Mandular boundary. The definition of LSZ reduction formalism is not clear in conformal field theory. In viewpoint of Lehmann-Källen form, 1-particle state is not well-defined in conformal field theory since every particles are massless. Therefore, traditional meaning of S-matrix is cubersome in conformal field theory and it is not a strange Coleman-Mandular theorem is bypassed by conformal theory.

Conformal symmetry is not directly visible in our life. We cannot imagine the scale invariance appears in our life like momentum conservation or angular momentum conservation. Neverthless, this theory often plays a key role in various places of theoretical physics. In this section, we will summarize three main motivations of studying conformal field theory : First,

second order phase transition. Second, Renormalization group flow. And Finally, AdS/CFT correspondence.

1.1 The Conformal Group

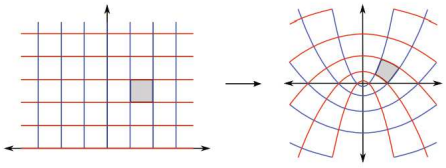

Figure 1: Conformal transformation is angle preserving transformation.

Let $g_{\mu\nu}$ denote the metric of D-dimensional spacetime. Conformal transformation is defined by angle-preserving transformation. The angle θ between two vectors x_1^μ, x_2^ν is defined by

$$\cos\theta = \frac{g_{\mu\nu}x_1^\mu x_2^\nu}{\sqrt{g_{\mu\nu}x_1^\mu x_1^\nu}\sqrt{g_{\mu\nu}x_2^\mu x_2^\nu}} \tag{1.3}$$

In the new coordinate system x', the angle θ is preserved under following transformation of metric.

$$g_{\mu\nu}(\mathbf{x}) \to g'_{\mu\nu}(\mathbf{x}') = \Lambda(\mathbf{x})g_{\mu\nu}(\mathbf{x}) \tag{1.4}$$

Under infinitesimal transformation $x'^\mu = x^\mu + \varepsilon^\mu(\mathbf{x})$, the metric transformed by $g_{\mu\nu} \to g_{\mu\nu} - (\partial_\mu\varepsilon_\nu + \partial_\nu\varepsilon_\mu)$. To preserve angle, we should impose

$$\partial_\mu\varepsilon_\nu + \partial_\nu\varepsilon_\mu = f(\mathbf{x})g_{\mu\nu} \tag{1.5}$$

with suitable factor $f(\mathbf{x})$. If we restrict ourselves on flat spacetime, we can replace $g_{\mu\nu}$ by $\eta_{\mu\nu}$. Then, it is easy to check that the factor $f(\mathbf{x})$ should satisfy

$$(D-1)\partial^2 f(\mathbf{x}) = 0 \tag{1.6}$$

for the case of spacetime dimension is larger than 2.[1] This means that ε_μ is at most quadratic in x. The most general solution of ε_μ is given by

$$\varepsilon_\mu = a_\mu + b_{\mu\nu}x^\nu + c_{\mu\nu\rho}x^\nu x^\rho, \qquad c_{\mu\nu\rho} = c_{\mu\rho\nu} \tag{1.7}$$

[1] $D = 2$ is special case. Their appears infinitely many generators and they called by Virasoro algebra. They do not discussed in this section since $D > 2$ CFT will be focused in this thesis.

The solution is classified by following table.

	Finite Transformation	Infinitesimal Transformation	Solutions
P_μ	$x'^\mu = x^\mu + a^\mu$	$-i\partial_\mu$	$\varepsilon^\mu = const$
$M_{\mu\nu}$	$x'^\mu = \Lambda^\mu_\nu x^\nu$	$i(x_\mu\partial_\nu - x_\nu\partial_\mu)$	$\varepsilon^\mu = x^\nu\omega_{[\nu\mu]}$
D	$x'^\mu = \lambda x^\mu$	$-ix^\mu\partial_\mu$	$\varepsilon^\mu = \lambda x^\mu$
K_μ	$x'^\mu = \frac{x^\mu - b^\mu x^2}{1-2b\cdot x+b^2x^2}$	$-i(2x_\mu x^\nu\partial_\nu - x^2\partial_\mu)$	$\varepsilon^\mu = 2(a\cdot x)x^\mu - x^2a^\mu$

Table 1: When spacetime dimension is larger than 2, we can classify all possible transformations by 4-classes.

In summary, only translation(P_μ), rotation($M_{\mu\nu}$), dilatation(D) and special conformal(K_μ) are appear in higher dimesional conformal algebra.

We can repackage conformal generators in following way.

$$J_{ab} \equiv \left[\begin{array}{c|c|c} 0 & D & J_{-1,\mu} \\ \hline -D & 0 & J_{0,\mu} \\ \hline J_{\mu,-1} & J_{\mu,0} & M_{\mu\nu} \end{array}\right]$$

Each component of this matrix is identified with conformal generators.

$$\begin{aligned} J_{-1,\mu} &= \frac{1}{2}(P_\mu - K_\mu), \quad J_{0,\mu} = \frac{1}{2}(P_\mu + K_\mu) \\ J_{-1,0} &= D, \quad J_{\mu\nu} = M_{\mu\nu} \end{aligned} \tag{1.8}$$

Then, this matrix J_{ab} satisfies following identity.

$$[J_{ab}, J_{cd}] = i(\eta_{ad}J_{bc} + \eta_{bc}J_{ad} - \eta_{ac}J_{bd} - \eta_{bd}J_{ac}) \tag{1.9}$$

We can interpret this as $D+2$ dimensional rotation generator. Therefore, we can consider conformal group as $SO(D,2)$. Indeed, this simple structure allows embedding space formalism which will be utilized later.

1.2 Phase Transition in condensed matter theory

Our quantum theory describes microscopic physics. Understanding macroscopic physics from quantum microscopic theory is a nontrivial problem. To see how this works, we will consider typical toy model in condensed matter theory. The most simple setup is spin-spin correlated system with each spin located at lattice and has the discrete value of ± 1. The

Hamiltonian of this system is given by

$$\mathcal{H} = -J\sum_{n.n} s_i s_j - h\sum_i s_i \tag{1.10}$$

From this Hamiltonian, we can compute various quantities like magnetization, heat capacity, susceptibility, etc.

The most simple approache is mean field theory. It decompose spin field s_i by mean value and small fluctuation. By ignoring quadratic fluctuation, it successfully describes phase transition of various quantities. However, the observed critical exponents and mean field theory do not well agrees, this indicates break down of mean field theory at near critical regime.

From the Gaussian model computation, the Green function $G(\mathbf{r}) = \langle s_i s_j \rangle - \langle s_i \rangle \langle s_j \rangle$ is given by,

$$G(\mathbf{r}) = \begin{cases} \frac{\xi e^{-\frac{r}{\xi}}}{(r\xi)^{(D-1)/2}} & \xi \ll r \\ \frac{1}{r^{D-2}} & \xi \gg r \end{cases} \tag{1.11}$$

Here, ξ is correlation length which defined by $|T - T_C|^{-\nu}$. The result at $\xi \ll r$ tells spin-spin correlation of two far seperated spins are almost 0, as naturally expected.

The other limit is nontrivial. $\xi \gg r$ corresponds to the limit of temperature approaches to critical temperature. In other words, it describes near critical behavior of system. In this limit, two point correlation function shows scaling behavior. This suggests that the scale-invariant physics is more appropriate to describe near critical behavior of condensed matter theory.

Later, we will back to the problem of finding critical exponents of D-dimensional ϕ^4 theory. The theoretical prediction of critical exponent of 3-dimensional IR physics(for instance, 3D Ising model) known to be well matched with experimental data. The typical example is λ-point phase transition of heat capacity of Helium-4 measurement [2]. The observed critical exponent is given by $\alpha = 1.5094(2)$, which is well captured by $O(2)$ symmetric XY model in 3-dimension.

1.3 Renormalization group flow

The idea of renormalization group flow provides the way of understanding macroscopic physics from microscopic physics. Basically, it starts from given scale and consider scaling $x \to x' = bx (b > 1)$ by integrating out local degrees of freedom. The resulting effective field theory expected to be describe macroscopic physics. In renormalization group flow viewpoint, this picture corresponds to RG flow from UV fixed point to IR fixed point.

For instance, let us consider deformation of 3-dimensional free field theory by quartic deformation.

$$S = \int d^3x \underbrace{\frac{1}{2}(\partial_\mu \phi(x))^2}_{\text{Free theory}} + \underbrace{\frac{\lambda}{4!}\phi(x)^4}_{\text{Quartic deformation}} \tag{1.12}$$

Under scale transformation $x \to x' = bx$ $(b > 1)$, we obtain effective coupling at new coordinate system x'.

$$\lambda \int d^3x \frac{1}{4!}\phi(x)^4 \longrightarrow \underbrace{\left(\frac{b}{\Lambda}\right)^{\Delta_{\phi^4}-3}\tilde{\lambda}'}_{\lambda'} \int d^3x \frac{1}{4!}\phi(x)^4 \tag{1.13}$$

Here Λ is cutoff scale. At near free theory, Δ_{ϕ^4} is given by engineering dimension 2. Therefore, effective coupling λ' shrinks as we taking high-energy limit $\Lambda \gg b$. Therefore, microscpic physics can be dealt with perturbation approache.

However, this not happens at macroscopic scale. An effective coupling at IR limit $\Lambda \ll b$ grows as scaling. This means we cannot utilize perturbative field theory for IR physics. This kind of non-perturbativity will be cared by ε-expansion, or conformal bootstrap. We will return to this issue at later section.

Generally, we can consider deformation near specific conformal field theory.

$$\mathcal{L} = \mathcal{L}_{\text{CFT}} + \sum_i \lambda_i O_i \tag{1.14}$$

Scaling dimension of them are $[\mathcal{L}] = D,\ [O_i] = \Delta_i,\ [\lambda_i] = D - \Delta_i$. Note that Δ_i is contains anomalous dimension. If we consider deformation near free field theory, then this scaling dimension agrees to engineering dimension.

Under scale $x \to bx$, effective coupling λ_i' is given by $\left(\frac{b}{\Lambda}\right)^{\Delta_{O_i}-D}\tilde{\lambda}_i'$. Depending on behavior under scaling, they are classified by 3-classes.

- When $D > \Delta_{O_i}$, quantum correction(effective coupling) dominant at long-distance area. This is called by *relevant operator*.
- When $D < \Delta_{O_i}$, quantum correction(effective coupling) dominant at short-distance area. This is called by *irrelevant operator*.
- When $D = \Delta_{O_i}$, this is called by *marginal operator*.

ϕ^4 operator corresponds to relevant at free theory. As scaling, this deformation eventually will dominant. Eventually, we expect to obtain non-trivial theory where interaction is given by quartic term. In this case, we call starting point free theory as UV fixed point while resulting interaction theory as IR fixed point.

As far as we considering asymptotically safety theory, any theory expected to have UV complete description. In principle, we can analyze any field theory by deforming UV theory by relevant operator. In this sense, we can say that UV conformal field theory is building block of field theory. By the way, existence of IR fixed point is not gauranteed. Later, we will see non-trivial IR Wilson-Fischer fixed point exist for the case of 3D ϕ^4 theory. Scaling dimension of ϕ^4 operator is quiet large, $\Delta_{\phi^4} \sim 3.84$. This exceeds spacetime dimension, therefore it is irrelevant operator at interacting theory. This means that even if we deform ϕ^4 theory by ϕ^4 deformation, this ignorable after sufficiently scaling. Therefore, RG flow inward directed to IR fixed point.

1.4 AdS/CFT correspondence

The distinguished property of QCD is asymptotic freedom, which allows perturbative expansion at large scale limit. Quark-antiquark pair potential behaves linearly, therefore quarks are strongly interact to each other at short distance limit. To deal with hadronic interaction(pion, nucleon, etc) at low energy area, more efficient method is required than perturbative QCD.

In 1968, Veneziano suggested dual resonance model for pion elastic scattering amplitude [3].

$$A_{\pi^+\pi^-\to\pi^+\pi^-} = \frac{\Gamma[1-\alpha(t)]\Gamma[1-\alpha(s)]}{\Gamma[1-\alpha(s)-\alpha(t)]} \tag{1.15}$$

s,t are Mandelstam variables and $\alpha(t)$ is Regge trajectory, behaves linearly with respect to t. This 4-point amplitude can be equivalently derived from 26-dimensional bosonic string theory. This suggests intrinsical connection between QCD and string theory.

t'Hooft large N_c limit gauge theory analysis gave another intuition on connection between gauge theory and string theory. Action of gluon and fermion matter that charged under adjoint representation of $SU(N_c)$ is given by,

$$S = \frac{1}{g_{YM}^2}\mathrm{Tr}F_{\mu\nu}^2 + \frac{1}{g_{YM}^2}\overline{\Psi}\not{D}\Psi \tag{1.16}$$

In this limit, $\frac{1}{N_c}$ expansion was suggested with fixed t'Hooft coupling $\lambda = g_{YM}^2 N_c$. The Feynman diagram of this theory consist of gluon propagator, fermion propagator and interaction vertex that behaves $\frac{1}{N_c}, \frac{1}{N_c}, N_c$ respectively. Therefore, for each Feynman diagram of E gluon/fermion propagators, F gluon loops, B quark loop and V vertices are

$$N_c^{F-E+V-B} = N_c^{\chi-B} = N_c^{2-2g-B} \tag{1.17}$$

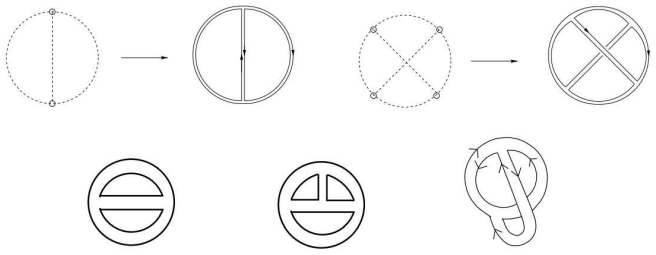

Figure 2: Various planar and non-planar vacuum Feynman diagrams

At large N_c limit, only planar diagram contributes. The quantum correction of gauge theory parametrized by double series with respect to N_c, λ.

$$\sum_{g=0}^{\infty} N^{2-2g-B} \sum_{i=0}^{\infty} c_{i,g} \lambda^i = \sum_{g=0}^{\infty} Z_g(\lambda) \tag{1.18}$$

This is precisely the topological expansion of string theory with respect to genus of world-sheet. The string coupling g_s corresponds to $\frac{1}{N_c}$, therefore large N_c limit is equivalent to small g_s limit. From this picture, open string is interpreted as ended on quark and antiquark.

Since string theory is now realized by quantum gravity, we can expect relation between strongly coupled($\lambda \gg 1$) gauge theory and weakly coupled($g_s \ll 1$) string theory. The specific example of this relation is AdS/CFT correspondence, which states

AdS/CFT correspondence

The quantum physics of strongly correlated conformal theory related to the classical dynamics of gravity in one higher dimension.

This correspondence can be understood two different view point for same physics. We start from N-stack of D3 brane, which is one of the fundamental object in Type IIB superstring theory in 10-dimension. This theory contains following bosonic degrees : a metric $g_{\mu\nu}$, a dilaton ϕ, Kalb-Ramond field $B_{\mu\nu}$ and potentials C_0, C_2, C_4.

First, we can consider this system as bulk with defect(N D3 brane) by DBI action. At leading order of α',

$$S \sim \frac{1}{g_s} d^4x \mathrm{Tr}(F^2) + \frac{1}{\alpha'^4} \int d^{10}x \sqrt{g} R e^{-2\phi} + \cdots \tag{1.19}$$

In low energy $\alpha' \to 0$ limit, interaction between D-brane and bulk is negligible. Since D3

brane is half-BPS object, this theory is 16 supercharge preserving Yang-Mills theory. This is called by $\mathcal{N}=4$ super Yang-Mills theory.

Second, the solution of extremal p-brane in supergravity could be utilized at $\alpha' \to 0$ limit. For the case of $p=3$, we have

$$\begin{aligned} ds^2 &= H^{-\frac{1}{2}} dx_\mu dx^\mu + H^{\frac{1}{2}}(dr^2 + r^2 d\Omega_5) \\ e^\phi &= g_s \equiv \frac{g_{YM}^2}{4\pi} \\ H &= 1 + \frac{g_{YM}^2 N \alpha'^2}{r^4} = 1 + \frac{g_{YM}^2 N}{\alpha'^2 \phi^4} \end{aligned} \tag{1.20}$$

At $r \to 0$, this solution is approximated by

$$ds^2 \sim \alpha' \left[R^2 \frac{d\phi^2}{\phi^2} + \frac{\phi^2}{R^2} dx^2 + R^2 d\Omega_5 \right], \quad R^2 = \alpha' \sqrt{g_{YM}^2 N} \tag{1.21}$$

This is corresponds to metric of $AdS_5 \times S^5$ with radius of Anti-de Sitter space is identified to radius of 5-sphere.

The parameters of two theories are related by

$$4\pi g_s = g_{YM}^2, \quad \frac{R^2}{\alpha'} = \sqrt{g_{YM}^2 N} \tag{1.22}$$

The supergravity approximation($g_s \to 0$) is valid only if curvature of AdS space is sufficiently larger than string scale. That is, $R = \alpha' \sqrt{g_{YM}^2 N} \gg \sqrt{\alpha'} = l_s$, or $\lambda \gg 1$. Therefore, this counting supports duality between strongly coupled conformal gauge theory and weakly coupled gravity.

1.5 Observables in conformal field theory

In this thesis, we will focus on specific two observables defined in conformal field theory : 4-point correlation function of scalar operator and light-like polygonal Wilson loop expectation value.

The polygonal Wilson loop defined on contour C_n parameterized by n-points $x_1, x_2, \cdots x_n$ and each neighborhood vertex connected by light-like segment. The total degree of freedom of polygonal Wilson loop can be counted by Poincare group or conformal group. In D-dimensional spacetime, it is given by

$$\text{D.O.F} = \begin{cases} (D-1)n - \frac{D(D+1)}{2} & \text{Number of Mandelstam variables} \\ (D-1)n - \frac{(D+2)(D+1)}{2} & \text{Number of Conformal cross ratio} \end{cases} \tag{1.23}$$

Counting the number of conformal cross-ratios (anharmonic ratios) in n-point correlation function is similar. Mathematically, counting the number of conformal cross-ratios (anharmonic ratios) amounts to counting the dimension of moduli space of n-points in D-dimensional space modulo conformal transformations. The conformal group $SO(D+1,1)$ in D-dimension has the dimension $\frac{(D+2)(D+1)}{2}$. So, one might naively suppose that the dimension of this moduli space is

$$\dim \mathcal{M}^{\text{conf}}(n,\mathbb{R}^D) = nD - \frac{(D+2)(D+1)}{2}. \tag{1.24}$$

However, this is not quite correct except for sufficiently large n for a given D. We tabulate the correct dimensions of the moduli space in Table 1. Fortuitously, for four-point correlation functions, $n=4$, the number of conformal cross-ratios is always 2 so long as the spacetime dimension is greater than 1.

So far we introduced the motivation of studying conformal field theory. The remaining part of this thesis is organized as follow. In section 2, we will focus on 4-point correlation function in conformal field theory. By utilizing crossing symmetry and unitarity constraint, we will rule out inconsistent theory. First we will see this *conformal bootstrap method* will provide us information of critical exponents in interacting IR theory. And next, we will turn to 5-dimensional $O(N)$ symmetric theory and figure out nontrivial UV fixed point by this bootstrap method. In section 3, we shortly introduce the story of gluon scattering amplitude and polygonal Wilson loop expectation value in $\mathcal{N}=4$ SYM. In section 4, we will focus on polygonal Wilson loop expectation value defined in 3D superconformal field theory, ABJM theory. Starting from explicit computation of hexagonal Wilson loop expectation value, we developed it to n-gon result by utilizing unresolved limit. Several consistent check were provided. In section 5, we summarize the main contents of this thesis and stated future direction.

d	2 pt	3 pt	4 pt	5 pt	6 pt	n(>6) pt
1	$P^\mu : 1$ $K^\mu : 1$ $n-2=0$	$D : 1$ $M^{\mu\nu} : 0$ $n-3=0$	$n-3=1$	$n-3=2$	$n-3=3$	$n-3$
2	$P^\mu : 2$ $K^\mu : 2$ $2n-4=0$	$D : 1$ $M^{\mu\nu} : 1$ $2n-6=0$	$2n-6=2$	$2n-6=4$	$2n-6=6$	$2n-6$
3	$P^\mu : 3$ $K^\mu : 3$ $3n-6=0$	$D : 1$ $M^{\mu\nu} : 2$ $3n-9=0$	$M^{\mu\nu} : 1$ $3n-10=2$	$3n-10=5$	$3n-10=8$	$3n-10$
4	$P^\mu : 4$ $K^\mu : 4$ $4n-8=0$	$D : 1$ $M^{\mu\nu} : 3$ $4n-12=0$	$M^{\mu\nu} : 2$ $4n-14=2$	$M^{\mu\nu} : 1$ $4n-15=5$	$4n-15=9$	$4n-15$
5	$P^\mu : 5$ $K^\mu : 5$ $5n-10=0$	$D : 1$ $M^{\mu\nu} : 4$ $5n-15=0$	$M^{\mu\nu} : 3$ $5n-18=2$	$M^{\mu\nu} : 2$ $5n-20=5$	$M^{\mu\nu} : 1$ $5n-21=9$	$5n-21$
d	$P^\mu : d$ $K^\mu : d$ $dn-2d$ $=0$	$D : 1$ $M^{\mu\nu} : d-1$ $dn-3d$ $=0$	$M^{\mu\nu} : d-2$ $dn-4d+2$ $=2$	$M^{\mu\nu} : d-3$ $dn-5d+5$ $=5$	$M^{\mu\nu} : d-4$ $dn-6d+9$ $=9$	$nd-$ $\frac{(d+2)(d+1)}{2}$

Table 2: *Dimension of moduli space for various cases. For sufficient large n, we have compact expression $nd-\frac{(d+2)(d+1)}{2}$ because of generators are fully used to fix the points. The 4-point correlation function has 2 degree of freedom when spacetime dimension larger than 2. Therefore, crossing symmetry constraint available even for the five-dimensional bootstrap.*

Chapter 2

Correlation function in conformal field theory

2.1 General structure of correlation function

Consider a conformal field theory in d-dimensional spacetime. The generators of the $SO(d+1,1)$ Euclidean conformal algebra are Poincaré translation P_μ, rotation $M_{\mu\nu}$, dilatation D, and special conformal translation K^μ. The correlation functions measure response of the system as a function of separations to perturbations sourced by local operators, so they should transform covariantly under the $SO(d+1,1)$. The conformal algebra fixes the structure of 2-point and 3-point correlation functions completely. In turn, conformal field theories are completely specified by 2- and 3-point correlation functions.

Denote local operators as O_I, where I refers collectively to all quantum numbers of the operator. Choosing the basis of local operators in orthonormal basis so that the 2-point correlation functions read

$$\langle O_I(x) O_J(y)\rangle = \frac{\delta_{IJ}}{|x-y|^{2\Delta_I}}, \tag{2.1}$$

where Δ_I refer to the conformal scaling dimension of I-th operator, the 3-point correlation functions

$$\langle O_I(x) O_J(y) O_K(z)\rangle = \frac{C_{IJK}}{|x-y|^{\Delta_I+\Delta_J-\Delta_K}|y-z|^{\Delta_J+\Delta_K-\Delta_I}|z-x|^{\Delta_K+\Delta_I-\Delta_J}} \tag{2.2}$$

are completely specified by the structure constants C_{IJK}. Owing to the conformal invariance, total set of these structure constants are encoded by the operator product expansions (OPE). The OPE is most compactly expressible in radial quantization by ordering two operators at two different radii (equivalently, conformal time). For instance, the OPE of two identical scalar operators O reads [9]

$$O(x)\times O(0) \sim \sum_{\Delta,\ell} C_{\Delta,\ell}\Phi_{\Delta,\ell}(x), \tag{2.3}$$

where the structure constants $C_{\Delta,\ell}$ are partial wave expansion coefficients and $\Phi_{\Delta,\ell}$ is the partial wave amplitudes. The partial wave amplitudes includes the set of conformal primary operators. The conformal invariance dictates that all multipole moments of the OPE are primary states and their conformal descendants. In conformal field theory, every operator prod-

uct is organized by conformal primary operators and their descendants, which are labeled by conformal dimension Δ and spin ℓ.

The 4- or higher-point correlation functions are not fully fixed by the conformal invariance. For instance, 4-point correlation function of local operators inserted at x_1, x_2, x_3, x_4 comes with two arbitrary degrees of freedom: the conformal cross-ratios (anharmonic ratios)of operator insertion points defined by

$$u := \frac{x_{12}^2 x_{34}^2}{x_{13}^2 x_{24}^2} \qquad \text{and} \qquad v := \frac{x_{14}^2 x_{23}^2}{x_{13}^2 x_{24}^2}, \tag{2.4}$$

where $x_{ij} \equiv x_i - x_j$. For instance, for local operators of the same kind, O, the 4-point correlation function takes the form

$$\langle O(x_1) O(x_2) O(x_3) O(x_4) \rangle = \frac{1}{(x_{12})^{2\Delta} (x_{34})^{2\Delta}} F(u,v), \tag{2.5}$$

Here, $F(u,v)$ is a scalar function .

By construction, u, v are invariant under the conformal transformation. As such, the function $F(u,v)$ has vanishing conformal weight, so further inputs are needed in order to constrain it. The conformal invariance allows to evaluate the multi-point correlation function by a sequence of operator product expansion (OPE). For the 4-point correlation function, this is reduced effectively to the OPE of two partial wave operators $\Phi_{\Delta,\ell}$. This OPE gives rise to the dependence on the square of the structure constant $C_{\Delta,\ell}$ and to a nontrivial function that depends on the conformal cross-ratios u, v. Therefore, the conformal partial wave expansion of the scalar function $F(u,v)$ takes the form

$$F(u,v) = \sum_{\Delta,\ell} C_{\Delta,\ell}^2 G_{\Delta,\ell}(u,v). \tag{2.6}$$

The function $G_{\Delta,\ell}(u,v)$ is referred as the conformal block. If the theory is unitary, the reflection positivity asserts that the partial-wave coefficient $C_{\Delta,\ell}$ is real and hence $C_{\Delta,\ell}^2$ is positive definite.

We can get more information about the conformal block $G_{\Delta,\ell}(u,v)$ from the underlying conformal symmetry, and is derivable from quadratic Casimir of the $SO(d,2)$ conformal algebra [8]. If the spacetime dimension is even, the conformal block has a closed form expression in terms of hypergeometric functions [7, 8]. If the spacetime dimension is odd, it is not known yet whether the conformal block is expressible in closed form. In numerical bootstrap approach, we do not actually need to have such closed form expressions, since we can evaluate the conformal block from its recursion relations [11].

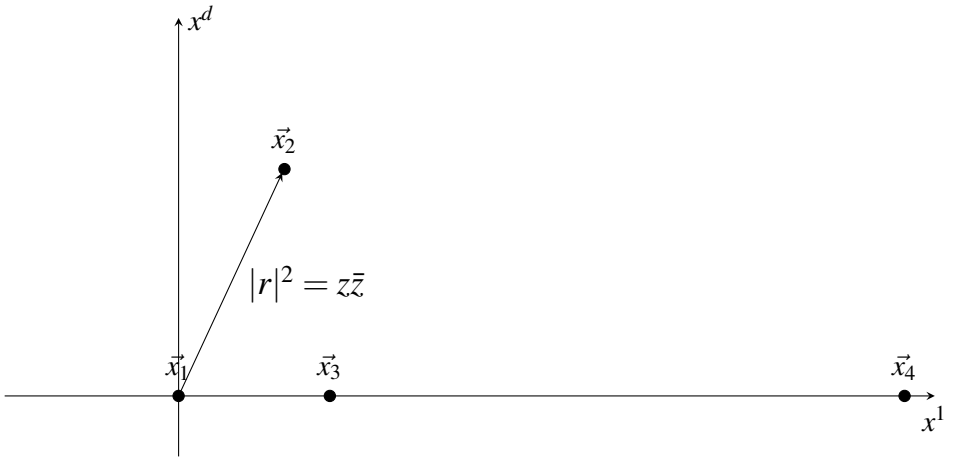

Figure 3: *Position of four insertion points of the sclar operators in. Using conformal symmetry, we fix $\vec{x}_1, \vec{x}_3, \vec{x}_4$. This leaves two degrees of freedom for the insertion point $\vec{x}_2$ lying in the (x^1, x^D)-subspace. The radial distance of $\vec{x}_2$ from origin is parametrized by $z, \bar{z}$. Therefore correlation function or conformal block is function of $z, \bar{z}$.*

2.2 Radial Representation of Conformal Block

Denote the four points the local operators are inserted as $\vec{x}_1, \vec{x}_2, \vec{x}_3, \vec{x}_4$. Utilizing the conformal invariance, we can fix location of three points $\vec{x}_1, \vec{x}_3, \vec{x}_4$ as in Figure 3. According to the result of previous subsection, there ought to be 2 remaining degree of freedom in arbitrary dimensions. Fixing 3 points as in figure 3 is consistent with this. Specifically, in five dimensions, we may conveniently put

$$\vec{x}_1 = (0,0,0,0,0), \quad \vec{x}_2 = (x_2^1, 0, 0, 0, x_2^5), \quad \vec{x}_3 = (1,0,0,0,0), \quad \vec{x}_4 = \infty \tag{2.7}$$

Length $|\vec{x_{12}}|^2$ is $(x_2^1)^2 + (x_2^5)^2$ for Euclidean space and $-(x_2^1)^2 + (x_2^5)^2$ for Minkowski space. Therefore, we introduce two variables so that this length equals to $z\bar{z}$. In Euclidean space, the new variables $(z, \bar{z})$ are two complex variables related each other by complex conjugation. In Minkowski space, the new variables $(z, \bar{z})$ are two real-valued light-cone variables.

In terms of the new variables $(z, \bar{z})$, the cross-ratios (2.4) are given by

$$u = z\bar{z} \qquad \text{and} \qquad v = (1-z)(1-\bar{z}). \tag{2.8}$$

Being now a function of complex variables, the conformal block is in general a multi-valued function over the z-plane. It can be seen from the closed-form expressions of the conformal

block in $d = 2, 4$:

$$G^{(d=4)}_{\Delta,\ell}(z,\overline{z}) = \frac{(-1)^\ell}{2^\ell}\frac{z\overline{z}}{z-\overline{z}}\left[k_{\Delta+\ell}(z)k_{\Delta-\ell-2}(\overline{z}) - k_{\Delta+\ell}(\overline{z})k_{\Delta-\ell-2}(z)\right]$$
$$G^{(d=2)}_{\Delta,\ell}(z,\overline{z}) = \frac{(-1)^\ell}{2^\ell}\left[k_{\Delta+\ell}(z)k_{\Delta-\ell}(\overline{z}) - k_{\Delta+\ell}(\overline{z})k_{\Delta-\ell}(z)\right] \tag{2.9}$$

where $k_\lambda(y)$ is the rescaled hypergeometric function:

$$k_\lambda(z) \equiv z^{\frac{\lambda}{2}}\ {}_2F_1\left[\frac{\lambda}{2},\frac{\lambda}{2},\lambda;z\right] \tag{2.10}$$

We recall that the hypergeometric function has a cut $z \in [1,\infty)$ along the real axis.

To avoid aforementioned branch cuts and render the conformal block single-valued, we need to restrict $z,\overline{z}$ outside the cut along $z \in [1,\infty)$. This can be achieved by changing the variables $(z,\overline{z})$ to

$$\rho = \frac{z}{(1+\sqrt{1-z})^2} \qquad \text{and} \qquad \overline{\rho} = \frac{\overline{z}}{(1+\sqrt{1-\overline{z}})^2}. \tag{2.11}$$

We are working in Euclidean space, so $(\rho,\overline{\rho})$ are complex conjugate each other. Under the change of variable, the z-plane outside the branch cut along $x \in [1,\infty)$ is mapped to the region inside a unit circle.

For the region inside a unit circle, we further change the variables to radial and polar variables:

$$r = |\rho| \quad \text{and} \quad \eta = \cos(\arg(\rho)), \qquad (0 \le r \le 1, \quad -1 \le \eta \le +1). \tag{2.12}$$

The conformal block is now a function of (r,η) in this bounded domain, so it can be expanded in double power series. This expansion turns out to converge sufficiently fast [18] and thus serve a useful basis for semi-definite programming. The power series takes the form

$$G_{\Delta,\ell}(r,\eta) = \sum_{n=0}^{\infty}\sum_{j\in D(\ell)} B_{n,j}(\ell) r^{\Delta+n}\frac{\Gamma(2\nu)\Gamma(j+1)}{\Gamma(2\nu+j)}C^\nu_j(\eta) \tag{2.13}$$

where $\nu = \frac{d}{2}-1$, $C^\nu_j(\eta)$ is the Gegenbauer polynomials, and the summation domain D is given by

$$D(\ell): \qquad j = \begin{cases} 0,2,4,\cdots,\ell+n & (\ell+n = 2\mathbb{Z}) \\ 1,3,5,\cdots,\ell+n & (\ell+n = 2\mathbb{Z}+1) \end{cases} \tag{2.14}$$

The series coefficient $B_{n,j}$ is determined by the differential equation for the Casimir operator

of the conformal algebra. It turns out the first component in radial expansion is given by

$$B_{0,j}(\ell) = 4^{\Delta}\delta_{j\ell}. \tag{2.15}$$

Therefore, at leading order in radial expansion, the conformal block reads

$$G_{\Delta,\ell}(r,\eta) = (4r)^{\Delta}\frac{\Gamma(2\nu)\Gamma(\ell+1)}{\Gamma(2\nu+\ell)}C_{\ell}^{\nu}(\eta) + O(r^{\Delta+1}) \tag{2.16}$$

We take the crossing symmetric point $z = \bar{z} = \frac{1}{2}$, which corresponds to $r = 3 - 2\sqrt{2}$. Higher order coefficients could be obtained similarly, but we do not need that information here.

One can compute the conformal block more efficiently by utilizing the Zamolodchikov recursive relation, as suggested in [6]. It is reduced to a set of recursive relation given by

$$\begin{aligned} h_{\Delta,\ell}(r,\eta) &\equiv r^{-\Delta}G_{\Delta,\ell}(r,\eta) \\ h_{\Delta,\ell}(r,\eta) &= h_{\ell}^{\infty}(r,\eta) + \sum_i \frac{c_i r^{n_i}}{\Delta-\Delta_i} h_{\Delta_i+n_i,\ell_i}(r,\eta) \end{aligned} \tag{2.17}$$

Here, the term $h_{\ell}^{\infty}(r,\eta)$ refers to a holomorphic function that specifies the 'boundary condition' at $\Delta \to \infty$. This term can be determined from the Sturm-Liouville problem of the quadratic Casimir operator of the conformal group and equals to

$$h_{\ell}^{\infty}(r,\eta) = \frac{\ell!}{(2\nu)_{\ell}} \frac{C_{\ell}^{\nu}(\eta)}{(1-r^2)^{\nu}\sqrt{(1+r^2)^2-4r^2\eta^2}}. \tag{2.18}$$

Detailed information of poles and coefficients c_i can be found in the original work [6].

2.3 Conformal Bootstrap Method

We are now at the stage of imposing the crossing symmetry and the unitarity. The conformal 4-point correlation function of same scalar operators is invariant under permutation of operator insertion points x_1, x_2, x_3, x_4. A nontrivial constraint follows from exchange of two points, say, x_1 and x_3. Acting on (2.5), this leads to the condition

$$v^{\Delta}F(u,v) = u^{\Delta}F(v,u). \tag{2.19}$$

In solving the crossing symmetry condition (2.19), the approach that has been practiced

widely is to expand the scalar function $F(u,v)$ as

$$F(u,v) = 1 + \sum_{\Delta,\ell}{}' C^2_{\Delta,\ell}\, G_{\Delta,\ell}(u,v), \tag{2.20}$$

where the identity operator is separated from all other operators: the summmation Σ' runs over all primary operators of nonzero scaling dimensions $\Delta \geq \Delta_{\text{min}} > 0$ for zero spin. For spin ℓ, summation contains all primary operator over unitary bound. So, an input we specify is the gap in the spectrum Δ_{min}. We refer this specification as one-gap bootstrapping. The crossing symmetry condition (2.19) is now recast as

$$\begin{aligned} v^\Delta - u^\Delta &= \sum_{\Delta,\ell}{}' C^2_{\Delta,\ell} \mathcal{F}(\Delta,\ell,u,v) \\ \mathcal{F}(\Delta,\ell,u,v) &:= u^\Delta G_{\Delta,\ell}(v,u) - v^\Delta G_{\Delta,\ell}(u,v). \end{aligned} \tag{2.21}$$

The crossing sum rule (2.21) can be solved by Taylor expanding it around the symmetric point $u = v = 1/4$. Changing the variables as (2.8), solving the sum rule (2.21) within analytic domain of $z, \bar{z}$ amounts to solving the set of infinitely many unfolded equations at the point $z = \bar{z} = 1/2$:

$$\mathcal{F}_0^{m,n}(\Delta,\ell,z,\bar{z}) = \sum_{\Delta,\ell}{}' C^2_{\Delta,\ell} \mathcal{F}^{m,n}(\Delta,\ell,z,\bar{z}) \tag{2.22}$$

where

$$\mathcal{F}^{m,n}(\Delta,\ell,z,\bar{z}) \equiv \partial_z^m \partial_{\bar{z}}^n \mathcal{F}(\Delta,\ell,z,\bar{z})\Big|_{z=\frac{1}{2},\bar{z}=\frac{1}{2}}, \tag{2.23}$$

subject to boundary condition:

$$\mathcal{F}_0 := (1-z)^\Delta (1-\bar{z})^\Delta - (z\bar{z})^\Delta. \tag{2.24}$$

The set of unfolded eqution (2.22) can be solved by the linear programming [**?**]. Define linear functional $\mathbb{L}[\cdot]$ by

$$\mathbb{L}[\mathcal{F}^{m,n}(\Delta,\ell,z,\bar{z})] := \sum_{m,n} \alpha_{m,n}\ \mathcal{F}^{m,n}(\Delta,\ell,z,\bar{z}), \tag{2.25}$$

where $\alpha_{m,n}$ denotes a real coefficient. Taking this linear functional on both side of (2.22),

$$\mathbb{L}[\mathcal{F}_0^{m,n}(\Delta,\ell,z,\bar{z})] = \sum_{\Delta,\ell}{}' C^2_{\Delta,\ell} \sum_{m,n} \alpha_{m,n} \mathbb{L}[\mathcal{F}^{m,n}(\Delta,\ell,z,\bar{z})]. \tag{2.26}$$

We need to solve (2.26) subject to the constraints that $C^2_{\Delta,\ell}$ is positive and all Δ's are above unitarity bound of respective spin($l > 0$). In practice, numerical method for solving (2.26) requires truncation of summation up to suitable order. In our computation below, we have done so by truncating the unfolded basis (m,n) up to $m+n \equiv k \leq 15$ and the spin basis ℓ up to $\ell \leq \ell_{\max} = 20$.

In solving the crossing symmetry condition, an approach widely used so far assumes a single gap Δ_{min} above the unitarity bound in scalar spectrum($l = 0$). The sums over (Δ,ℓ) in (2.26) contain all continuous operators in scalar sector($\ell = 0$) but above Δ_{min} and all continuous operator in higher-spin sector($\ell \neq 0$). If there is set of $\alpha_{m,n}$ that satisfy positiveness of both side of (2.26) under assumption of spectrum with specific value of $\Delta_{\min}$, it potentially represents a conformal field theory consistent with unitarity and crossing symmetry. If not, it may still represent a conformal field theory but it must be a non-unitary one. Numerically, the unfolded conditions (2.26) was solved originally in linear programming [**?**] and later in semi-definite programming [17].

2.3.1 ε-expansion

The IR physics of 3-dimensional ϕ^4 theory is non-perturbative with resepct to effective coupling λ'. Therefore, perturbative quantum field theory is cannot be applied for this theory. The alternative way of analysis this physics suggested by Wilson, often called by $D = 4-\varepsilon$ expansion. It assumes computation in quantum field theory can be extended for non-integer valued spacetime dimension D. In other words, even if our theories only well-defined on integer-valued spacetime dimension D, extension of this parameter into real-value is successfully working.

The leading order beta function of $D = 4-\varepsilon$-dimensional $O(N)$ ϕ^4 theory is given by

$$\beta(\lambda) = -\varepsilon\lambda + (N+8)\frac{\lambda^2}{8\pi^2} \tag{2.27}$$

We have two fixed point corresponds to $\lambda = 0$ and $\lambda = \frac{8\pi^2}{(N+8)}\varepsilon$. First one corredponds to Gaussian fixed point, which is free-field theory that we already expected. The another one is non-trivial fixed point called by Wilson-Fischer fixed point, corresponds to IR fixed point. Figuring out this fixed point is not available via 3-dimensional quantum field theory, but ε-expansion successfully converted non-perturbative problem into perturbative problem.

At Wilson-Fischer fixed point, the anomalous dimension of ϕ and ϕ^2 operators are given

by,

$$\Delta_\phi = \frac{D}{2} - 1 + \gamma_\phi = 1 - \frac{\varepsilon}{2} + \frac{N+2}{4(N+8)^2}\varepsilon^2 + O(\varepsilon^3)$$
$$\Delta_{\phi^2} = D - 2 + \gamma_{\phi^2} = 2 - \frac{6}{N+8}\varepsilon + O(\varepsilon^2) \tag{2.28}$$

From Callan-Symanzik equation, we can see that these quantities related to the value of critical exponents, $\Delta_\phi = \frac{1}{2} + \frac{\eta}{2}$ and $\Delta_{\phi^2} = 3 - \frac{1}{\nu}$.

This critical exponent can be calculated by several way. One can continue higher-loop Feynman diagram computation for anomalous dimension of ϕ and ϕ^2 operators. This higher-loop computation were done up to 7-loop. Since $O(N)$ theory is Borel summable, inserting $\varepsilon = 1$ will give convergent series after resummation procedure. Indeed, theoretical computation of critical exponents well fits to experimental data. Alternative approach for critical exponent is Monte-Carlo simulation. The numerical value of both method agrees with high accuracy.

2.3.2 Bootstrapping 3 dimensional critical theory

Although 3-dimensional $\mathbb{Z}_2$ or $O(N)$ theory are strongly coupled at IR regime, we saw ε expansion alternatively suggested the way of computing critical exponents. Fortunately, this systems are Borel summable, therefore well-behaving convergent series emergent after resummation even if for the large value of $\varepsilon = 1$.

The conformal bootstrap method independently provides equivalent numerical value for critical exponents. By linear programming or semi-definite programming, the observed results are quiet remarkable.

We have two inputs in bootstrap. First one is conformal dimension of scalar operator σ, which is $\mathbb{Z}_2$ odd field. Operator product expansion of this σ field expected to be

$$\sigma \times \sigma \sim 1 + \varepsilon + \cdots \tag{2.29}$$

Here ε field is $\mathbb{Z}_2$ even and lowest operator that first appears in $\sigma \times \sigma$ OPE. The second input parameter is conformal dimension of ε field, Δ_ε. Varying these two parameters and running convex optimization result is expressed in above figure. The colored region means do not viloates unitarity and crossing symmetry while white region violates unitarity and crossing symmetry.

The remarkable point is kink appeared in upper boundary. We can read critical exponents η and ν from coordinates of this kink. Suprisingly, this result very close to known numerical value of η and ν. By imposing only unitary and crossing symmetry, bootstrap program

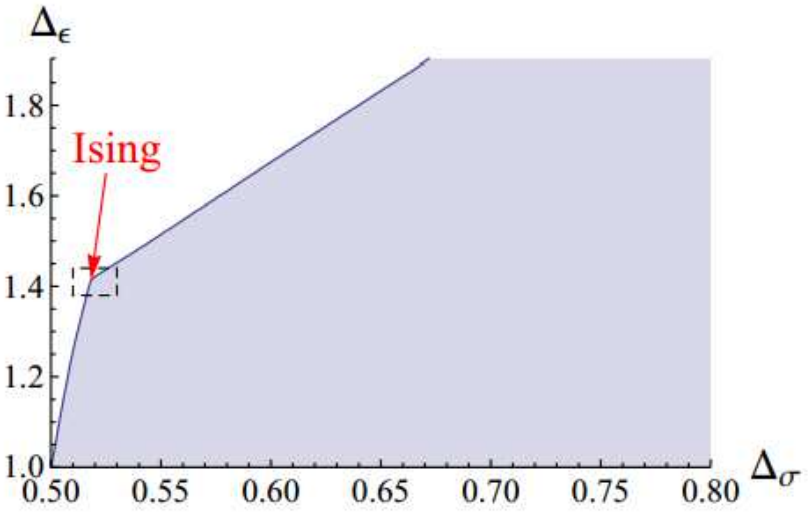

Figure 4: The result of 3D bootstrapping, obtained in [11]. The x-axis means conformal dimension of external operator σ and y-axis means the lowest operator appearing in $\sigma \times \sigma$ OPE. Colored region is consistent with unitarity and crossing symmetry. On its boundary, it has special kink. Remarkably, this kink indicates 3D IR critical theory(Ising theory).

provides physical quantities independently from other methods. For comparison, following table shows obtained value of critical exponents by various method.

Critical exponent	ε expansion(1998) [12]	Monte-Carlo(2010) [13]	Bootstrap(2014) [14]
η	0.03650(500)	0.03627(10)	0.03631(3)
ν	0.63050(250)	0.63002(10)	0.62999(5)

Table 3: The three different method of computing critical exponents of Ising theory. Bootstrap gives numerical value of critical exponent with high accuracy. Moreover, it is intrinsically non-perturbative method.

It is straightforward to impose global symmetry in bootstrap program. Especially, $O(N)$ global symmetry can be implied into here utilizing $SO(N)$ representation can be splitted into singlet, symmetric traceless and anti-symmetric part. The 3-dimensional $O(N)$ bootstrap result is summarized by following figure.

This is the result of singlet bound of $O(N)$ symmetric CFT in 3-dimension for various value of N. The cross in this figure indicates result of large N expansion result. Likewise $\mathbb{Z}_2$ symmetric case, there appears non-trivial kinks for various N results. For sufficiently large N, the location of kink well agrees to cross point. This agreement breaks down when N is small, since large N perturbation is no longer valid in this regime.

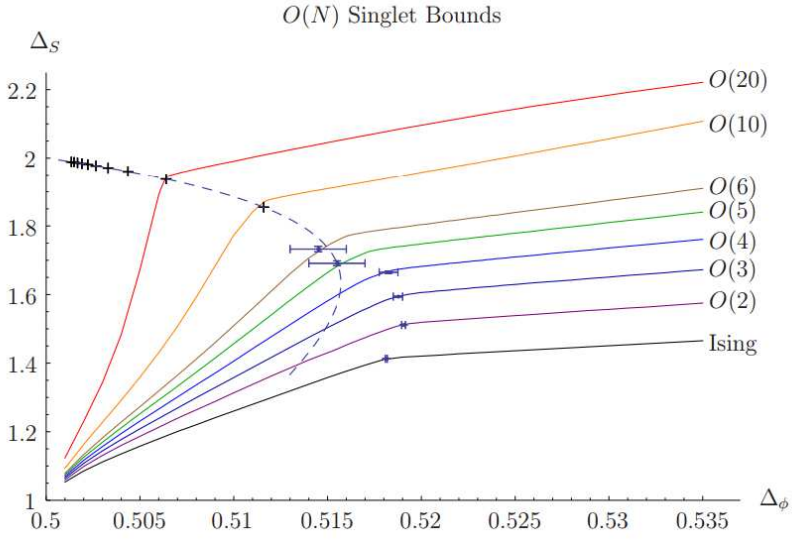

Figure 5: The result of 3D bootstrapping with $O(N)$ symmetry, obtained in [6]. The x-axis means conformal dimension of external operator ϕ and y-axis means the lowest operator appearing in $\phi \times \phi$ OPE in symmetric traceless sector. For diverse value of N, it has special kink on its boundary. Again, this kink indicates critical $O(N)$ theory. As N grows up, the location of kink well-matched with large-N expansion.

2.4 Non-trivial fixed point in 5 Dimension

The role of ϕ^4 operator in 5-dimension is distinguished from 3-dimensioanl one. In 3-dimensional case, deformation by this operator was relevant at Gaussian fixed point while irrelevant at Wilson-Fischer fixed point. Therefore, effective coupling grows as scaling, IR fixed point was hard to analyze by perturbation method.

The situation of 5-dimension is reversed. ϕ^4 deformation at free theory is irrelevant, which means Gaussian fixed point is now IR fixed point. Now existence of UV fixed point is non-trivial, hard to approach by perturbative computation.

At this stage, ε-expansion can be revisited. Rather than $D = 4 - \varepsilon$ expansion, we can consider $D = 4 + \varepsilon$ expansion. In this case, coupling constant λ at UV fixed point has negative value. It causes instability, suggests UV fixed point is not stable fixed point.

Although ε-expansion do not works well in higher dimension, we have several signals on existance of UV fixed point. First, we can utilize duality between $O(N)$ symmetric conformal field theory and higher spin theory defined on AdS_4 background. By adjusting boundary condition, higher spin theory provides two fixed points, which corresponds to Gaussian fixed point and Wilson-Fischer fixed point of 3-dimensionl $O(N)$ CFT. Likewise, we can extend this game for arbitrary dimensional AdS background. For the case of AdS_6 higher-spin, we expect there should be two fixed point as before, which characterized by UV/IR fixed point of 5-dimensional $O(N)$ CFT.

Second, we can utilize large-N expansion. Regardless of spacetime dimension, this technique can be applied and do not suffers from instability due to negative ε. We will see how this large-N expansion works and shows possibility of existance of UV fixed point in higher dimensional conformal field theory.

2.4.1 Hubbard-Stratonovich transformation

To get around the difficulty and to find nontrivial ultraviolet fixed point of $O(N)$ symmetry in higher spacetime dimensions, an alternative approach based on Hubbard-Stratonovich method was considered [4,5]. The theory, consisting of scalar fields ϕ^i, σ of $O(N)$ vector and scalar representations, is defined by the Lagrangian density:

$$\mathcal{L} = \frac{1}{2}(\partial_m \phi^i)^2 + \frac{1}{2}(\partial_m \sigma)^2 + \frac{\lambda_1}{2}\sigma\phi^{i2} + \frac{\lambda_2}{3!}\sigma^3 \qquad (i = 1, 2, \cdots N). \tag{2.30}$$

In six-dimensional spacetime, both λ_1 and λ_2 are marginal couplings. The fixed points are classifiable by the associated $O(N)$ symmetry. Two limiting situations are of interest. If the ϕ^i field becomes heavy and decoupled, the theory is reduced to a system of $O(0)$ symmetry in which the σ scalar field dominates the dynamics with cubic self-interaction. At the

fixed point, the coupling λ_2 is driven to a purely imaginary value. Therefore, this theory belongs to the universality class of the Lee-Yang edge singularity (which is a non-unitary theory). Otherwise, the $O(N)$ vector field ϕ^i couples to a system of the σ scalar field with bosonic Yukawa-type interactions. Starting from the Gaussian fixed point, there would be the renormalization group flows leading to non-trivial ultraviolet fixed point.

The perturbative computation of this system in $1/N$ and ε double expansion was performed in [4, 5]. Their result indicates that both situations of the fixed point is captured as N is varied: fixed point values of the coupling constants λ_1, λ_2 are real-valued for sufficiently large N, while complex-valued for sufficiently small N. The spacetime dimension is above the Ginzburg criterion, so the flow between ultraviolet fixed point and the infrared fixed point is reversed compared to the spacetime dimension less than four.

In five-dimensional spacetime, the scaling dimensions of ϕ^i and σ are computable perturbatively. They were computed up to third orders in $1/N$-expansion [4, 24]. The result is

$$\begin{aligned}\Delta_\phi &= \frac{3}{2} + \frac{0.216152}{N} - \frac{4.342}{N^2} - \frac{121.673}{N^3} + \cdots \\ \Delta_\sigma &= 2 + \frac{10.3753}{N} + \frac{206.542}{N^2} + \cdots\end{aligned} \tag{2.31}$$

For sufficiently large N, we expect the critical theory to exist at $(\Delta_\phi, \Delta_\sigma) = (\frac{3}{2}, 2)$, distinguished from the free theory at $(\Delta_\phi, \Delta_\sigma) = (\frac{3}{2}, 3)$. However, the above perturbtive result indicates that, for sufficiently small N, negative contribution of $\frac{1}{N}$ corrections dominate. In this case, Δ_ϕ falls below the unitary bound $3/2$ of five-dimensional scalar operator. This suggests that, at sufficiently small N, the critical fixed point should be interpreted as describing a non-unitary theory.

2.4.2 5-dimesional conformal bootstrap : one-parameter result

We performed the numerical bootstrap with one-gap approach. The result is shown in Figure 6. The result indicates that, in sharp contrast to the numerical bootstrap results for spacetime dimensions less than 4, the nontrivial ultraviolet fixed point predicted by large-N and ε-expansions lies well below the upper boundary of the allowed region. Moreover, there is no kink structure on the upper bounary. We thus conclude that the one-gap approach does not render any specific information on nontrivial fixed point. Clearly, the one-gap approach being incapable of pinning down the critical point precisely, a better approach is sought for.

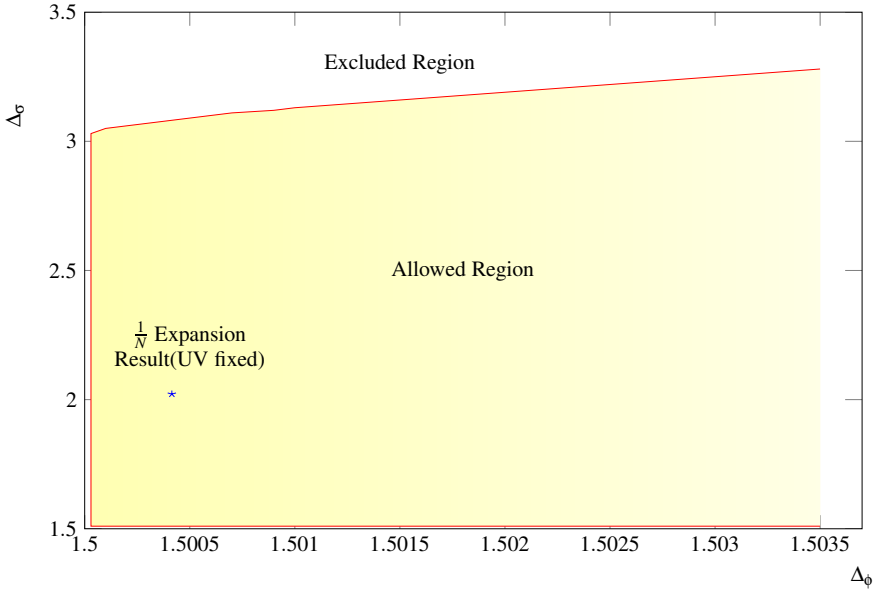

Figure 6: *The result of one-gap numerial boostrap for* $N = 500$. *The colored region is the values scaling dimensions consistent with the unitarity and crossing symmetry. The ultraviolet fixed point predicted by the* $1/N$*-expansion lies at an interior of the region.*

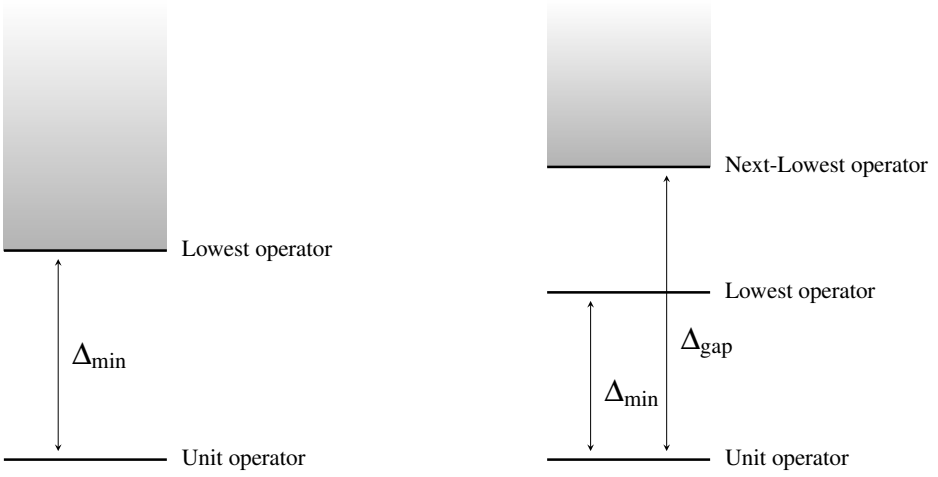

Figure 7: *Low-lying spectrum of one-gap approach traditionally used for* $d < 4$ *versus two-gap approach we propose in this work. Left figure illustrates typical one-gap setup in bootstrap program. Right figure depicts our input of two-gap in the scalar operator spectrum. Above the unit operator, we have an isolated scalar operator of conformal scaling dimension* Δ_{min}. *All other operators of higher scaling dimension starts at* Δ_{gap}.

2.4.3 5-dimesional conformal bootstrap : two-parameter result

To remedy the problem alluded above that the one-gap approach is not capable of locating the ultraviolet critical point, the idea we put forward is to use two-gap approach. By this, we mean that we assume that the lowest scalar operator (other than the identity operator) has scaling dimension Δ_{min} and that all other scalar operators start with scaling dimension at least Δ_{gap}. Our approach is most transparently depicted in Figure 7.

The idea is this: Compared to the one-gap bootstrapping, our two-gap bootstrapping expected to be carve out more space. This is because we are depleting primary operators in the scalar sector whose conformal scaling dimension lies between Δ_{min} and Δ_{gap}. Suppose a potential conformal fixed point has a scaling operator in the scalar sector spectrum between Δ_{min} and Δ_{gap}. The one-gap approach should capture this fixed point as a solution to the numerical bootstrap. On the other hand, the two-gap approach would consider this fixed point as an inconsistent theory. Therefore, we expect the two-gap approach constrains a putative conformal field theory further. A similar idea was considered in three-dimensional bootstrap program and there it also pointed to further restrictions for exploring ultraviolet and infrared fixed points [11]. As we will see later, however, a sharp difference is that nontrivial fixed points in spacetime dimensions less than four are already located by the one-gap approach, while those in spacetime dimensions larger than four necessitates the two-gap approach at the least.

More specifically, with the $O(N)$ global symmetry at hand, the operator product of two primary scalar fields ϕ_i in the fundamental representation of $O(N)$ is schematically given by [23]

$$\phi_i \times \phi_j \quad \sim \quad \sum_S \delta_{ij} O + \sum_T O_{(ij)} + \sum_A O_{[ij]}, \tag{2.32}$$

where the three terms in the right-hand side refer to the singlet, symmetric traceless, and antisymmetric irreducible representation sectors, respectively. As for the spin ℓ, the singlet and the symmetric traceless tensor sectors contain even spins only, while the antisymmetric tensor sector contain odd spins only. Reflecting this structure, sum rule for this case reads

$$\sum_{S,\Delta,\ell=\text{even}} c_{\Delta,\ell} V_{S,\Delta,\ell} + \sum_{T,\Delta,\ell=\text{even}} c_{\Delta,\ell} V_{T,\Delta,\ell} + \sum_{A,\Delta,\ell=\text{odd}} c_{\Delta,\ell} V_{A,\Delta,\ell} = 0, \tag{2.33}$$

where

$$V_{S,\Delta,\ell} = \begin{pmatrix} 0 \\ \mathcal{F}^-_{\Delta,\ell}(u,v) \\ \mathcal{F}^+_{\Delta,\ell}(u,v) \end{pmatrix}, \quad V_{T,\Delta,\ell} \begin{pmatrix} \mathcal{F}^-_{\Delta,\ell}(u,v) \\ (1-\frac{2}{N})\mathcal{F}^-_{\Delta,\ell}(u,v) \\ -(1+\frac{2}{N})\mathcal{F}^+_{\Delta,\ell}(u,v) \end{pmatrix}, \quad V_{A,\Delta,\ell} = \begin{pmatrix} -\mathcal{F}^-_{\Delta,\ell}(u,v) \\ \mathcal{F}^-_{\Delta,\ell}(u,v) \\ -\mathcal{F}^+_{\Delta,\ell}(u,v) \end{pmatrix}$$

and

$$\mathcal{F}^{\pm} \equiv v^{\Delta} G_{\Delta,l}(u,v) \pm u^{\Delta} G_{\Delta,l}(v,u). \tag{2.34}$$

In our two-gap approach, we propose to introduce two parameters $(\Delta_{\text{min}}, \Delta_{\text{gap}})$ into the singlet sector $V_{S,\Delta,\ell}$. For nonsinglet sectors $V_{T,\Delta,\ell}$ and $V_{A,\Delta,\ell}$, we include all operators in so far as their scaling dimensions are above the unitary bound.

For the numerical optimization, we converted this problem into semi-definite programming [17]. We proceeded as follows. Firstly, using the radial approximation and the Zamolodchikov recursion relation (2.17), we expressed the function $\mathcal{F}^{m,n}(\Delta,\ell,z,\bar{z})$ as a sum over conformal blocks, in which structure of this building block is given by $\Pi_i\big(\frac{1}{\Delta-\Delta_i}\big)P_\ell^{m,n}(\Delta)$. This is because, successive iteration of recursion relation (2.17) generates product of $\frac{1}{\Delta-\Delta_i}$, which appears in (2.17). As $\Pi_i\big(\frac{1}{\Delta-\Delta_i}\big)$ is positive-definite, it suffices to focus on the polynomial $P_\ell^{m,n}(\Delta)$. Secondly, we parametrized scaling dimension of operators above Δ_{gap} in scalar sector by $\Delta = \Delta_{\text{gap}}(1+\alpha),\ \alpha \in (0,\infty]$. This puts $P_\ell^{m,n}(\Delta = \Delta_{gap}(1+\alpha))$ a polynomial of α. Likewise, spin sector parametrized by $\Delta = (l+d-2)(1+\alpha),\ \alpha \in (0,\infty]$. This parametrization means we consider all operators over unitary bound. Therefore, regardless of spin, the function $P_\ell^{m,n}(\Delta)$ is essentially polynomial of α. This polynomial structure of $P_\ell^{m,n}(\alpha)$ enables to put the optimization into semi-definite programming.

Below, we provide the pseudocode for our optimization of (2.26):

`Semi-Definite Programming:` $\mathbb{L}$

$$\begin{aligned}
&\texttt{Minimize} \quad \mathbb{L}[\mathcal{F}_0^{m,n}(\Delta,l,z,\bar{z})] \\
&\quad \texttt{subject to} \quad \mathbb{L}(P^{m,n}(\Delta_{\text{min}})) > 0; \\
&\qquad \vec{\alpha} = (1,\alpha,\alpha^2,\cdots,\alpha^d) \\
&\qquad \mathbb{L}(P^{m,n}(\Delta_0(1+\alpha))) = \vec{\alpha}^{\mathrm{T}}\mathbb{A}_\ell\,\vec{\alpha} + \alpha(\vec{\alpha}^{\mathrm{T}}\mathbb{B}_\ell\,\vec{\alpha}) \\
&\qquad \Delta_0 = \Delta_{\text{gap}}(1+\alpha) \quad \texttt{if} \quad \ell = 0 \\
&\qquad\qquad \Delta_\ell(1+\alpha) \quad \texttt{else} \quad \ell > 0 \\
&\qquad \mathbb{A}_\ell \succeq 0, \quad \mathbb{B}_\ell \succeq 0; \\
&\quad \texttt{given} \quad (N,\Delta_{\text{gap}},\Delta_\ell); \\
&\texttt{Run} \quad \ell = 0 \\
&\qquad\quad \ell = \ell + 1 \\
&\texttt{Stop} \quad \ell = \ell_{\text{max}}
\end{aligned} \tag{2.35}$$

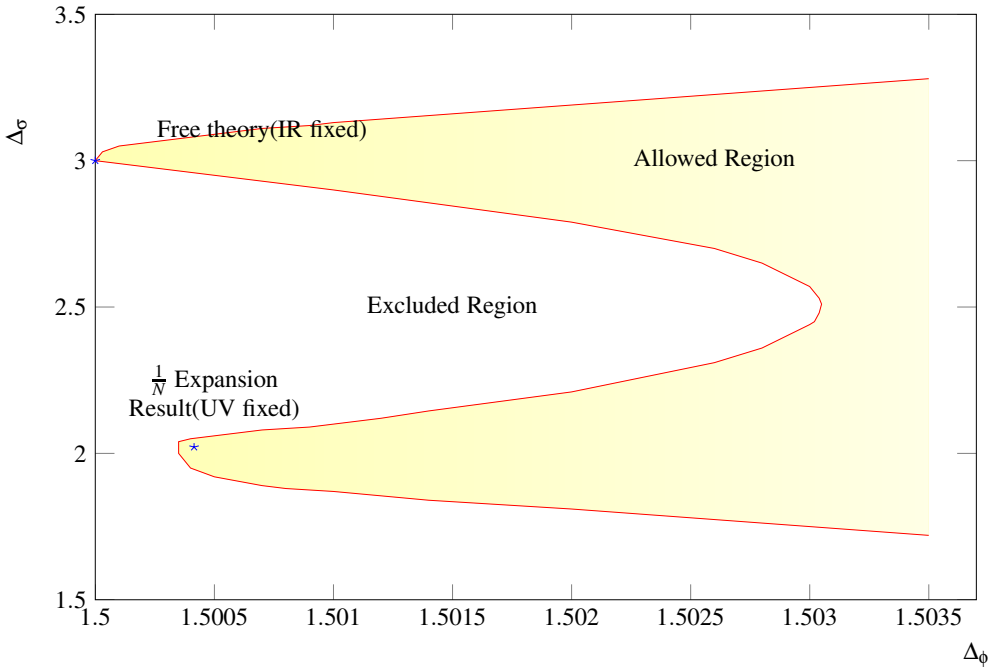

Figure 8: *Result of two-gap approach for $N = 500$ and $k = 15$. Yellow-colored part is the allowed region, consistent with the unitarity and the crossing symmetry of 4-point correlation function. Compared to the one-gap approach result in Figure 2, the two-gap approach carves out regions of low values above the unitarity bound. Its boundary features two cusps. The ultraviolet nontrivial fixed point is located at its lower tip, while the infrared Gaussian fixed point is located at its upper tip.*

In the code, Δ_ℓ is the unitary bound for spin-ℓ operators, given by $(D-2+\ell)$. In our computation, we truncated the spins to $\ell \leq \ell_{\max} = 20$. Also, $\mathbb{A}_\ell$ and $\mathbb{B}_\ell$ are matrices that built from the polynomials $P^{m,n}(\alpha)$. In our computation, we calculated the numerical value of $\mathbb{A}_\ell, \mathbb{B}_\ell$ matrix entries by `Mathematica`. These matrix entries are the input parameters of semi-definite programming. For numerical optimization of semi-definite programming with respect to the parameters $\alpha_{m,n}$, we used the open source `SDPA-GMP`.

2.4.4 Bootstrap Results

We considered the $O(N)$ global symmetric bootstrap, where the sum rule was decomposed according to (2.34). We carried out the numerical bootstrapping with the proposed two-gap approach in the scalar sector $V_{S,\Delta,\ell}$ by semi-definite programming. We identified regions in $(\Delta_\phi, \Delta_\sigma)$ space where the unitarity and the crossing symmetry conditions are satisfied. We repeated the procedure with varying $N, \Delta_{\min}, \Delta_{\text{gap}}$ and addressed the following questions.

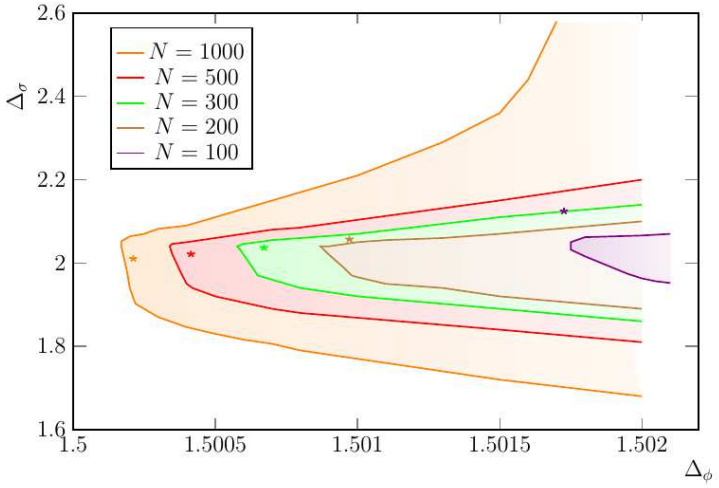

Figure 9: *Result for* $\Delta_{\text{gap}} = 8.0$. *Here we zoomed in around near lower tip. From leftmost, each bound stands for* $N = 1000, N = 500, N = 300, N = 200, N = 100$, *respectively. The star marks indicate location of perturbative* $\frac{1}{N}$ *expansion result for each* N. *For sufficiently large* N, *star mark location gradually approaches to boundary of allowed region.*

- Does the two-gap approach constrain the theory space more than the one-gap approach? Is the two-gap approach enough to locate both the Gaussian and nontrivial fixed points on its allowed region boundary?
- What is the range of validity of perturbative $1/N$-expansions?
- How do locations of the fixed points move around as the theory parameters N, Δ_{gap} are varied?
- At extreme values of N, Δ_{gap}, do fixed points appear or disappear? If so, what are critical value $N^{\text{crit}}, \Delta_{\text{gap}}^{\text{crit}}$ for onset of such behavior?
- From scaling consideration, we expect that bootstrapping for $d > 4$ and bootstrapping for $d < 4$ are dual each other in that ultraviolet and infrared regimes are interchanged. Do we find such 'duality' from the result?

We first explore whether the two-gap approach carves out regions that were allowed within the one-gap approach. For the representative choice of $N = 500$, the result is shown in Figure 8.

We already presented physical reason why we expect the two-gap approach puts more restrictive result than one-gap approach. Indeed, the two-gap approach result in Figure 8 further carves out the region allowed by the one-gap approach. In this result, we have set

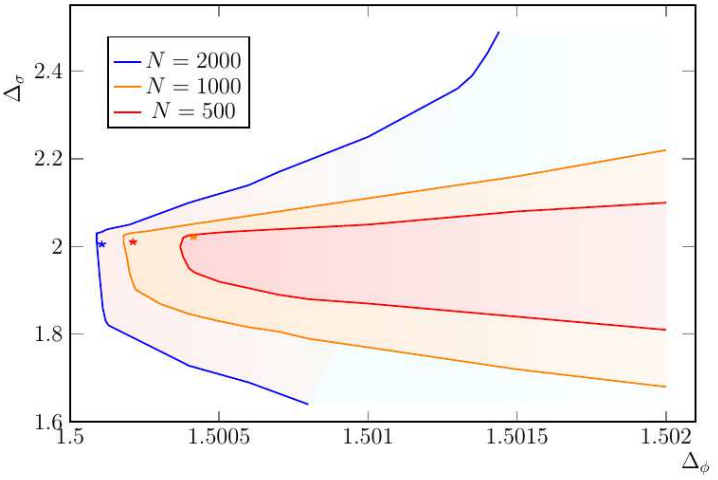

Figure 10: *Result for* $\Delta_{\text{gap}} = 40.0$. *Here, we zoomed in near lower tip. From leftmost, each bound presents* $N = 2000, N = 1000, N = 500$, *respectively. Each star mark is the location of perturbative result from (2.31). The endpoint of tip agrees to star mark, identified as the ultraviolet fixed point.*

Δ_{gap} to 8.00 and $k = 15$. The result manifests two pronounced tips. The apex of upper tip region indicates free theory. Surprisingly, end of lower tip is quiet close to perturbation result (2.31).

Next, we bootstrapped with various N, fixing parameter $\Delta_{gap} = 8.0$ as before. To see agreement of UV fixed point and shrapened end of tip, we zoomed in near low-tip area. The result displayed in Figure 9. Each star mark is perturbation result from (2.31). Perturbative result of $\frac{1}{N}$ expansion for $N = 100, 200$ lies outside of allowed region. Our result shows bootstrap result and large-N expansion are comparable when N is larger than 300. Another notable point here is appearance of kink at lower bound. For $N = 100$, kink do not appears while other case shows sudden change of slope.

We also examined the impact of varying the parameter Δ_{gap} at a fixed value of N. We increased it to $\Delta_{\text{gap}} = 40.0$, which is much larger than the value we set in Figure 9. Since we are now ruling out more theories than for $\Delta_{gap} = 8.0$, we expect the result carving more space out. The result displayed in Figure 10 indeed demonstrate that our intuition is met.

The pattern of carving out is worth of nothing. Overall, the boundary curve of the allowed region retains the shape of Σ. As the gap Δ_{gap} is increased, the depletion mines out and pushes the mid-part of the boundary curve (the part that takes $>$-shape) to the right. On ther other hand, the outer boundaries – the upper boundary emanating from the upper tip and lower boundary emanating from the lower tip - are little changed. We confirmed that this

behavior persists even if Δ_{gap} is increased up to 100.0.

We also checked validity of the $1/N$-expansion. Even if the band gap is large, as in Figure 10 with $\Delta_{\text{gap}} = 40.0$, the ultraviolet nontrivial fixed point predicted by $1/N$ expansion (note that this expansion comes with large coefficients) sits close to the tip of the allowed region. This is the behavior we already observed for lower value of Δ_{gap}, as in Figure 8 for $\Delta_{\text{gap}} = 8.0$.

From the proximity of the pertubative fixed point to the boundary of allowed region, we also draw a conclusion that the $1/N$-expansion becomes less reliable at larger band gap Δ_{gap}. This can be gleaned from the data for $N = 500$. For $\Delta_{\text{gap}} = 8.0$, Figure 9 indicates the perturbative fixed point was enclosed by the boundary curve. On the other hand, for $\Delta_{\text{gap}} = 40.0$, Figure 10 indicates the perturbative fixed point hits the boundary curve. Inferred from Figure 9 to the trend of varying N, it is expected that the perturbative fixed point will lies outside the allowed region for N less than 500.

We consider the large-N match in $(\Delta_\phi, \Delta_{\text{min}})$-space between the nontrivial fixed point predicted by large-N expansion and the tip of allowed Σ-region is a strong indication that the two-gap approach is a useful method for locating nontrivial fixed point at any N.

Chapter 3

Interlude : Scattering amplitude versus Polygonal Wilson loop in $\mathcal{N}=4$ SYM

The $\mathcal{N}=4$ super Yang-Mills theory is maximally supersymmetric Yang-Mills theory defined in 4-dimension. The structure of tree-level gluon scattering amplitude is same with QCD since three-point interaction is identical. Therefore, we can utilize Parke-Taylor expression which developed in QCD. However, loop correction would be different with QCD. This theory suffers from IR *logarithmic* divergence. To manage it, we should utilize dimensional regularization. Since now spacetime dimension shifted 4 to $4-2\epsilon$, the conformal symmetry is broken. Therefore, Ward identity with respect to $\mathbb{D}$ or $\mathbb{K}_\mu$ is violated. The conformal anomaly governed by anomalous conformal Ward identity. Solution of this differential equation well matched with perturbtive computation. In this section, we will discuss remarkable properties of gluon scattering amplitude defined in $\mathcal{N}=4$ SYM. The dual conformal symmetry, all-loop ansatz, conformal Ward identity and relation with polygonal Wilson loop will be discussed.

3.1 Gluon Scattering Amplitude in $\mathcal{N}=4$ SYM

In this section, we will focus on gluon n-point amplitude defined in Yang-Mills Theory in 4-dimension. Since gluon field in this theory is massless, states are labeled by helicity, which is given by ± 1. The benifit of tree level amplitude in Yang-Mills theory is, the information of gauge group is factorized due to identity of Lie algebra. The remained part often called by color ordered amplitude. In summary, full amplitude is consist of non-cyclic permutation of color ordered amplitude.

$$\mathcal{A}_n = \mathrm{Tr}[T^{a_1}T^{a_2}\cdots T^{a_n}]A_n^{h_1,h_2,\cdots h_n}(p_1,p_2,\cdots,p_n) + \text{permutations} \tag{3.1}$$

Since we are considering $SU(N)$ gauge theory, color indices a_i runs from 1 to N^2-1. $A_n^{+++\cdots+}(p_1,p_2,\cdots,p_n)$ and $A_n^{-++\cdots+}(p_1,p_2,\cdots,p_n)$ are vanished due to supersymmetry. First nontrivial contribution in amplitude is called by Maximally Helicity Violation amplitude(MHV), $A_n^{++-\cdots-}(p_1,p_2,\cdots,p_n)$ or $A_n^{--+\cdots+}(p_1,p_2,\cdots,p_n)$.

To compute tree-level amplitude, we should consider all possible diagrams in principle. The complexity of computation is rapidly increase as growing particle number n. Up to

$n = 10$, number of diagram is summarized in following table.

Number of external gluons	4	5	6	7	8	9	10
Number of diagrams	4	25	220	2485	34300	559405	10525900

It is almost impossible counting all these diagrams. Nevertheless, extremely remarkable simplification occurs in $\mathcal{N} = 4$ SYM. To explain it, let us recall the concept of twistor formalism.

We define the momentum $p^{\alpha\dot{\alpha}}$ by,

$$p^{\mu} \to \hat{p}^{\alpha\dot{\alpha}} = p^{\mu}\sigma_{\mu}^{\alpha\dot{\alpha}} = \begin{pmatrix} p^0 + p^3 & p^1 + ip^2 \\ p^1 - ip^2 & p^0 - p^3 \end{pmatrix} \tag{3.2}$$

It is easy to recognize that on-shell gluon momenta $p^2 = 0$ corresponds to vanishment of determinant $\hat{p}$. Now, we introduce twisor λ^{α} and anti-twistor $\tilde{\lambda}^{\dot{\alpha}}$ by

$$\hat{p}^{\alpha\dot{\alpha}} = \lambda^{\alpha}\tilde{\lambda}^{\dot{\alpha}} \tag{3.3}$$

The inner product of twistor is defined by

$$\langle ij \rangle \equiv \lambda_i^{\alpha}\lambda_{j,\alpha}, \quad [ij] \equiv \lambda_i^{\dot{\alpha}}\tilde{\lambda}_{j,\dot{\alpha}}, \quad \langle ij] \equiv \lambda_i^{\alpha}\tilde{\lambda}_{j,\dot{\alpha}}, \tag{3.4}$$

By utilizing these definition, we can replace mometum dependence by twistor variables.

The n-point MHV gluon tree level amplitude has very simple structure in twistor variable :

$$A_n^{Tree}(1^-2^-3^+\cdots n^+) = \frac{\langle 12 \rangle^4}{\langle 12 \rangle\langle 23 \rangle\cdots\langle n1 \rangle}\delta^{(4)}(\sum p_i) \tag{3.5}$$

The loop correction is enters by scalar factor M_n, they are factorized from tree level amplitude.

$$A_n = A_n^{Tree} \times M_n = A_n^{Tree} \times (1 + M_n^{(1)} + M_n^{(2)} + \cdots) \tag{3.6}$$

Note that the information of helicity is completely imposed in tree level amplitude.

Bern, Smirnov and Dixon explicitly computed 4-point loop amplitude up to 3-loop. They found that very remarkable recursive relation appears for loop amplitude. For instance, 2-loop amplitude is related by 1-loop amplitude by

$$M_4^{(2)}(\varepsilon) = \frac{1}{2}\left(M_4^{(1)}(\varepsilon)\right)^2 + f^{(2)}(\varepsilon)M_4^{(1)}(2\varepsilon) + C^{(2)} + O(\varepsilon) \tag{3.7}$$

They found this kind of recursive relation still holds to 3-loop. Based on this observation,

they made all-loop n-point ansatz on gluon scattering amplitude.

$$\mathcal{M}_n \equiv 1 + \sum_{l=1} \alpha^l M_n^{(l)} = \exp\Big[\sum_{l=1} \alpha^l \big(f^{(l)}(\varepsilon) M_4^{(1)}(l\varepsilon) + C^{(l)} + O(\varepsilon)\big)\Big] \tag{3.8}$$

For the case of 4-point amplitude, expression is simply summarized.

$$\begin{aligned} A_4 &= A_{\text{Tree}} (A_{\text{div},s})^2 (A_{\text{div},t})^2 \exp\Big(\frac{f(\lambda)}{8}\big(\text{Log}\frac{s}{t}\big)^2 + \text{const}\Big) \\ A_{\text{div},s} &= \exp\Big(-\frac{1}{8\varepsilon^2} f^{(-2)}\big(\frac{\lambda\mu^{2\varepsilon}}{s^\varepsilon}\big) - \frac{1}{4\varepsilon} g^{(-1)}\big(\frac{\lambda\mu^{2\varepsilon}}{s^\varepsilon}\big)\Big) \end{aligned} \tag{3.9}$$

The function $f^{(-2)}\big(\frac{\lambda\mu^{2\varepsilon}}{s^\varepsilon}\big)$ is related to cusp anomalous dimension.

This BDS ansatz is consistent with dual conformal Ward identity. To describe dual conformal symmetry, let us first introduce dual coordinate from momentum p_i.

$$p_i \equiv x_{i+1} - x_i \tag{3.10}$$

The dual conformal symmetry is generated by conformal generator based on dual coordinate x_i. This non-local symmetry is hidden symmetry of $\mathcal{N}=4$ SYM. In summary, $\mathcal{N}=4$ SYM theory has superconformal symmetry and dual conformal symmetry. Together, they are called by Yangian symmetry. This dual conformal symmetry can be utilized for computing higher loop correction of scattering amplitude.

We can express loop integration with this dual variables. For instance, 1-loop box integration is reexpressed by

$$I_4^{(1)} = \int \frac{d^4q}{q^2(q-p_1)^2(q-p_1-p_2)^2(q+p_4)^2} = \int \frac{d^4x_5}{x_{15}^2 x_{25}^2 x_{35}^2 x_{45}^2} \tag{3.11}$$

Here, internal momenta q is identified with $x_5 - x_1$. By dual inversion, this 4-point 1-loop amplitude behaves covariantly. Reflecting this, we can equivalently express above 1-loop amplitude by

$$I_4^{(1)} = \frac{\Phi(u,v)}{x_{13}^2 x_{24}^2} \tag{3.12}$$

This structure is very parallel to 4-point correlation function defined in conformal field theory. For the case of 3-loop amplitude, there are two class of amplitudes : Ladder diagram and tennis court diagram. By utilizing dual conformal symmetry, indeed one can see these two diagrams are equivalent. This way, dual conformal way makes loop computation more easier.

3.2 Polygonal Wilson loop expectation value in $\mathcal{N}=4$ SYM

The striking discovery in $\mathcal{N}=4$ SYM is that equivalent relation between gluon scattering amplitude and polygonal Wilson loop expectation value holds for out of Regge limit. In other words, this theory is Regge exact. There are several benifit to considering polygonal Wilson loop rather than scattering amplitude. First, number of diagrams appearing in Wilson loop side is generally less than scattering amplitude. For large n, polygonal Wilson loop computation is still doable while scattering amplitude is very hard to compute. Second, dual conformal symmetry is realized in Wilson loop by conformal symmetry. This is because, Wilson loop contour and location of cusp are realized by dual coordinate. If contour is smooth, one get UV divergence as two point of contour approaches to each other. However, this divergence correspond to power divergence, irrelevant to dimensional regularization. Therefore, we need not worry about break down of conformal symmtery. When contour has cusp, the divergent corresponds to logarithmic divergence. This should be regularized by dimensional regularization, eventually cause measure anomaly. This anomaly realized by non-vanishing Ward identity for special conformal generator K_μ. This operator is defined by

$$K_\mu = \sum_i \Big[x_{i\mu} x_i \cdot \frac{\partial}{\partial x_i} - \frac{1}{2} x_i^2 \frac{\partial}{\partial x_i^\mu} \Big] \tag{3.13}$$

Operating on finite part of Wilson loop expectation valueF_n^{WL} gives

$$K^\mu F_n^{WL} = \frac{1}{2}\Gamma_{\text{cusp}}(a) \sum_i (2x_i^\mu - x_{i-1}^\mu - x_{i+1}^\mu) \text{Log} x_{i-1,i+1}^2 \tag{3.14}$$

The solution of this differential equation is given by

$$F_4 = \frac{1}{4}\Gamma_{\text{cusp}}(a) \text{Log}^2\Big(\frac{x_{13}^2}{x_{24}^2}\Big) + \text{const}$$

$$\begin{aligned}
F_5 &= -\frac{1}{8}\Gamma_{\text{cusp}}(a) \sum_{i=1}^{5} \text{Log}\Big(\frac{x_{i,i+2}^2}{x_{i,i+3}^2}\Big) \text{Log}\Big(\frac{x_{i+1,i+3}^2}{x_{i+2,i+4}^2}\Big) + \text{const} \\
F_6 &= \frac{1}{4}\Gamma_{\text{cusp}}(a) \sum_{i=1}^{6} \Big[-\text{Log}\Big(\frac{x_{i,i+2}^2}{x_{i,i+3}^2}\Big) \text{Log}\Big(\frac{x_{i+1,i+3}^2}{x_{i,i+3}^2}\Big) + \frac{1}{4}\text{Log}^2\Big(\frac{x_{i,i+3}^2}{x_{i+1,i+4}^2}\Big) \\
&\qquad - \frac{1}{2}\text{Li}_2\Big(1 - \frac{x_{i,i+2}^2 x_{i+3,i+5}^2}{x_{i,i+3}^2 x_{i+2,i+5}^2}\Big)\Big] + f(u_1,u_2,u_3;a) + \text{const}
\end{aligned} \tag{3.15}$$

These solution exactly corresponds to result of BDS ansatz. We have additional part $f(u_1, u_2, u_3; a)$ that appears at F_6. Indeed, BDS anstaz is known to be breaks down at 6-point amplitude. The reason is simply figured out from this anomalous conformal Ward identity. From 6-point amplitude, we can define non-trivial three cross ratios u_1, u_2, u_3. Since conformal cross ratio is invatiant under conformal transformation, this differential equation cannot fix the structure of $f(u_1, u_2, u_3; a)$. This function is called by remainder function.

The analytic structure of this remainder function of hexagon Wilson loop was obtained in [35]. There, central tool was to utilize the special limit of the quasi-multi Regge kinematics(QMRK). It was found that the remainder function could be written with the uniform transcendentality in terms of the Goncharov polylogarithms. The structure was very involved but was reduced to a combination of classical polylogarithms of uniform transcendentality of degree four [36]. These techniques were also utilized in subsequent works investigating analytic structure of the remainder function up to three loop order [37, 38]. It was further extended to analytic structure of the non-maximal helicity violating (nMHV) amplitudes at two loop order with help of the symbols [39].

Chapter 4

Polygonal Wilson loop in ABJM theory

We now turn to the ABJM theory and compare known results about scattering amplitudes and lightlike Wilson loops with those of the $\mathcal{N}=4$ SYM theory. Given that both theories are superconformal, one might anticipate from the AdS/CFT correspondence that the Wilson loops / scattering amplitudes duality would hold equally and result in identical functional structure, at least at strong coupling regime. This is not the case. In the ABJM theory, the n-parton scattering amplitudes is definable only for even integers $n=4,6,8,\cdots$ (since the dynamical matter fields are in bifundamental representations), while the n-gon Wilson loops exist for all integers $n=4,5,6,\cdots$. So, a possibility is that the duality holds only for even integers n, while leaving Wilson loops of odd-sided polygons a class of its own. Secondly, the open superstring in $\mathrm{AdS}_4\times\mathbb{CP}^3$ does not possess the fermionic T-duality. Absence of fermionic T-duality symmetry implies no relation between scattering amplitudes and light-like Wilson loops. This then rules out the duality relation between scattering amplitude and Wilson loop in ABJM theory.

4.1 Main Results

Firstly, we obtained analytic result of the light-like hexagon Wilson loop at second-order in 't Hooft coupling constant $\lambda=(N/k)$. Regularizing the UV divergence by supersymmetric dimensional reduction scheme with $d=3-2\varepsilon$, the result reads

$$\left\langle W_{\square}[C_6]\right\rangle^{(2)}_{\mathrm{ABJM}}=\lambda^2\left[-\frac{1}{2}\sum_{i=1}^{6}\frac{(x_{i,i+2}^2\tilde{\mu}^2)^{2\varepsilon}}{(2\varepsilon)^2}+\mathrm{BDS}_6^{(2)}(x)+\left(\frac{9}{2}\mathrm{Log}^2(2)+\frac{\pi^2}{3}\right)\right]. \tag{4.1}$$

Here, x_i $(i=1,\cdots,6)$ are hexagon vertex positions, and $\tilde{\mu}^2:=8\pi e^{\gamma_E}\mu^2$. The second term is the UV-finite "BDS" function [1] :

$$\mathrm{BDS}_6^{(2)}(x)=\frac{1}{2}\sum_{i=1}^{6}\left[\frac{1}{4}\mathrm{Log}^2(\frac{x_{i,i+3}^2}{x_{i+1,i+4}^2})-\mathrm{Log}(\frac{x_{i,i+2}^2}{x_{i,i+3}^2})\mathrm{Log}(\frac{x_{i+1,i+3}^2}{x_{i,i+3}^2})-\frac{1}{2}\mathrm{Li}_2(1-\frac{x_{i,i+2}^2x_{i+3,i+5}^2}{x_{i,i+3}^2x_{i+2,i+5}^2})\right]+\frac{\pi^2}{2} \tag{4.2}$$

[1] Hereafter, we shall adopt the terminology of corresponding quantities in the $\mathcal{N}=4$ SYM theory

This function depends on the vertex positions the same way as the UV-finite, leading order BDS function of the $\mathcal{N}=4$ SYM theory. All the finite parts in Eqs.(4.1, 4.2) exhibit the property of the uniform transcendentality.

Secondly, we obtained the ABJM antenna function relevant for lightlike polygon Wilson loops. Recall that, in the $\mathcal{N}=4$ SYM theory, the splitting function in the scattering amplitudes is defined by the IR factorization associated with multiple collinear limit of massless particles. Here, in ABJM theory, we dwell on special kinematic configuration and focus on the limit of the Wilson loop contour. For reasons that will become clear later, we focus on a sort of operator product expansion involving two collinear edges of fraction h_1, h_3 and one soft edge of fraction h_2 in between. This limit defines the triple antenna function: lightlike n-gon Wilson loop is decomposable into a product of $(n-2)$-gon light-like Wilson loop and this antenna function. At second order in 't Hooft coupling λ, the triple antenna function consists of two parts: the pure Chern-Simons part and matter-dependent part. Our result is

$$\begin{aligned}\left[\frac{\mathrm{Ant}^{(2)}[C_n]}{\mathrm{Ant}^{(0)}[C_n]}\right]_{\mathrm{CS}} &= \frac{\mathrm{Log}(2)}{2\varepsilon} \\ &+ \frac{1}{2}\mathrm{Log}(2)\mathrm{Log}(h_1) + \frac{1}{2}\mathrm{Log}(2)\mathrm{Log}(h_3) + \frac{1}{2}\mathrm{Log}(2)\mathrm{Log}(x_{24}^2) + \frac{1}{2}\mathrm{Log}(2)\mathrm{Log}(x_{35}^2) \\ &- \frac{7\pi^2}{24} + \mathrm{Log}^2(2) \end{aligned} \tag{4.3}$$

for the pure Chern-Simons part and

$$\begin{aligned}\left[\frac{\mathrm{Ant}^{(2)}[C_n]}{\mathrm{Ant}^{(0)}[C_n]}\right]_{\mathrm{matter}} &= \frac{1}{4\varepsilon^2} + \frac{1}{4\varepsilon}(\mathrm{Log}(h_1) + \mathrm{Log}(h_3) + \mathrm{Log}(x_{24}^2) + \mathrm{Log}(x_{35}^2)) \\ &+ \frac{1}{2}\mathrm{Log}(h_1)\mathrm{Log}(x_{24}^2) + \frac{1}{2}\mathrm{Log}(h_3)\mathrm{Log}(x_{35}^2) + \frac{1}{2}\mathrm{Log}(x_{35}^2)\mathrm{Log}(x_{24}^2) \\ &- \frac{1}{2}\mathrm{Log}(h_1)\mathrm{Log}(h_3) - \frac{\pi^2}{6} \end{aligned} \tag{4.4}$$

for the matter-dependent part. The result demonstrates that splitting function also displays the property of maximal transcendentality. Moreover, the result is independent of n, suggesting that the triple antenna function holds universally for all n. The total triple antenna function is strikingly similar to triple splitting function in the limit middle parton becomes soft. We found, however, they are still subtly different.

Thirdly, combining the two results above, we obtained the simplest functional form of lightlike polygon ABJM Wilson loop to the second-order in 't Hooft coupling. The requisite shape of lightlike polygon must be Euclidean and satisfy vanishing Gram determinant condition.

It turns out such kinematics requirements limit the lightlike polygon only to the one with even number of cusps, marking a stark difference from the $\mathcal{N}=4$ SYM theory. Demanding IR factorization of the Wilson loop with the universal antenna function, we obtained a version of operator product expansion, leading to a linear recursion relation among the light-like Wilson loops:

$$\Big\langle W_{\square}[C_n]\Big\rangle \quad \longrightarrow \quad \mathrm{Ant}[C_n]\cdot\Big\langle W_{\square}[C_{n-2}]\Big\rangle. \tag{4.5}$$

Solving this recursion with the hexagon Wilson loop (4.1) as an input, we finally find that

$$\boxed{\Big\langle W_{\square}[C_n]\Big\rangle^{(2)}_{\mathrm{ABJM}} = \lambda^2\left[-\frac{1}{2}\sum_{i=1}^{n}\frac{(x^2_{i,i+2}\tilde{\mu}^2)^{2\varepsilon}}{(2\varepsilon)^2}+\mathrm{BDS}^{(2)}_n(x)+\mathrm{Rem}^{(2)}_n(u)\right],} \tag{4.6}$$

where $\mathrm{Rem}_n(u)$ is the remainder function that depends on the Mandelstam invariants only through conformal cross-ratios u's. At two loops, the remainder function is independent of u's and reads

$$\boxed{\mathrm{Rem}^{(2)}_n(u)=\left[n\left(\frac{\pi^2}{12}+\frac{3}{4}\mathrm{Log}^2(2)\right)-\frac{\pi^2}{6}\right].} \tag{4.7}$$

Here, we extracted this analytic result by utilizing the PSLQ algorithm to the high precision numerical integrations. As a nontrivial check, we derived the spacelike circular Wilson loop expectation value from the $n\to\infty$ continuum limit and found perfect agreement with the previous results.

4.2 Light-like Polygon Wilson loop in ABJM Theory

4.2.1 ABJM Theory

The ABJM theory describes $(2+1)$-dimensional supersymmetric matter interacting with Chern-Simons gauge system. It has $\mathcal{N}=6$ superconformal symmetry (having 24 conserved supercharges) and $U(N)\times\overline{U(N)}$ gauge group with Chern-Simons levels $+k,-k$, respectively. The gauge fields are denoted as $A_m(x)\in u(N)$ and $\overline{A}_m(x)\in\overline{u(N)}$. For foregoing considerations, it suffices to note that the action includes the pure Chern-Simons density [25]

$$S_{\mathrm{CS}} = +\frac{k}{4\pi}\int d^dx\varepsilon^{mnp}\mathrm{Tr}\Big(A_m\partial_nA_p+\frac{2i}{3}A_mA_nA_p\Big) \tag{4.8}$$

$$\overline{S}_{\mathrm{CS}} = -\frac{k}{4\pi}\int d^dx\varepsilon^{mnp}\overline{\mathrm{Tr}}\Big(\overline{A}_m\partial_n\overline{A}_p+\frac{2i}{3}\overline{A}_m\overline{A}_n\overline{A}_p\Big). \tag{4.9}$$

Here, the Chern-Simons density has levels $+k$ and $-k$, respectively. Invariance of the action under large gauge transformation puts k integer-valued. The action is invariant under the

generalized parity that simultaneously reverts one spatial coordinates and exchanges the two gauge fields. In this theory, the ABJM Wilson loop operator in the fundamental representation $(\Box,1)\oplus(1,\Box)$ of the gauge group $U(N)\times\overline{U(N)}$ is defined by [40]:

$$\mathcal{W}^{\prime}_{\Box}[C] := \frac{1}{2}\Big(W_{\Box}[C]+\overline{W}_{\Box}[C]\Big), \tag{4.10}$$

where $W_{\Box}[C]$ and $\overline{W}_{\Box}[C]$ refer to the Wilson loop of the fundamental representation of $U(N)$ and $\overline{U(N)}$ gauge groups, respectively.

The close contour C is a geometric datum of the Wilson loop operator. Hereafter, we shall exclusively deal with Lorentzian contour C_n connecting n vertices $x_1,x_2,\cdots,x_n$ whose adjacent points are lightlike-separated. The total set C_n with $n=4,5,6,\cdots$ form lightlike n-gons. Denote the distance vectors between a pair of vertices by

$$x_{i,j}\equiv[x_i-x_j] \qquad\qquad i,j=1,\cdots,n. \tag{4.11}$$

Among them are the lightlike-separated edges $x_{i+1,i}$. Denote a point on i-th edge by z_i. In parametrized form, it is

$$z_i(\tau)=x_i+y_i\tau \qquad \text{where} \qquad y_i\equiv x_{i+1,i}, \qquad 0\leq\tau\leq 1. \tag{4.12}$$

We relegate notations for various Lorentz invariants of x_i's to Appendix A.

The lightlike n-gon Wilson loop operators for $SU(N)$ and $\overline{SU(N)}$ gauge groups take the form

$$W_{\Box}[C_n]=\frac{1}{N}\mathrm{Tr}\mathcal{P}\exp\left[i\oint_{C_n}d\tau A_m(x(\tau))\dot{x}^m(\tau)\right] \tag{4.13}$$

$$\overline{W}_{\Box}[C_n]=\frac{1}{N}\overline{\mathrm{Tr}}\mathcal{P}\exp\left[i\oint_{C_n}d\tau \overline{A}_m(x(\tau))\dot{x}^m(\tau)\right]. \tag{4.14}$$

Both are $1/6$-BPS operators preserving 4 supercharges. Under the generalized parity, the two Wilson operators are interchanged each other. On the other hand, the ABJM Wilson loop $\mathcal{W}^{\prime}_{\Box}[C]$ is $1/2$-BPS operator preserving 12 supercharges. By construction, it is invariant under the generalized parity. The n vertices of C_n break all supersymmetries. This implies that the expectation values of these Wilson loops receive quantum corrections. Analyzing these corrections in the regime of infinite number of color $N\to\infty$ and weak 't Hooft coupling $\lambda=(N/k)\ll 1$ is the main focus of this paper.

4.2.2 Previous Results

Our goal is to compute the vacuum expectation value of the lightlike polygon Wilson loop. In the planar limit, we evaluate it in perturbation theory of the 't Hooft coupling λ:

$$\left\langle \mathcal{W}_{\square}[C] \right\rangle = \sum_{\ell=0}^{\infty} \lambda^{\ell} \left\langle \mathcal{W}_{\square}[C] \right\rangle^{(\ell)} \tag{4.15}$$

and similarly for $\left\langle W_{\square}[C] \right\rangle$ and $\left\langle \overline{W}_{\square}[C] \right\rangle$. The Wilson loops $\left\langle W_{\square}[C] \right\rangle$ and $\left\langle \overline{W}_{\square}[C] \right\rangle$ are 1/6-BPS configurations and in general receive perturbative corrections to all orders in λ. On the other hand, the ABJM Wilson loop $\left\langle \mathcal{W}_{\square}[C] \right\rangle$ is 1/2-BPS configuration and receive perturbative corrections only at even order of λ. This is an elementary consequence of the fact that the ABJM Wilson loop is invariant under the generalized parity. Since the net effect of the generalized parity is to flip k to $-k$, equivalently, λ to $-\lambda$, it follows immediately that

$$\left\langle W_{\square}[C] \right\rangle^{\ell=\text{odd}} = -\left\langle \overline{W}_{\square}[C] \right\rangle^{\ell=\text{odd}} \tag{4.16}$$

Actually, the result is stronger at linear order in λ. At this order, kinematical considerations indicate that $\left\langle W_{\square}[C_n] \right\rangle^{(1)}$ and $\left\langle \overline{W}_{\square}[C_n] \right\rangle^{(1)}$ vanish separately. By the generalized parity transformation, it also follows that

$$\left\langle W_{\square}[C] \right\rangle^{\ell=\text{even}} = \left\langle \overline{W}_{N}[C] \right\rangle^{\ell=\text{even}}. \tag{4.17}$$

We conclude that

$$\left\langle \mathcal{W}_{\square}[C] \right\rangle = \sum_{\ell=0}^{\infty} \lambda^{2\ell} \left\langle W_{\square}[C] \right\rangle^{(2\ell)} = \sum_{\ell=0}^{\infty} \lambda^{2\ell} \left\langle \overline{W}_{\square}[C] \right\rangle^{(2\ell)}. \tag{4.18}$$

The leading-order correction arises at two-loop order $O(\lambda^2)$. The diagrams contributing to this order are categorized to three groups [42]: matter-dependent diagrams, gauge boson ladder diagrams, and gauge boson triple-vertex diagrams. The contribution of the matter diagrams is equivalent to one-loop contribution in the $\mathcal{N} = 4$ SYM theory. This is because, in the ABJM theory, the finite one-loop correction to the gauge boson propagator is precisely the same as the tree-level gauge boson propagator in the $\mathcal{N} = 4$ SYM theory [**?**]. This means that differences between the ABJM theory and the $\mathcal{N} = 4$ SYM originate from ladder diagrams and triple-vertex diagrams. Both diagrams originate from gauge boson interactions through the Chern-Simons parts. Computationally, these two contributions are the most complicated.

The general structure of the two-loop corrections to the light-like Wilson loop expecta-

tion value can be obtained by requiring the anomalous conformal Ward identities. For this consideration, we can split the contributions to two parts: the matter contribution and the Chern-Simons contribution.

As explained above, the matter contribution is structurally the same as the one-loop contribution to the lightlike Wilson loops in $\mathcal{N}=4$ SYM theory. Therefore, it is useful to recall how the anomalous conformal Ward identities determined the Wilson loop expectation value in the $(3+1)$-dimensional SYM theory. There, the dilatation generator $\mathbb{D}$ and the special conformal generator $\mathbb{K}$ were perturbatively modified by quantum corrections. The dilatation symmetry is broken by the UV regularization and its Ward identity gets anomalous. To $O(\lambda_{\rm SYM})$, the $(3+1)$-dimensional SYM theory exhibits

$$\mathbb{D}\langle W[C_n]\rangle\Big|_{\rm SYM} = -\lambda_{\rm SYM}\left[\sum \frac{(x^2_{i-1,i+1}\mu^2)^\varepsilon}{\varepsilon} + O(\varepsilon^0)\right]. \tag{4.19}$$

The $O(\varepsilon^0)$ term refers that this Ward identity is verified up to ε^0-order. Using the elementary relation

$$\mathbb{D}\Big((x^2_{i,j})^\varepsilon\Big) = 2\varepsilon(x^2_{i,j})^\varepsilon, \tag{4.20}$$

we can find particular solution to the dilatational Ward identity as

$$\langle W[C_n]\rangle\Big|_{\rm SYM} = \lambda_{\rm SYM}\left[-\frac{1}{2}\sum \frac{(x^2_{i-1,i+1}\mu^2)^\varepsilon}{\varepsilon^2} + O(\varepsilon^0)\right]. \tag{4.21}$$

Consideration of the special conformal generator $\mathbb{K}$ confirmes the result and further provides information for the $O(\varepsilon^0)$ part, so-called the BDS function, BDS_n. Homogeneous solution to the conformal Ward identities is referred as the remainder function Rem_n. It depends only on the conformal cross-ratios u of the n-sided polygon. Putting together and replacing $\lambda_{\rm SYM}$ by λ^2, we deduce that the matter contribution in the ABJM theory takes the form

$$\langle W_\square[C_n]\rangle^{(2)}\Big|_{\rm matter} = \left[-\frac{1}{2}\sum_{i=1}^{n}\frac{(-x^2_{i,i+2}\mu^2)^{2\varepsilon}}{(2\varepsilon)^2} + \mathrm{BDS}^{(2)}_n(x) + \mathrm{Rem}^{(2)}_{n,\rm SYM}(u) + O(\varepsilon)\right]. \tag{4.22}$$

The subscript in the remainder function refers to the fact that it was deduced from the one-loop counterpart in the $\mathcal{N}=4$ SYM theory.

The pure Chern-Simons contribution is subject to the UV divergence. To regulate the divergence while preserving the supersymmetry, we use the dimensional reduction scheme, $d=(3-2\varepsilon)$. The scheme also contributes anomalies to the conformal and special conformal

Ward identities. The resulting anomalous Ward identities are [42]

$$\begin{aligned}\mathbb{D}\langle W[C_n]\rangle\Big|_{\rm CS} &= -{\rm Log}(2)\Big(\sum_{i=1}^{n}1\Big)+O(\varepsilon)\\ \mathbb{K}^m\langle W[C_n]\rangle\Big|_{\rm CS} &= -2{\rm Log}(2)\Big(\sum_{i=1}^{n}x_i^m\Big)+O(\varepsilon)\end{aligned} \tag{4.23}$$

The full solution to these equations takes the form

$$\langle W_\square[C_n]\rangle^{(2)}\Big|_{\rm CS} = -\frac{{\rm Log}(2)}{2}\sum_{i=1}^{n}\frac{(-x_{i,i+2}^2\mu^2)^{2\varepsilon}}{2\varepsilon}+{\rm Rem}^{(2)}_{n,{\rm CS}}(u)+O(\varepsilon). \tag{4.24}$$

For the tetragon Wilson loop, $n=4$, the two-loop result was computed in [42]. The Chern-Simons contribution in (4.24) is absorbable to the matter-dependent part by redefining the UV regularization scale μ. Remarkably, the final result coincides with the one loop result in $\mathcal{N}=4$ SYM theory. Explicitly, the matter-dependent contribution and the ladder plus triple-vertex contribution take the form [68]

$$\langle W_\square[C_4]\rangle^{(2)}\Big|_{\rm matter} = -\frac{(-x_{13}^2 4\pi e^{\gamma_E}\mu^2)^{2\varepsilon}}{(2\varepsilon)^2}-\frac{(-x_{24}^2 4\pi e^{\gamma_E}\mu^2)^{2\varepsilon}}{(2\varepsilon)^2}+\frac{1}{2}{\rm Log}^2\Big(\frac{x_{13}^2}{x_{24}^2}\Big)+{\rm Rem}_4^{(2)}(u)\Big|_{\rm matter} \tag{4.25}$$

$$\langle W_\square[C_4]\rangle^{(2)}\Big|_{\rm CS} = -\frac{{\rm Log}(2)}{2}\sum_{i=1}^{4}\frac{(-x_{i,i+2}\pi e^{\gamma_E}\mu^2)^{2\varepsilon}}{2\varepsilon}+{\rm Rem}_4^{(2)}(u)\Big|_{\rm CS} \tag{4.26}$$

Hereafter, we denote ${\rm Rem}^{(2)}_{n,{\rm matter}}(u)$ for the IR finite part of $\langle W_\square[C_n]\rangle^{(2)}_{\rm matter}$ modulo the BDS finite part. Also, ${\rm Rem}^{(2)}_{n,{\rm CS}}(u)$ is the IR finite part of $\langle W_\square[C_n]\rangle^{(2)}_{\rm CS}$. For the tetragon Wilson loop, $n=4$, these numerical constants are given by

$$\begin{aligned}{\rm Rem}_4^{(2)}(u)\Big|_{\rm matter} &= \frac{\pi^2}{4}\\ {\rm Rem}_4^{(2)}(u)\Big|_{\rm CS} &= \frac{5\pi^2}{12}-2{\rm Log}^2(2).\end{aligned} \tag{4.27}$$

Finally, the two contributions, (4.25) and (4.26), can be combined to the following compact form for the ABJM theory

$$\langle W_\square[C_4]\rangle^{(2)}_{\rm ABJM} = -\frac{(-x_{13}^2\tilde{\mu}^2)^{2\varepsilon}}{(2\varepsilon)^2}-\frac{(-x_{24}^2\tilde{\mu}^2)^{2\varepsilon}}{(2\varepsilon)^2}+\frac{1}{2}{\rm Log}^2\left(\frac{x_{13}^2}{x_{24}^2}\right)+{\rm Rem}_4^{(2)}(u)+O(\varepsilon). \tag{4.28}$$

Here, $\tilde{\mu}$ is the uniformizing UV regulator scale related to μ by

$$\widetilde{\mu}^2 = 8\pi e^{\gamma_E}\mu^2. \tag{4.29}$$

The remainder function $\text{Rem}_4^{(2)}(u)$ is

$$\begin{aligned}\text{Rem}_4^{(2)}(u) &= \text{Rem}_4(u)\Big|_{\text{matter}} + \text{Rem}_4(u)\Big|_{\text{CS}} + 5\text{Log}^2(2) \\ &= +3\text{Log}^2(2) + \frac{2\pi^2}{3}.\end{aligned} \tag{4.30}$$

The last term in the first line is from the uniformization (4.29) of the regulator scale. The remainder function is independent of the conformal cross-ratios u's, much the same way as the one-loop result in the $\mathcal{N}=4$ SYM theory. Moreover, it displays the uniform transcendentality property.

4.3 Hexagon Wilson Loops at Two Loops

Our goal in this paper is to obtain the remainder function $\text{Rem}_n^{(2)}(u)$ in (4.24) for general $n \geq 6$. For later convenience, we decompose the second-order corrections to the Wilson loop expectation value as

$$\begin{aligned}\left\langle W_\square[C_n]\right\rangle^{(2)}_{\text{ABJM}} &= \left[\left\langle W_\square[C_n]\right\rangle^{(2)}_{\text{matter}} + \left\langle W_\square[C_n]\right\rangle^{(2)}_{\text{ladder}} + \left\langle W_\square[C_n]\right\rangle^{(2)}_{\text{vertex}}\right]_{\widetilde{\mu}} \\ &= \left[\left\langle W_\square[C_n]\right\rangle^{(1)}_{\mathcal{N}=4\text{ SYM}}\right]_{\text{BDS}} + \text{Rem}_n^{(2)}\end{aligned} \tag{4.31}$$

In the second line, we related the functional form of the ABJM Wilson loop expectation value to that of the $\mathcal{N}=4$ SYM Wilson loop expectation value. The BDS part is abelian, so it must be that both are the same. The remainder function is theory specific. In ABJM theory, Rem_n is related by

$$\text{Rem}_n^{(2)} := \text{Rem}_n^{(2)}\Big|_{\text{matter}} + \text{Rem}_n^{(2)}\Big|_{\text{CS}} + \frac{5}{4}n\text{Log}^2(2) \tag{4.32}$$

The last term constant originated from uniformizing the UV regulator scale as in (4.29). The contribution $\text{Rem}^{(2)}_{n,\text{CS}}$ is computationally most complicated.

Our first task is to compute $\text{Rem}_n^{(2)}(u)$ for $n=6$ analytically. For $n>6$, we will determine $\text{Rem}_n^{(2)}(u)$ using recursion relations that we will derive in later from soft-collinear factorization of the light-like Wilson loop and analytic result for $n=6$ as an input.

It turns out the anomalous conformal Ward identities demand that the Wilson loop ex-

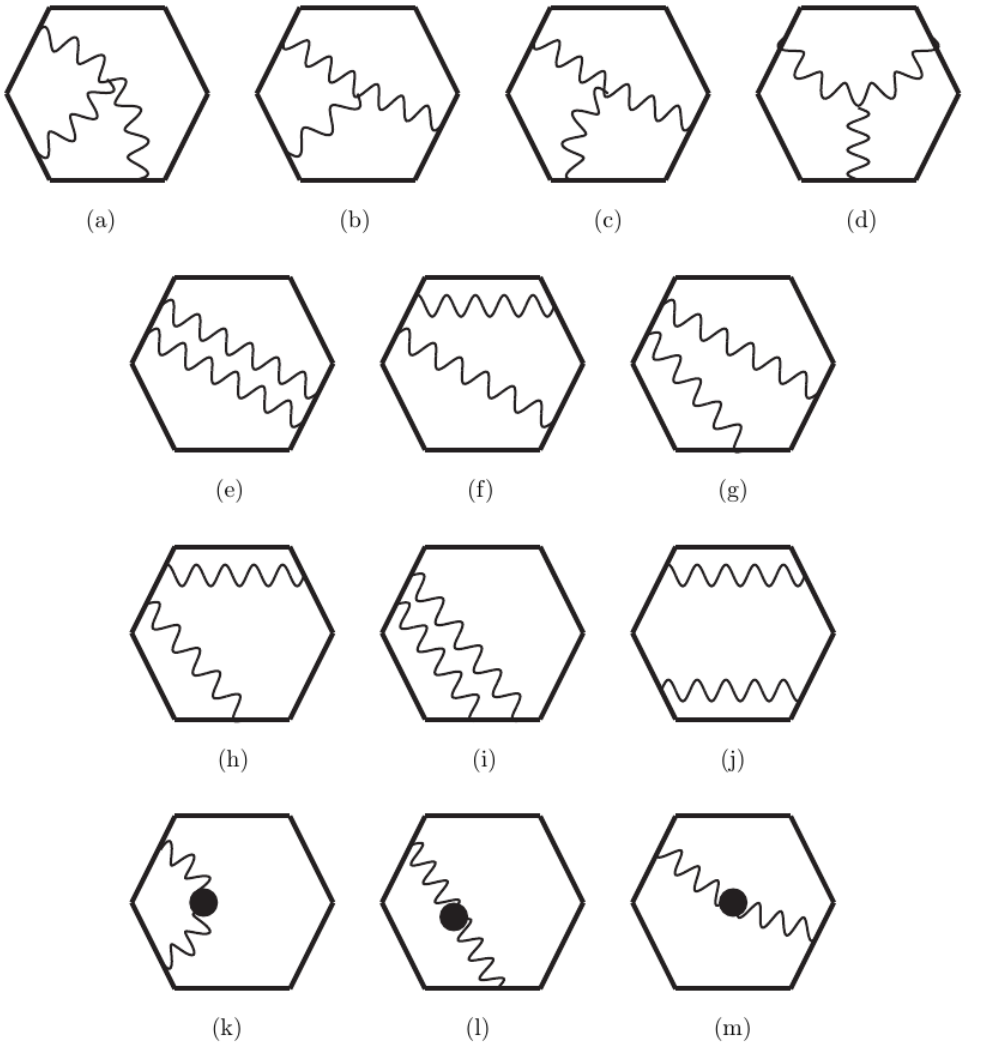

Figure 11: The Feynman diagrams contributing to the light-like hexagon Wilson loop at leading order are (a) $\sim$ (m) and cyclic permutations of the six edges. We classify them by (a) $\sim$ (d) as triple-vertex contributions, (e) $\sim$ (j) as ladder contributions, and (k) $\sim$ (m) as matter contributions.

pectation value must take the form Eq.(4.31). Here, we want to determine the remainder function Rem_n in Eq.(4.31). To this end, we evaluate all contributing Feynman diagrams to two loop orders. We shall regularize the UV divergences in the dimensional regularization $d = (3-2\varepsilon)$ and adopt the dimensional reduction scheme DRED that treats the Levi-Civita symbol ε_{mnp} as 3-dimensional tensor while all others as d-dimensional tensors.

In above Figure, we display the relevant diagrams. The complete list of the contributing diagrams include them and their cyclic permutations with respect to the hexagon edges. For foregoing discussions, we classify the diagrams in Figure 1 into three groups: triple-vertex diagrams for (a)-(d), ladder diagrams for (e)-(j), and matter-dependent diagrams (k)-(m). Computationally, we found that the triple-vertex diagrams the most complex. All of them involve the gauge field propagator $(\Delta_{mn})(x,y)$. We take the Landau gauge. In this gauge, the tree-level gauge field propagator is parity-odd and is given in position space by

$$(\Delta_{mn})^{(0)}(x,y) = \frac{\lambda}{N}\,\mathbb{I}\otimes\mathbb{I}\,Z_{\mathrm{o}}\frac{\varepsilon_{mnp}(x-y)^p}{[(x-y)^2]^{\frac{d}{2}}} \qquad \text{where} \qquad Z_{\mathrm{o}} = \pi^{(2-d)/2}\Gamma(d/2). \tag{4.33}$$

4.3.1 Matter Contribution

For the diagrams (k)-(m) in Figure, it suffices to first consider the self-energy of the gauge fields. At one-loop, the gauge field propagators receive corrections from vacuum polarization of matter fields. The one-loop corrected self energy is equal to the tree-level gauge field propagator in $\mathcal{N}=4$ SYM [40, 41] In position space, the one-loop corrected gauge field propagator $\Delta^{(1)}_{mn}(x,y)$ is parity-even and takes the form

$$\Delta^{(1)}_{mn}(x,y) = -\frac{\lambda^2}{N}\,\mathbb{I}\otimes\mathbb{I}\,Z_{\mathrm{e}}\frac{g_{mn}}{((x-y)^2)^{d-2}} \quad \text{where} \quad Z_{\mathrm{e}} = \pi^{2-d}\Gamma^2\Big(d/2-1\Big) \tag{4.34}$$

The matter contribution is computable parallel to the leading-order in the $\mathcal{N}=4$ SYM theory, except replacing the propagator with $\Delta^{(1)}_{mn}(x,y)$ in (4.34):

$$\begin{aligned}\big\langle W_\square[C_n]\big\rangle^{(2)}_{\text{matter}} &= \frac{1}{\lambda^2}\frac{1}{N}\mathrm{Tr}\mathcal{P}\oint dx_i^m\oint dx_j^n\big(i^2\Delta^{(1)}_{mn}(z_i,z_j)\big)\\ &= \Big((4\pi e^{\gamma_E})^{2\varepsilon}+\frac{\pi^2}{2}\varepsilon^2+O(\varepsilon^3)\Big)\sum_{i>j=1}^{n} I_{ij}\end{aligned} \tag{4.35}$$

Here, I_{ij} is the integral of one gauge boson exchange between edges i,j along the contour C_n:

$$I_{ij}(x) = \int_0^1 d\tau_i\int_0^1 d\tau_j\frac{y_i\cdot y_j}{[(z_i-z_j)^2]^{d-2}} \qquad (i,j=1,2,\cdots,n) \tag{4.36}$$

It is straightforward to evaluate these integrals (4.36), as was done in [52]. Singular loci of the denominator are where the UV divergences arise and they occur precisely at the cusps, viz. when the gauge propagator connects two points on adjacent edges and approach toward the cusp in between.

For the adjacent diagrams, the integration is straightforward. The leading UV divergence is readily obtained as

$$I_{i+1,i}(x) = \int d\tau_i \int d\tau_{i+1} \, \frac{y_i \cdot y_{i+1}}{[(z_{i+1} - z_i)^2]^{d-2}} = -\frac{1}{2} \frac{(x_{i,i+2}^2)^{2\varepsilon}}{(2\varepsilon)^2}. \tag{4.37}$$

Non-adjacent diagrams are UV finite. Summing them over all possible distinct permutations, we obtain the so-called the BDS function $\mathrm{BDS}_n^{(2)}$:

$$\mathrm{BDS}_n^{(2)}(x) \equiv \sum_{i>j+1}^{n} I_{ij}(x) \tag{4.38}$$

These integrals can be evaluated analytically, as was done in [52]:

$$I_{ij}(x) = \frac{1}{2} \left[-\mathrm{Li}_2(1-as) - \mathrm{Li}_2(1-at) + \mathrm{Li}_2(1-aP^2) + \mathrm{Li}_2(1-aQ^2) \right]_{ij}. \tag{4.39}$$

Here, the parameter a is given by [52]

$$a = \frac{s+t-P^2-Q^2}{st-P^2Q^2}, \quad \text{where} \quad P^2 = x_{i,j+1}^2, \quad Q^2 = x_{i+1,j}^2, \quad s = x_{i,j}^2, \quad t = x_{i+1,j+1}^2. \tag{4.40}$$

Combining this with Eq.(4.35), it follows that the matter contribution to the Wilson loop expectation value is given by

$$\left\langle W_\square[C_n] \right\rangle_{\text{matter}}^{(2)} = -\frac{1}{2} \sum_{i=1}^{n} \frac{(x_{i,i+2}^2 4\pi e^{\gamma_E} \mu^2)^{2\varepsilon}}{(2\varepsilon)^2} + \mathrm{BDS}_n^{(2)}(x) + \mathrm{Rem}_n^{(2)}(u)\Big|_{\text{matter}} + O(\varepsilon). \tag{4.41}$$

Here, the matter contribution to the remainder function is given by

$$\boxed{\mathrm{Rem}_n^{(2)}(u)\Big|_{\text{matter}} = -\frac{1}{16} n\pi^2.} \tag{4.42}$$

For the special case of $n = 4$, this result reproduces (4.25) and the remainder function (4.27).

4.3.2 Gauge Boson Ladder diagram

The pure Chern-Simons term generates ladder diagrams and triple-vetex diagrams. The ladder diagram contributes to the Wilson loop expectation value as

$$\left\langle W_{\square}[C_n]\right\rangle^{(2)}_{\text{ladder}} = \left(\frac{\Gamma\left(\frac{d}{2}\right)}{\pi^{\frac{d-2}{2}}}\right)^2 \sum_{\mathcal{P}(i,j,k,l)} I_{\text{ladder}}(x) \tag{4.43}$$

Here, $\mathcal{P}(i,j,k,l)$ refers to sum over path-ordered, pairwise connections among the four segments (i,j,k,l) and the I_{ladder} integral is given by

$$I^{\{i,j,k,l\}}_{\text{ladder}} = \int d\tau_i \cdots \int d\tau_l \frac{\varepsilon(y_i, y_l, z_i - z_l)}{[(z_i - z_l)^2]^{\frac{d}{2}}} \frac{\varepsilon(y_j, y_k, z_j - z_k)}{[(z_j - z_k)^2]^{\frac{d}{2}}}, \tag{4.44}$$

where the superscript $\{i,j,k,l\}$ labels the edges that the gauge field is attached. For instance, for the hexagon, the six configurations

$$\{i,j,k,l\} = \{4,4,1,1\}, \{5,4,1,1\}, \{4,3,1,1\}, \{5,3,1,1\}, \{3,3,1,1\}, \{5,4,2,1\} \tag{4.45}$$

and their cyclic permutations should be summed over . Importantly, these ladder diagrams are all UV finite.

4.3.3 Triple-Vertex Diagram

The triple-vertex diagrams are reduced to tensor integrals involving the Levi-Civita tensor ε_{mnp}. We deal with such tensor integrals by reducing them to scalar integrals via the relations

$$I^{mnp}(x,y,z) = \frac{\partial}{\partial y^n}\frac{\partial}{\partial z^p} I^m(y-x, z-x), \tag{4.46}$$

where $I^m(y-x,z-x)$ is given by

$$I^m(a,b) = \int d^d w \frac{w^m}{|w|^d |w-(y-x)|^d |w-(z-x)|^d} \ . \tag{4.47}$$

Contracting the Levi-Civitat tensors with the segment vectors of the polygon, one obtains integrals in readily evaluatable forms.

Triple-vertex diagram contributes to the Wilson loop expectation value as

$$\left\langle W_{\square}[C_n]\right\rangle^{(2)}_{\text{vertex}} = \frac{i}{2\pi}\left(\frac{\Gamma\left(\frac{d}{2}\right)}{\pi^{\frac{d-2}{2}}}\right)^3 \sum_{\text{path-ordered}} I^{\{i,j,k\}}_{\text{vertex}} \tag{4.48}$$

Here again, the superscript $\{i,j,k\}$ labels the edges where the gauge field is attached. The path ordering restricts $i>j>k$ case only. In self-explaining notation, the integral takes the form

$$I_{\text{vertex}}^{\{i,j,k\}}(x)=\int_{\mathbb{R}^{2,1}}d^dw\left[\int\cdots\int d\tau_i d\tau_j d\tau_k\varepsilon^{abc}\frac{\varepsilon(y_i,a,w-z_i)\varepsilon(y_j,b,w-z_j)\varepsilon(y_k,b,w-z_k)}{[(w-z_i)^2]^{\frac{d}{2}}[(w-z_j)^2]^{\frac{d}{2}}[(w-z_k)^2]^{\frac{d}{2}}}\right]. \tag{4.49}$$

In the case of hexagon, the four configurations

$$\{i,j,k\}=\{3,2,1\},\{4,2,1\},\{4,3,1\},\{5,3,1\} \tag{4.50}$$

and their cyclic permutation generate all possible diagrams. Among them, divergence appears only through $\{3,2,1\}$-type configuration.

Note that the triple-vertex diagrams are UV-divergent. These divergences arise from configurations whose three attached points of the gauge bosons approach a single segment. The $\{3,2,1\}$ diagram is an example of such configuration. After the Mellin-Barnes transformation, the integral $I_{\text{vertex}}^{\{3,2,1\}}$ can be brought to a form that can be evaluated in part analytically and in part numerically with high precision.

The result reads

$$I_{\text{vertex}}^{\{3,2,1\}}(x)=\frac{i\pi^{\frac{d}{2}}\Gamma(d-1)}{8\Gamma(\frac{d}{2})^3}\Big(4\pi\text{Log}(2)\frac{(x_{13}^2\mu^2)^{2\varepsilon}}{\varepsilon}+4\pi\text{Log}(2)\frac{(x_{24}^2\mu^2)^{2\varepsilon}}{\varepsilon}+I_{\text{finite}}^{\{3,2,1\}}\Big). \tag{4.51}$$

Summing over all possible path-ordered triples (i,j,k), we find that

$$\sum_{\mathcal{P}(i,j,k)}I_{\text{vertex}}^{\{i,j,k\}}(x)=\frac{i\pi^{\frac{d}{2}}\Gamma(d-1)}{8\Gamma(\frac{d}{2})^3}\left(8\pi\text{Log}(2)\sum_{i=1}^{n}\frac{(x_{i,i+2}^2\mu^2)^{2\varepsilon}}{2\varepsilon}+I_{\text{finite}}\right), \tag{4.52}$$

The leading UV-divergence is $\frac{1}{\varepsilon}$, in contrast to $\frac{1}{\varepsilon^2}$ leading UV-divergence in matter contribution.

4.3.4 Wilson Loop of the Pure Chern-Simons Theory

In pure Chern-Simons theory, the contribution $\langle W_\square[C_n]\rangle_{\text{CS}}^{(2)}$ is obtained by combining $\langle W_\square[C_n]\rangle_{\text{ladder}}^{(2)}$ and $\langle W_\square[C_n]\rangle_{\text{vertex}}^{(2)}$. To evaluate these expectation values, we carry out tensor integral $\sum_{i>j>k>l}I_{i,j,k,l}^{\text{ladder}}$ and $\sum_{i>j>k}I_{i,j,k}^{\text{vertex}}$.

The result is

$$\begin{aligned}\langle W_\square[C_n]\rangle^{(2)}_{\rm CS} &= \langle W_\square[C_n]\rangle^{(2)}_{\rm ladder} + \langle W_\square[C_n]\rangle^{(2)}_{\rm vertex} \\ &= \Big(\frac{\Gamma\big(\frac{d}{2}\big)}{\pi^{\frac{d-2}{2}}}\Big)^2 \sum_{i>j=1}^{n} I^{i,j}_{\rm ladder} + \frac{i}{2\pi}\Big(\frac{\Gamma\big(\frac{d}{2}\big)}{\pi^{\frac{d-2}{2}}}\Big)^3 \sum_{i>j>k=1}^{n} I^{i,j,k}_{\rm vertex} \end{aligned} \tag{4.53}$$

Inserting (4.52), we finally obtain

$$\begin{aligned}\langle W_\square[C_n]\rangle^{(2)}_{\rm CS} &= -\Big(\frac{\Gamma(d-1)}{2}\frac{\pi^{2-d}}{8}\Big)\Big(4\pi{\rm Log}(2)\sum_{i=1}^{n}\frac{(x^2_{i,i+2}\mu^2)^{2\varepsilon}}{\varepsilon} + I^{\rm finite}_{\rm vertex}\Big) + \Big(\frac{\Gamma\big(\frac{d}{2}\big)}{\pi^{\frac{d-2}{2}}}\Big)^2 \sum_{i>j>k>l} I^{i,j,k,l}_{\rm ladder} \\ &= -\Big(\frac{\Gamma(d-1)}{2}\frac{\pi^{2-d}}{8}\Big)\Big(4\pi\log(2)\sum_{i=1}^{n}\frac{(x^2_{i,i+2}\mu^2)^{2\varepsilon}}{\varepsilon}\Big) + I_{\rm CS} + O(\varepsilon) \\ &= -\frac{{\rm Log}(2)}{2}\sum_{i=1}^{n}\frac{(x^2_{i,i+2}\pi e^{\gamma_E}\mu^2)^{2\varepsilon}}{2\varepsilon} + {\rm Rem}^{(2)}_{n,{\rm CS}}(u) + O(\varepsilon) \end{aligned} \tag{4.54}$$

In second line, we used the fact that $I^{\rm finite}_{\rm vertex}$ and $\sum_{i>j>k>l} I^{i,j,k,l}_{\rm ladder}$ are finite quantity. For convenience, we defined here

$$I_{\rm CS} = -\frac{1}{16\pi} I^{\rm finite}_{\rm vertex} + \frac{1}{4}\sum_{i>j>k>l} I^{i,j,k,l}_{\rm ladder}. \tag{4.55}$$

Explicit expansion of the last line in (4.54) yields relation between $I_{\rm CS}$ and ${\rm Rem}_{n,{\rm CS}}(u)$:

$${\rm Rem}^{(2)}_{n,{\rm CS}}(u) = I_{\rm CS} + \frac{n}{2}{\rm Log}(2). \tag{4.56}$$

We will evaluate $I_{\rm CS}$ numerically. Before proceeding, we will need to digress to general consideration of free kinematic variables in light-like polygon, viz. the moduli space of light-like polygon.

4.4 Euclid, Mandelstam and Gram

The first step in evaluating the remainder function is to specify the geometry of lightlike polygon. We shall call it the kinematics. In this section, we present general considerations of the moduli space of a lightlike n-gon C_n.

4.4.1 Moduli Space of Lightlike Polygon

The contour C_n is specified by the set of points $x_1, \cdots, x_n$. They are lightlike separated with adjacent neighbors, and can always be brought to

$$x_1 + \cdots + x_n = 0. \tag{4.57}$$

by translation invariance. Equivalently, C_n can be specified by the segment vectors $y_1, \cdots, y_n$. They are all light-like ($y_i^2 = 0$), and trivially satisfy the closedness condition

$$y_1 + \cdots + y_n = 0. \tag{4.58}$$

The two are discrete, polygon counterpart of the statement that a smooth curve can be described either by specifying position vectors of the curve or by specifying tangent vectors of the curve. Either way, one finds that the moduli space $\mathcal{M}[C_n]$ of n-sided polygon C_n in d-dimensional embedding space is given by

$$\dim \mathcal{M}[C_n] = (dn - n) - d - \frac{1}{2}d(d-1). \tag{4.59}$$

The dimension of the moduli space (4.59) grows linearly with n, the number of x's or y's. For instance, consider the $n = 6$ hexagon. We can specify 6 position vectors, $x_1, \cdots, x_6$ subject to (4.57). Out of $6 \times 3 = 18$ components, light-like conditions $x_{i,i+1}^2 = 0$ eliminates 6, (4.57) eliminates 3 and $so(2,1)$ Lorentz transformation eliminates 3. The remaining 6 independent variables are the moduli of C_6. Alternatively, we can also specify 6 segment vectors $y_1, \cdots, y_6$ subject to (4.58). Out of $6 \times 3 = 18$ components, light-like conditions $y_i^2 = 0$ eliminate 6, (4.58) eliminates 3 and $so(2,1)$ Lorentz transformation eliminates 3. The remaining 6 independent variables are the moduli of C_6.

On the other hand, by the Poincaré invariance, the lightlike Wilson loops are not functions of x_i's or y_i's themselves, but are functions of the Mandelstam invariants x_{ij}^2, $i, j = 1, \cdots, n$. They vanish for $j = i, i \pm 1$, so the net number of nontrivial invariants is given by

$$\dim M(C_n) = \frac{1}{2}n(n-3). \tag{4.60}$$

Alternative choice of the Mandelstam invariants are y_{ij}^2. They range over $i, j = 1, \cdots, (n-1)$ because of the closedness condition (4.58). They also vanish for $j = i$. Altogether, the net number of nontrivial invariants is given again by (4.60). Their number grows quadratically with n, so would outgrow the dimension of n-gon moduli space (4.59). It must be that many of the Mandelstam invariants are redundant.

The projection of the space of Mandelstam invariants to the space of polygon moduli is achieved by the geometric condition that n vectors in d dimensional spacetime are necessarily linearly dependent for $n > d$. To this end, consider the Gram matrix G, whose (i, j) entry is given by $y_i \cdot y_j$:

$$G \equiv M^{\mathrm{T}} \cdot M = \begin{pmatrix} y_1 \cdot y_1 & y_1 \cdot y_2 & y_1 \cdot y_3 & \cdots & y_1 \cdot y_n \\ y_2 \cdot y_1 & y_2 \cdot y_2 & y_2 \cdot y_3 & \cdots & y_2 \cdot y_n \\ y_3 \cdot y_1 & y_3 \cdot y_2 & y_3 \cdot y_3 & \cdots & y_3 \cdot y_n \\ \vdots & \vdots & \vdots & \ddots & \vdots \\ y_n \cdot y_1 & y_n \cdot y_2 & y_n \cdot y_3 & \cdots & y_n \cdot y_n \end{pmatrix} \tag{4.61}$$

Here, M is $(d \times n)$ matrix whose entries are the segment vectors $M = (y_1^m, y_2^m, \cdots, y_n^m)$. Determinant of G, called Gram determinant, is nothing but the square of the hypercube volume spanned by the segment vectors:

$$\mathrm{Det}G(i, j) = ||y_1 \wedge y_2 \wedge y_3 \wedge \cdots \wedge y_n||^2. \tag{4.62}$$

Because of the closedness condition (4.58), the Gram determinant vanishes identically. Moreover, d-dimensional spacetime accommodates at most d many linearly independent vectors. Hence, in Gram matrix, determinant of any $(d+1) \times (d+1)$ sub-matrices ought to vanish identically. There are $(n-d-1)(n-d)/2$ many such choices, so these Gram subdeterminant conditions project the space of Mandelstam variables down to the space of independent scalar invariants of dimension

$$\dim \Pi_G M(C_n) = \frac{1}{2} n(n-3) - \frac{1}{2}(n-d-1)(n-d) = (d-1)n - \frac{1}{2} d(d+1). \tag{4.63}$$

This matches precisely with the dimension of the moduli space of n-sided lightlike polygon (4.59).

4.4.2 Euclidean Configuration

In evaluating the lightlike polygon Wilson loop operator expectation value , the input data of C_n are the vectors x_i's or y_i's of the polygon. On the other hand, the expectation value is

Poincaré invariant, so it must depend on these vectors only through scalar products:

$$y_i \cdot y_j = \frac{1}{2}\left[x_{i,j+1}^2 + x_{i+1,j}^2 - x_{i,j}^2 - x_{i+1,j+1}^2\right]. \tag{4.64}$$

This suggests it natural to take the Mandelstam variables as input parameters. This is what we shall do for numerical computations. On the other hand, as we saw above, the Mandelstam variables are not mutually independent and need to be further supplemented by the Gram sub-determinant conditions.

A complication is that, typically, the Gram sub-determinant conditions are too involved to solve explicitly. In evaluating the Feynman loop integrals, we shall employ the Mellin-Barnes transformations. During the evaluation, we shall provisionally assume that the Mandelstam variables are linearly independent until we perform the Mellin-Barnes transformations. We then evaluate the transformed expressions numerically, and at this stage we shall impose the Gram sub-determnant conditions by taking special kinematics of C_n such that it becomes consistent with these conditions.

We found numerically that $\mathrm{Rem}(u)$ yields physically meaningful values when Mandelstam variables are restricted by the Gram sub-determinant conditions and that, in solving the anomalous conformal Ward identity, the remainder function $\mathrm{Rem}(u)$ is expressed in terms of cross ratios only after the Gram sub-determinant conditions are imposed to the Mandelstam variables.

Often, the Mellin-Barnes transformed integrals involve spurious poles. To avoid them, it is necessary to impose all the Mandelstam variables to have the same sign. We shall call this condition as "Euclidean condition". It turns out that, for the segment vectors y_i's, the condition is satisfied by making timelike components of adjacent edge vectors to have opposite signs. As the segment vectors y's are subject to the closedness condition, this condition then implies that only even numbers of edges $n = 2\mathbb{N}$ are permissible. This purely kinematical consideration imposes that the polygons relevant for the lightlike ABJM Wilson loops [2] must be restricted to those with even numbers of the edge. Though lacking a general argument, we think that this is a general kinematic condition.

To illustrate this, consider the case of hexagon. A choice of the edge vectors $y_1, \cdots, y_6$ satisfying the Euclidean condition and the closedness condition $y_1 + \cdots + y_6 = 0$ are

$$\begin{array}{lll} y_1 = (-\sqrt{a^2+b^2}, a, b) & y_2 = (+\sqrt{c^2+d^2}, c, d) & y_3 = (-\sqrt{e^2+f^2}, e, f) \\ y_4 = (+\sqrt{g^2+h^2}, g, h) & y_5 = (-\sqrt{p^2+q^2}, p, q) & y_6 = (+\sqrt{r^2+s^2}, r, s) \end{array} \tag{4.65}$$

First, we set the time-component of the edge vectors of alternating sign so that every Mandel-

[2] This restriction applies to any conformal field theories in three dimensions.

stam variables are positive. Take for example the hexagon. Among 9 Mandelstam variables, 6 variables are inner product of consecutive segment vector, viz. $2y_i \cdot y_{i+1}$. Then,

$$x_{1,3}^2 = 2y_1 \cdot y_2 = \pm 2\sqrt{a^2+b^2}\sqrt{c^2+d^2} \pm 2ac \pm 2bd. \tag{4.66}$$

By triangle inequality, sign of this Mandelstam variable is determined by the first term. To make it positive, we see that the edge vectors must be chosen to have consecutively alternating signs of their time components.

Moreover, the Euclidean condition requires other 3 Mandelstam variables($x_{14}^2, x_{25}^2, x_{36}^2$) should be also positive. This further constraints number of independent variables appearing in (4.65). Nevertheless there are 9 possible combination of Mandelstam variables, arbitrarily choice of them may cause inconsistency with Euclidean and closedness condition. Follwing from counting (4.63), number of independent Mandelstam variables are given by 6, not 9.

Such kinematical restrictions bear the following geometric implications to the 'triple-collinear factorization' we will study in the next section. Recall that, by construction, a lightlike polygon is made of oriented edges which are all lightlike. When we take a polygon and let two non-adjacent vertices $x_i, x_j (j \neq i \pm 1)$ become lightlike, we see we can decompose the lightlike contour of the parent polygon as a sum of two lightlike contours of daughter polygons. The absence of polygons with odd numbers of the edge also puts the constraint that the factorization must involve even number of consecutive vertices. This condition is also compatible with the requirement that the time component of edge vectors must be sign alternating. We see that such factorization gives rise to a nonlinear recursion relations among the lightlike Wilson loops.

4.4.3 Moduli Space of Conformal Lightlike Polygon

Up until now, in counting the moduli space of lightlike polygons, we only took into account the Poincaré symmetry of embedding spacetime. We now further endow the polygons with conformal symmetry. Replacing the Poincaré symmetry $so(d-1,1)$ by the conformal symmetry $so(d,2)$, we see that the dimension of moduli space of conformal lightlike polygons is modified to

$$\dim \mathcal{M}_c[C_n] = (d-1)n - \frac{1}{2}(d+1)(d+2). \tag{4.67}$$

On the other hand, we elaborated in the previous section that the geometry of lightlike polygons is more conveniently described in terms of Mandelstam variables but these variables are not mutually independent. The requisite projection of the Mandelstam variables is the Gram condition. Below, we explain how this can be achieved.

The dimension of parameter space of conformally invariant Mandelstam variables, viz. the conformal cross-ratios

$$u_{i,j} = \frac{x^2_{i,j+1}x^2_{i+1,j}}{x^2_{i,j}x^2_{i+1,j+1}}, \tag{4.68}$$

is given by

$$\dim M_c[C_n] = \frac{1}{2}n(n-1) - n - n = \frac{1}{2}n(n-5), \tag{4.69}$$

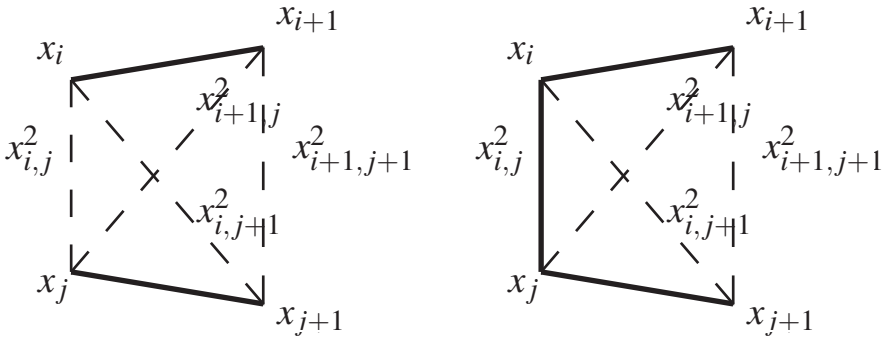

The counting is simple. To construct a cross-ratio, we need two distinct edges. There are $n(n-1)/2$ possible pairs of edges. However, the resulting cross-ratio vanishes if the two edges chosen are nearest neighbors or next-nearest neighbors.

We are again in a situation that, in a given spacetime dimension, the dimension of the moduli space of conformal cross-ratios (4.69) outgrows dimension of moduli space of conformal lightlike polygon (4.67) we want to describe. The requisite projection to the conformal cross-ratios is achieved by the Gram condition modulo conformal equivalence relations.

Let's be more explicit. A conformal covariant vector x^m in $\mathbb{R}^{d-1,1}$ can be equivalently described by projection of a vector $X^A = (X_1, X_0, X_1, \cdots, X_d)$ in embedding Minkowski space $\mathbb{R}^{d,2}$ onto the lightlike hyperboloid:

$$\eta_{AB}X^AX^B = -(X_{-1})^2 - (X_0)^2 + (X_1)^2 + \cdots + (X_d)^2 = \eta_{mn}X^mX^n - 2X^+X^- = 0. \tag{4.70}$$

Choosing the lightcone coordinates $X^\pm = (X_{-1} \pm X_d)/\sqrt{2}$ are the lightcone coordinates, the vector x^m is projectively obtained by

$$x^m = \frac{X^m}{X^+}. \tag{4.71}$$

The action of the conformal group $SO(d,2)$ to the vector x^m is equivalent to the action of linear transformations acting on X^A lying on the lightlike hyperboloid (4.70). It is known that the space of x-vectors is $\mathbb{R}^{d-1,1}$ provided the $SO(d,2)$ is gauge-fixed to $X^+ = 1$. In this gauge,

$$X_{ij}^2 = -2X_i \cdot X_j = x_{ij}^2. \tag{4.72}$$

From this, it also follows that

$$Y_i := (X_{i+1} = X_i) = (y_i, 0, Y_i^-) \qquad (i = 1, \cdots, n) \tag{4.73}$$

are lightlike in $\mathbb{R}^{d,2}$. We thus associated the conformal edge vectors y_i's of a conformal lightlike polygon in the physical spacetime $\mathbb{R}^{d-1,1}$ with the edge vectors Y_i's of a lightlike polygon in the embedding space $\mathbb{R}^{d,2}$. This then implies that the space of conformal cross-ratios in $\mathbb{R}^{d-1,1}$ is the same as the space of Mandelstam variables in $\mathbb{R}^{d,2}$. Therefore, the dimension of the moduli space of conformal cross-ratios is given by

$$\dim M_c(C_n) = \frac{1}{2}n(n-1) - n - n = \frac{1}{2}n(n-5). \tag{4.74}$$

We subtracted n for choosing adjacent edge pairs, and n for choosing next-adjacent edge pairs.

How do we match this moduli space to the moduli space of conformal lightlike polygons? The idea is that the Gram sub-determinants of the vectors project the cross-ratios down to the space of independent ones. The Gram determinant in the embedding space is now given by

$$G_c = M_c^T \cdot M_c = \begin{pmatrix} Y_1 \cdot Y_1 & Y_1 \cdot Y_2 & \cdots & Y_1 \cdot Y_n \\ Y_2 \cdot Y_1 & Y_2 \cdot Y_2 & \cdots & Y_2 \cdot Y_n \\ \vdots & \vdots & \ddots & \vdots \\ Y_n \cdot Y_1 & Y_n \cdot Y_2 & \cdots & Y_n \cdot Y_n \end{pmatrix} \tag{4.75}$$

Because of the closedness condition, the Gram determinant itself vanishes identically. Since the embedding space $\mathbb{R}^{d,2}$ accommodates at most $(d+2)$ many linearly independent vectors, Therefore, there are $(n-(d+1))(n-(d+1)-1)/2$ many Gram sub-determinant conditions.

Therefore, the dimension of conformal cross-ratios is

$$\dim\Pi_G M_c[C_n] = \frac{1}{2}n(n-5) - \frac{1}{2}(n-d-1)(n-d-2) = (d-1)n - \frac{1}{2}(d+1)(d+2). \tag{4.76}$$

This matches precisely the dimension of moduli space of conformal lightlike polygons (4.67).

4.5 The Hexagon Remainder Function

In this section, we compute the remainder function $\mathrm{Rem}^{(2)}_{6,\mathrm{CS}}$, relevant for the hexagon ABJM Wilson loop expectation value. We explained that this computation involves multi-dimensional scalar integrals. In this section, we compute them.

We expect from the anomalous conformal Ward identity that the remainder function $\mathrm{Rem}_{n,\mathrm{CS}}$ depends only on the conformal cross-ratios. In setting up the computation, we can readily verify this property of the remainder function by varying shapes, equivalently, Mandelstam variables of the lightlike polygon. Not all the Mandelstam variables are independent and, as we explained in section 4, it is necessary to impose the Gram sub-determinant conditions. This condition turns out a stark difference from what were known for extracting the remainder function in the four-dimensional $\mathcal{N}=4$ SYM. In section 5.5.1, we recall this situation in detail.

For the computation of multi-dimensional integrals, we utilize public packages. The scalar integrals we need to compute span up to 8-dimensional complex integrations. The traditional `MB` package [53] turns out not powerful enough to render the result with requisite numerical precisions. Instead, we utilize the package `FIESTA2`, [54]. In the following subsections, we present details of the computation. In section 5.5.2, we present numerical computations performed using the `FIESTA2` package. In section 5.5.3, for the special shapes of the hexagon discussed in the previous section, we reduce our multi-dimensional integrals to lower-dimensional integrals. The reduction facilitates to achieve high precision to the numerical computations. In section 5.5.4, we utilize the PSLQ algorithm and infer analytic expressions of the $\mathrm{Rem}_{6,\mathrm{CS}}$ from the numerical results.

4.5.1 Remainder Function in $\mathcal{N}=4$ Super Yang-Mills Theory

We explained that the Mandelstam variables are the Lorentz scalars convenient for specifying the geometry of lightlike polygon, they need to be further projected down to the space of conformal cross-ratios since they are not mutually independent. We alluded that such projection is achieved by the Gram sub-determinant conditions. Therefore, in the numerical

computation in this section of the hexagon remainder function, we shall cover the moduli space of the lightlike hexagon by varying the Mandelstam invariants over the subspace that the Gram sub-determinant conditions are satisfied.

While our prescription is the most natural steps to take, this was not what was practiced when the hexagon remainder function was computed in the (3+1)-dimensional $\mathcal{N}=4$ SYM theory. There, the anomalous conformal Ward identities also put the remainder function to be a function of conformal cross-ratios. The lightlike Wilson loops were again specified by Mandelstam invariants. Remarkably, it was observed that two sets of Mandelstam invariants, one obeying the Gram sub-determinant conditions and another not, yielded an identical result for the remainder function. In so far as the cross-ratios are the same, any choice of the Mandelstam variable set is allowed regardless of solving the Gram sub-determinant conditions. Indeed, this explains why lightlike Wilson loops with odd numbers of edges are admissible configurations in the $\mathcal{N}=4$ SYM theory.

As the Mandelstam variables can be chosen freely thus they can be taken 'unphysical' values outside the moduli space of the hexagon, wide variety of kinematic limits become available in so far as evaluation of the remainder function is concerned. In the $(3+1)$-dimensional $\mathcal{N}=4$ SYM theory, this freedom was maximally taken into advantage. A particularly useful limit was the quasi multi-Regge kinematics (QMRK), since this kinematics enabled determination of the hexagon remainder function and understanding its analytic structure. For $(2+1)$-dimensional ABJM theory, we concluded in section 4 that such kinematic limits are not available and we should impose the Gram sub-determinant conditions throughout.

The Gram sub-determinant conditions essential for the ABJM theory bears further impact. In the the $(3+1)$-dimensional $\mathcal{N}=4$ SYM theory, another useful kinematic limit was to take the lightlike polygon to $(1+1)$-dimensional subspace. This limit brought in enormous simplification and facilitated computation of the remainder function analytically tractable. Unfortunately, for kinematical reasons again, this limit is also not available for $(2+1)$-dimensional ABJM theory. This is because the $(1+1)$-dimensional kinematics cruially relies on the Euclidean condition and the closedness of edge vectors. Take for instance the lightlike hexagon and restrict it to the $(1+1)$-dimensional lightlike basis, $(1,-1)$ and $(1,1)$. The 6 edge vectors obeying the Euclidean condition are parametrized as

$$y_1=(a,-a),\quad y_2=(b,b),\quad y_3=(c,-c),\quad y_4=(d,d),\quad y_5=(e,-e),\quad y_6=(f,f), \tag{4.77}$$

where a,b,c,d,e,f are restricted to be positive. To obey the closedness, both $a+b+c+d+e+f=0$ and $a-b+c-d+e-f=0$ should be satisfied. We see that these conditions cannot be met, since the positivity of a,b,c,d,e,f violates first equation. Therefore,

$(1+1)$-dimensional lightlike condition, Euclidean condition and closedness are not mutually compatible.

4.5.2 Scalar Invariants and Gram Sub-Determinant Conditions

Here, we first study how the hexagon remainder function depends on the Mandelstam variables and the Gram sub-determinant conditions. We shall find that the dependence in the $(2+1)$-dimensional ABJM theory is very different from the dependence in the $(3+1)$-dimensional $\mathcal{N}=4$ SYM theory.

We computed numerically both the triple-vertex diagrams and the ladder diagrams listed in Figure 2. Adding them, we obtained the hexagon remainder function at two loops, $\mathrm{Rem}^{(2)}_{6,\mathrm{CS}}$ as a function of 9 Mandelstam variables of the hexagon.

	x^2_{13}	x^2_{24}	x^2_{35}	x^2_{46}	x^2_{15}	x^2_{26}	x^2_{14}	x^2_{25}	x^2_{36}	$\mathrm{Rem}^{(2)}_{6,\mathrm{CS}}$
A	−1.0000	−1.0000	−1.0000	−1.0000	−1.0000	−1.0000	−1.0000	−1.0000	−1.0000	−3.47537352
B	−6.8764	−18.194	−21.887	−77.498	−48.781	−14.780	−24.467	−30.720	−3.3327	−3.47342610
C	−4.8757	−11.282	−6.1981	−42.828	−19.339	−8.1903	−15.616	−10.007	−2.5719	−3.47622947
D	−3.5979	−7.3282	−1.4275	−24.543	−7.9792	−4.5361	−10.424	−2.6875	−1.9989	−3.47688979
E	−116.29	−4.0000	−116.29	−2.0350	−4.0000	−2.0350	−4.0000	−4.0000	−59.160	−3.48197748
F	−4.0000	−2.3528	−9.0000	−1.0000	−1.3057	−1.0000	−1.0000	−2.2500	−3.6892	−3.47579959
G	−4.0000	−1.0000	−8.8965	−4.4482	−1.0000	−2.0000	−1.0000	−1.0000	−5.5504	−3.47576202
H	−1.2027	−2.5332	−2.0000	−3.0000	−6.2344	−13.512	−2.1782	−3.6253	−0.82827	−3.47561202

Table 4: *Results of $R_{CS,6}$ for eight configurations of hexagon's Mandelstam variables. It suggests that $R^{(2)}_{6,\mathrm{CS}}$ takes a constant value over wide ranges of the conformal cross-ratios.*

In Table 1, we generated eight configurations (A)∼(H) of the 9 Mandelstam variables $x^2_{13},\cdots,x^2_{36}$, subject to the Gram sub-determinant conditions. Equivalently, these configurations are generated by lightlike segment vectors $y_1,\cdots,y_6$ subject to the $SO(3,2)$ conformal invariance. The results indicates that the hexagon remainder function $\mathrm{Rem}^{(2)}_{6,\mathrm{CS}}$ is a constant number, independent of the Mandelstam variables and hence the conformal cross-ratios.

To test neessity of the Gram sub-determinant conditions, we chose a configuration, say (D), and permuted subset of the 9 Mandelstam variables while keeping their conformal cross-ratios fixed. Obviously, permuting the Mandelstam variables so violates the Gram sub-determinant conditions. We computed the hexagon remainder function $\mathrm{Rem}^{(2)}_{6,\mathrm{CS}}$ and the results are tabulated in Table 2.

In Table 2, we generated configurations (D1) and (D2) that have the same conformal ratios as (D) but violates the Gram sub-determinant condition [3]. We observe that the remainder function at (D),(D1),(D2) do not agree one another even though all three sets have one

[3]This is equivalent to saying that there is no suitable choice of x_i's or y_i's vectors which generate (D1) and (D2) configurations.

	x_{13}^2	x_{24}^2	x_{35}^2	x_{46}^2	x_{15}^2	x_{26}^2	x_{14}^2	x_{25}^2	x_{36}^2	$\mathrm{Rem}_{6,\mathrm{CS}}^{(2)}$
D1	−3.5979	−7.9792	−1.4274	−24.543	−7.3282	−4.5361	−10.424	−2.6875	−1.9989	−3.70845563
D2	−3.5979	−7.9792	−4.5361	−24.543	−7.3282	−14.780	−10.424	−2.6875	−1.9989	−3.99210938

Table 5: *Through this configuration, we tried to examine whether* $\mathrm{Rem}_{6,\mathrm{CS}}^{(2)}$ *maintain same values for various configurations which has same conformal cross ratios. One of remarkable observation on remainder function in* $\mathcal{N}=4$ *SYM was that it has equivalent values as long as conformal cross ratios agree, even Gram determinant was not satisfied. However, this result suggest such useful property is absent in ABJM theory.*

and the same conformal cross-ratio. We thus conclude that, in stark contrast to the $(3+1)$-dimensional $\mathcal{N}=4$ SYM theory, the lightlike hexagon Wilson loop expectation value in the ABJM theory is consistent with the anomalous conformal Ward identity only if the Mandelstam variables were to satisfy the Gram sub-determinant conditions. Therefore, if two sets of the hexagon Mandelstam variables satisfy the Gram sub-determinant conditions and yield the same conformal cross-ratio, then their values of the remainder function should be the same. In our numerical computations, we have confirmed this.

	x_{13}^2	x_{24}^2	x_{35}^2	x_{46}^2	x_{15}^2	x_{26}^2	x_{14}^2	x_{25}^2	x_{36}^2	$\mathrm{Rem}_{6,\mathrm{CS}}^{(2)}$
X	−6.0000	−2.0000	−3.0000	−9.0000	−5.0000	−7.0000	−1.0000	−4.0000	−8.0000	−3.99713002
Y	−1.0000	−5.0000	$-\frac{3}{16}$	−27.000	−1.0000	−7.0000	−2.0000	−1.0000	−2.0000	−3.84236164
Z	−1.0000	$-\frac{1}{3}$	−1.0000	−1.0000	−2.0000	$-\frac{2}{3}$	−1.0000	$-\frac{2}{3}$	−1.0000	−3.41789832

Table 6: *Three sets of 'unphysical' Mandelstam variables were chosen arbitrarily. They are unphysical since they do not satisfy the Gram sub-determinant conditions. The values of the remainder function* $R_{CS,6}$ *do not agrees with the values in Table 1 for 'physical' Mandelstam variables.*

As another check, we considered randomly chosen configuration (X) and another configuration (Y) having the same conformal cross-ratios as (X). The two configurations yield different values for the remainder function. This affirms that configurations violating the Gram sub-determinant condition do not obey the anomalous conformal Ward identitie since these identities put the remainder function to a function only of conformal cross-ratios. As such, we call them 'unphysical' configurations. We also considered the configuration (Z) whose cross-ratios all have value 1 and hence relevant for the $(1+1)$-dimensional configuration of the hexagon. Result (Z), however, shows that it does not yield the physical result, because the closedness, $(1+1)$-dimensional lightlikeness, and the Euclidean conditions cannot be satisfied simultaneously.

Summarizing, we learned that although the polygon kinematics is most conveniently described in terms of the Mandelstam invariants, they are subject to various restrictions to correspond to physical configurations. Some of these restrictions are universal, inde-

pendent of spacetime dimensions, while some other restrictions are specific to $(2+1)$-dimensional spacetime. Unfortunately, the latter restrictions were stringent enough not to allow the QMRK that played powerful role in understanding the analytic structure of the Wilson loop expectation values in the $(3+1)$-dimensional $\mathcal{N}=4$ SYM theory.

To avoid such difficulty, we identified alternative special kinematics that satisfy the Gram sub-determinant conditions and also permit continuous deformation within the moduli space of the lightlike polygon. The idea is to take the deformation parameters to asymptotic limit and reduce Mellin-Barnes integrals as simple as possible. We shall study these kinematic limits in the next sections. For now, we present numerical result for several configurations that turn out representative of 1- and 2-parameter subspaces.

	x_{13}^2	x_{24}^2	x_{35}^2	x_{46}^2	x_{15}^2	x_{26}^2	x_{14}^2	x_{25}^2	x_{36}^2	$\mathrm{Rem}_{6,\mathrm{CS}}^{(2)}$
J1	-100.00	-1.0000	-1.0000	$-\frac{1}{100}$	-1.0000	-1.0000	-1.0000	-1.0000	-1.0000	-3.4857518
J2	-100.00	-2000.0	-100.00	-100.00	-5.0000	-100.00	-100.00	-100.00	-100.00	-3.4778556

Table 7: *These configurations satisfy the Gram sub-determinant conditions. We checked (J1) and (J2) could be generated from y_i's with suitable choice of components. Since we want to take asymptotic limit while keeping the Gram sub-determinant conditions, some special kinematics should be considered. These results provide numerical evidence that both one-parameter family and two parameter family indeed gives satisfactory results for the remainder function. See Table 1 for comparison.*

The configuration (J1) belongs to 1-parameter group, while (J2) belongs to 2-parameter group. We examined numerically the effect of changing these free parameters. As seen in table 4, the remainder function $\mathrm{Rem}_{6,\mathrm{CS}}^{(2)}$ takes a constant value over the ranges we changed these parameters. The result hints that we can take certain asymptotic limits of these moduli parameters and simplify the Mellin-Barnes transformation integrals.

4.5.3 Special Shapes and Asymptotic Limits

The strategy

Our goal is to compute the hexagon remainder function with high precision and infer from it analytic result. In the previous subsection, we presented the remainder function computed using the package `FIESTA2`. The numerical error is rather large, $O(10^{-2})$. Here, we propose an alternative strategy for computing the remainder function with better numerical precision than `FIESTA2`. We begin with the Mellin-Barns transformation to our 2-loop integrals, for which we used the Mathematica package `MB`. The problem of this transformation is that it results in multi-dimensional scalar integrals, for which numerical precision is difficult to attain. The idea is to lower the dimension of numerical integral maximally so that higher

numerical precision can be achieved. The way we achieve this is as follows. Recall that the dimension of numerical integral is closely related to the number of independent terms inside the denominator Δ_y in the two-loop integral involving the gauge boson triple-vertex diagrams. By choosing judiciously a set of the Mandelstam variables that satisfy the Gram sub-determinant conditions and that reduce the number of terms in Δ_y, we can bring down the dimension of numerical integrals and obtain the result with high numerical precisions. Below, we explain how we performed high precision numerical computation for the gauge boson triple-vertex diagrams.

Computational Details

Our strategy for the numerical computation is as follows. We apply the Mellin-Barnes transformation to every loop integrals resulting from the gauge boson triple-vertex and gauge boson ladder diagrams derived in section 3. We then take special limits of the polygon shape deformed by one- or two-moduli parameters. The integrals are defined in the complex domain. Utilizing the packages `MB` and `MBresolve` [55], we resolve singularity structure of each complex integrals. We then apply the Barnes lemma to reduce the integrals to lower-dimensional integrals. We made this procedure automatic using the package `barnesroutines` [56]. Next, we apply the package `MBasymptotics` [59] to the chosen moduli parameters and obtain simpler expressions for the integrals. We find that these expressions are reducible to at most three-dimensional complex integrals. Finally, we evaluate them using the `MB` package and obtain numerical result with high precision.

What special limits can we choose for the Mandelstam variables of the lightlike hexagon? Subject to the Gram sub-determinant conditions, let's consider the following two special limits: the first one has 1-moduli parameter, while second one has 2-moduli parameters.

- **one-parameter hexagon**

x_{13}^2	x_{24}^2	x_{35}^2	x_{46}^2	x_{15}^2	x_{26}^2	x_{14}^2	x_{25}^2	x_{36}^2
$-e^a$	-1	-1	$-e^{-a}$	-1	-1	-1	-1	-1

  The moduli parameter a ranges over $-\infty < a < +\infty$. We take the Euclidean configuration, and this puts all the Mandelstam variables to negative definite values.

- **two-parameter hexagon**

x_{13}^2	x_{24}^2	x_{35}^2	x_{46}^2	x_{15}^2	x_{26}^2	x_{14}^2	x_{25}^2	x_{36}^2
$-e^\alpha$	$-e^{\alpha+\beta}$	$-e^\alpha$	$-e^\alpha$	$-e^{\alpha-\beta}$	$-e^\alpha$	$-e^\alpha$	$-e^\alpha$	$-e^\alpha$

  The moduli parameters α, β range over $-\infty < \alpha, \beta < +\infty$. Again, taking the Euclidean configuration, all the Mandelstam variables are negative definite.

We found that the hexagon remainder function $\mathrm{Rem}^{(2)}_{6,\mathrm{CS}}$ remains constant-valued for a wide range of the moduli parameters a, α, β. In the previous subsection, we already presented one such choice in the result for the configurations (J1) and (J2) in the previous subsection. The result suggested that the hexagon remainder function $\mathrm{Rem}^{(2)}_{6,\mathrm{CS}}$ is indeed a constant up to two loops in the ABJM theory. We performed numerical computation for both configurations and found that the two-parameter configuration yields the result with better numerical precision. Hereafter, we will exclusively discuss the two-parameter configuration results. The simplest integral is I_{321} in (F.11). Inserting the two-moduli parameter contour to (F.11), we observe that the four-fold integration is reduced to three-fold integration. For instance, the denominator is reduced to

$$\Delta_y\Big|_{\text{2-parameter}} \quad \longrightarrow \quad e^{\alpha}\cdot x\bar{x}y\bar{s_1}s_2 + e^{\alpha-\beta}\cdot \bar{x}\bar{y}\bar{s_2}s_3 + e^{\alpha-\beta}\cdot x\bar{y}s_1s_3 + e^{\alpha}\cdot x\bar{y}\bar{s_1}. \tag{4.78}$$

By itself, five terms in the denominator Δ_y are reduced to three terms, so the two-parameter configuration does not appear to simplify the multi-dimensional integrals considerably. It turned out the two-parameter configuration is more effective for other triple-vertex diagrams involving higher-dimensional integrals. The most complicated integrals resulted from the contribution I_{531}. The Mellin-Barns transformation of this contribution yielded 8-dimensional complex integrals. With the two-parameter special kinematics, we were able to reduce these integrals to five-dimensional integrals. We could do even better. By taking the asymptotic limits for α, β sequentially,

$$\alpha \to -\infty \quad \text{then} \quad \beta \longrightarrow +\infty. \tag{4.79}$$

we were able to reduce the five-dimensional integrals down to at most three-dimensional integrals.

Result

The high precision computation yielded

$$\mathrm{Rem}^{(2)}_{6,\mathrm{CS}} = -3.470168804. \quad \Big(0.000489814\Big). \tag{4.80}$$

Utilized the PSLQ algorithm, we converted thi to an analytic expression. The result is

$$\mathrm{Rem}^{(2)}_{6,\mathrm{CS}} = -\frac{17}{4}\zeta(2) + 3\mathrm{Log}(2) + 3\mathrm{Log}^2(2). \tag{4.81}$$

Numerical value of the right-hand side is -3.470169200670522, and this agrees to our numerical result -3.47016880435048 within the $O(10^{-6})$ precision.

The final result for the two-loop, lightlike hexagon ABJM Wilson loop expecation value is obtained by combining the purely abelian, matter-dependent contribution (4.41) and the pure Chern-Simons contribution (4.54) for $n=6$. It takes the form:

$$\begin{aligned}\left\langle W_{\square}[C_6]\right\rangle^{(2)}_{\text{ABJM}} &= -\Big[\frac{1}{2}\text{Log}(2)\sum_{i=1}^{6}\frac{(x_{i,i+2}^2\pi e^{\gamma_E}\mu^2)^{2\varepsilon}}{2\varepsilon}+\text{Rem}^{(2)}_{6,\text{CS}}-3\text{Log}(2)\\ &\quad+\frac{1}{2}\sum_{i=1}^{n}\frac{(x_{i,i+2}^2 4\pi e^{\gamma_E}\mu^2)^{2\varepsilon}}{(2\varepsilon)^2}-\text{BDS}_6^{(2)}+\frac{3}{8}\pi^2\Big]\\ &= -\Big[\frac{1}{2}\sum_{i=1}^{6}\frac{(x_{i,i+2}^2 8\pi e^{\gamma_E}\mu^2)^{2\varepsilon}}{(2\varepsilon)^2}-\text{BDS}_6^{(2)}+\text{Rem}^{(2)}_{6,\text{CS}}-3\text{Log}(2)+\frac{3\pi^2}{8}-\frac{15}{2}\text{Log}^2(2)\Big]\\ &= -\frac{1}{2}\sum_{i=1}^{6}\frac{(x_{i,i+2}^2 8\pi e^{\gamma_E}\tilde{\mu}^2)^{2\varepsilon}}{(2\varepsilon)^2}+\text{BDS}_6^{(2)}+\Big(\frac{9}{2}\text{Log}^2(2)+\frac{\pi^2}{3}\Big),\end{aligned}\tag{4.82}$$

where the BDS contribution $\text{BDS}_6^{(2)}$ is already known. This is one of the main results of this paper. Like the lightlike tetragon Wilson loop expectation value, the UV finite part in (4.82) exhibits the uniform transcendentality.

While we have succeeded in obtaining two-loop analytic result for the hexagon Wilson loop expectation value, we have yet no clue for the structure of the remainder function $\text{Rem}^{(2)}_{n,\text{CS}}$ for polygons of $n\geq 8$. To crack down its structure, we will need to understand further configurational structures of the lightlike polygon Wilson loop expectation value. This is what we will undertake in the next section.

4.6 Lightlike Factorization and Antenna Function

Conformal field theories are subject to infrared divergences due to collinear and soft bremsstrahlung partons. These divergences then allow universal factorization and scaling behavior of physical processes. A class of such processes is the parton scattering amplitudes in gauge theories. The universal factorization and scaling behavior allowed accurate prediction at fixed order perturbation theory and resummation of dominant logarithms.

Our goal in this section is to demonstrate that universal factorization and scaling behavior are also present in the lightlike polygon Wilson loops. We then introduce 'universal antenna function' for a certain limit of the polygon shape, which we will utilize it in the next section to solve for the ABJM Wilson loop expectation value for arbitrary n.

4.6.1 Infrared Factorization in Gauge Theories

Let us recall the IR factorization in gauge theories and draw intuitions for what we may expect for the lightlike Wilson loops. The color-ordered scattering amplitude in gauge theories has the factorization property with respect to the IR divergence. First, consider the collinear limit that lightlike momenta k_i and k_{i+1} of two partons i and $i+1$ become parallel and coalesce to a new lightlike momentum k_P. Kinematically, this situation described by

$$k_i \longrightarrow hk_P \quad \text{and} \quad k_{i+1} \longrightarrow (1-h)k_P, \qquad (0 \leq h \leq 1) \tag{4.83}$$

so the two collinear partons carry the fraction $h,(1-h)$ of the momentum k_P.

For the L-loop n-point scattering amplitude $A_n^{(L)}(k_1,\cdots,k_n)$, the collinear limit exhibits factorization [60]

$$A_n^{(L)}(k_1,\cdots,k_n) \longrightarrow \sum_{\lambda=\pm}\sum_{\ell=0}^{L} \mathrm{Split}_{-\lambda}^{(L-\ell)}(h;k_i,\lambda_i;k_{i+1},\lambda_{i+1})A_{n-1}^{(\ell)}(k_P,\lambda,\cdots k_n)) \tag{4.84}$$

Here λ labels the polarization state of the factorizing parton. In the summation, $L,\ell=0$ denote the tree-level amplitude. Helicity structure is fixed by the Poincaré invariance, so both the scattering amplitudes and the splitting functions can be decomposed to their tree-level counterparts times scalar functions summarizing loop corrections.

We define reduced scattering amplitudes $M_n^{(L)}$ for the ratio of the L-loop scattering amplitude to the tree-level scattering amplitude:

$$A_n^{(L)}(k_1,\lambda_1,\cdots,k_n,\lambda_n) = A_n^{(0)}(k_1,\lambda_1,\cdots,k_n\lambda_n)\cdot M_n^{(L)}(k_1,\cdots,k_n). \tag{4.85}$$

Similarly, we define the reduced splitting functions $R_s^{(L)}(\varepsilon,z,k_P)$ for the ratio of the L-loop splitting function to the tree-level splitting function

$$\mathrm{Split}_{-\lambda}^{(L)}(h;k_i,\lambda_i;k_{i+1},\lambda_{i+1}) = \mathrm{Split}_{-\lambda}^{(0)}(h;k_i,\lambda_i;k_{i+1},\lambda_{i+1})\cdot R_s^{(L)}(\varepsilon,h;k_P), \tag{4.86}$$

where we use the dimensional regularization for the IR divergences. In the collinear limit, the tree-level scattering amplitudes are expected to factorize as follows:

$$A_n^{(0)} \longrightarrow \sum_{\lambda=\pm} \mathrm{Split}_{-\lambda}^{(0)}(h;k_i,\lambda_i;k_{i+1},\lambda_{i+1})A_{n-1}^{(0)}(k_P,\lambda). \tag{4.87}$$

This is illustrated in next Figure.

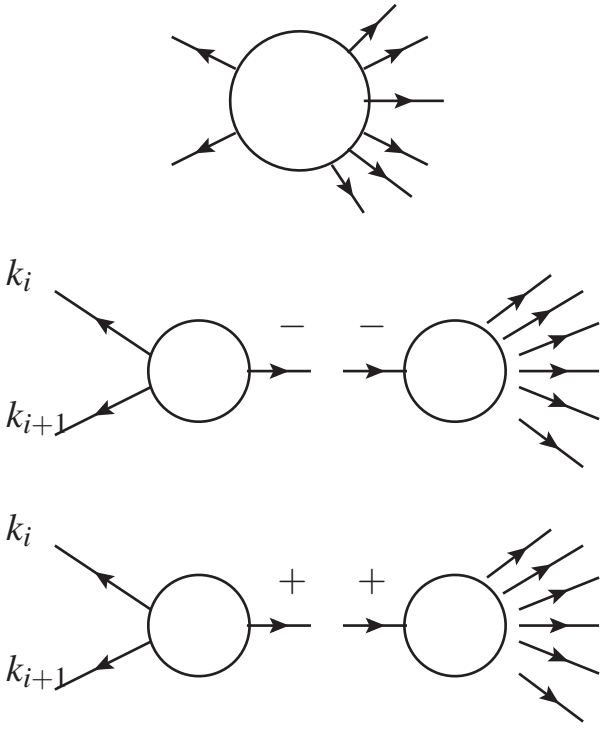

Inserting the relation (4.84) to (4.87), we get

$$M_n^{(L)} \longrightarrow \sum_{\ell=0}^{L} R_s^{(\ell)} M_{n-1}^{(L-\ell)} \tag{4.88}$$

By definition, $R_s^{(0)} = 1$ and $M_n^{(0)} = 1$. The reduced amplitudes $M_n^{(L)}$ at one- and two-loops factorize to

$$M_n^{(1)} \longrightarrow M_{n-1}^{(1)} + R_s^{(1)} \tag{4.89}$$

$$M_n^{(2)} \longrightarrow M_{n-1}^{(2)} + R_s^{(1)} M_{n-1}^{(1)} + R_s^{(2)}. \tag{4.90}$$

In the $(3+1)$-dimensional SYM theory, it is known that (4.89) and (4.90) are related each other by the collinear relation [33]:

$$M_n^{(2)}(\varepsilon) = \frac{1}{2}\big(M_n^{(1)}(\varepsilon)\big)^2 + f^{(2)}(\varepsilon) M_n^{(1)}(2\varepsilon) + C^{(2)}. \tag{4.91}$$

Here, $C^{(2)}$ is a finite constant, equal to $-\frac{1}{2}\zeta_2^2$. Also, $f^{(2)}(\varepsilon) = -(\zeta_2 + \zeta_3\varepsilon + \zeta_4\varepsilon^2 + \cdots)$.

Substituting (4.89) to (4.91),

$$M_n^{(2)}(\varepsilon) = \frac{1}{2}(M_{n-1}^{(1)}(\varepsilon) + R_s^{(1)}(\varepsilon))^2 + f^{(2)}(\varepsilon)(M_{n-1}^{(1)}(2\varepsilon) + R_s^{(1)}(2\varepsilon)) + C^{(2)}$$
$$= M_{n-1}^{(2)}(\varepsilon) + R_s^{(1)}(\varepsilon)M_{n-1}^{(1)} + \frac{1}{2}(R_s^{(1)}(\varepsilon))^2 + f^{(2)}(\varepsilon)R_s^{(1)}(2\varepsilon). \tag{4.92}$$

In the second line, we utlized the above collinear relation for $M_{n-1}^{(2)}$. Comparing this with (4.90), we obtain recursive relation for the splitting function:

$$R_s^{(2)}(\varepsilon) = \frac{1}{2}(R_s^{(1)})^2 + f^{(2)}(\varepsilon)R_s^{(1)}(2\varepsilon) + O(\varepsilon). \tag{4.93}$$

More generally, the scalar splitting function $R_s^{(\ell)}$ also follows from the BDS-like relation for all higher $\ell > 1$ loops. Indeed, for QCD and $(3+1)$-dimensional $\mathcal{N} = 4$ SYM theory, the scalar splitting function $R_s^{(1)}$ was calculated explicitly and its universality was established [**?**], [33].

Another source of the IR divergences in gauge theories is emission of the soft partons. These divergences also provide another kind of factorization. More explicitly, in the limit of one parton becomes soft, the scattering amplitudes exhibit an abelian factorization that it becomes a product of an eikonal factor with a lower-point scattering amplitude. At tree-level, when b-parton becomes soft, $k_b \simeq 0$, the soft factorization is given by

$$A_n^{(0)}(k_1,\cdots,k_a,k_b,k_c,\cdots k_n) \quad \longrightarrow \quad S^{(0)}(k_a,k_b,k_c)A_{n-1}^{(0)}(k_1,\cdots,k_a,k_c,\cdots,k_n) \tag{4.94}$$

where $S^{(0)}(k_a,k_b,k_c)$ denotes the tree-level eikonal factor,

$$S^{(0)}(k_a,k_b,k_c) = \frac{-1}{\sqrt{2}}\left[\frac{\varepsilon_b^{\pm}\cdot k_a}{k_a\cdot k_b} - \frac{\varepsilon_b^{\pm}\cdot k_c}{k_b\cdot k_c}\right]. \tag{4.95}$$

The soft bremsstrahlung factorization has the feature that this eikonal factor does not depend on the helicity of external particles. The soft factorization also holds at higher loops. For example, at one loop, the scattering amplitude factorizes in the soft limit as

$$A_n^{(1)}(k_1,\cdots,k_a,k_b,k_c,\cdots,k_n)$$
$$\longrightarrow S^{(0)}(k_a,k_b,k_c)A_{n-1}^{(1)}(k_1,\cdots,k_a,k_c,\cdots,k_n) + S^{(1)}(k_a,k_b,k_c)A_{n-1}^{(0)}(k_1,\cdots,k_a,k_c,\cdots,k_n). \tag{4.96}$$

Here, $S^{(1)}$ is the one-loop eikonal function. In dimensional regularization, it reads [**?**]:

$$S^{(1)}(k_a,k_b,k_c) = -S^{(0)}(k_a,k_b,k_c)\frac{1}{(4\pi)^{2-\varepsilon}}\frac{\Gamma(1+\varepsilon)\Gamma^2(1-\varepsilon)}{\Gamma(1-2\varepsilon)}\frac{1}{\varepsilon^2}\left(\frac{(-s_{ac})\mu^2}{(-s_{ab})(-s_{bc})}\right)^{\varepsilon}\frac{\pi\varepsilon}{\sin(\pi\varepsilon)}, \tag{4.97}$$

where $s_{ab} = 2k_a \cdot k_b$, etc. So, the soft factorization behavior is analogous to that of the collinear limit, just replacing the splitting function of the latter to the eikonal function.

The antenna function is a universal function introduced to describe in a unified manner all leading infrared singularities of tree-level scattering amplitudes as the color-connected set of momenta becomes collinear or soft. Consider, in color-order scattering amplitude, two hard momenta k_a, k_b and one momentum k_c in between. The unified factorization then takes the form

$$A_n^{(0)}(k_1,\cdots,k_a,k_c,k_b,\cdots,k_n) \quad \to \quad \sum_{\lambda}\mathrm{Ant}(\hat{a},\hat{b}\leftarrow a,c,b)A_{n-1}(k_1,\cdots,-k_{\hat{a}},-k_{\hat{b}},\cdots,k_n), \tag{4.98}$$

where the antenna function Ant contains information of the parton c:

- collinear splitting function for $k_c\cdot k_a \to 0$ and $k_c\cdot k_b =$ finite ($k_{\hat{a}} = -(k_a+k_c), k_{\hat{b}} = -k_b$)
- collinear splitting function for $k_c\cdot k_b \to 0$ and $k_c\cdot k_a =$ finite ($k_{\hat{a}} = -k_a, k_{\hat{b}} = -(k_c+k_b)$)
- soft eikonal function for both $k_c\cdot k_a \to 0$ and $k_c\cdot k_b \to 0$ ($k_{\hat{a}} = -k_a, k_{\hat{b}} = -k_b$).

The momentua $k_{\hat{a}}, k_{\hat{b}}$ are reconstructed from the original momenta via the reconstruction function [57]. The antenna function can also be extended to higher loops in terms of parton currents J that was used in the Berends-Giele recursion relations [58]. At L-loops,

$$\mathrm{Ant}^{(L)}(\hat{a},\hat{b}\leftarrow a,c,\cdots,m,b) = \sum_{\ell=0}^{L}\sum_{i=1}^{m} J^{(\ell)}(a,c,\cdots,i;\hat{a})J^{(L-\ell)}(i+1,\cdots,m,b;\hat{b}) \tag{4.99}$$

Then, the factorization of the leading-color contribution to higher-loop scattering amplitudes can be derived by matching to known purely collinear limit or purely soft bremsstrahlung limit. This leads to

$$A_n^{(L)}(k_1,\cdots,k_n) \longrightarrow \sum_{\ell=0}^{L}\sum_{\lambda}\mathrm{Ant}^{(\ell)}(\hat{a},\hat{b}\leftarrow a,1,b)\cdot A_{n-1}^{(L-\ell)}(k_1,\cdots,-k_{\hat{a}},-k_{\hat{b}},\cdots,k_n). \tag{4.100}$$

This can be generalized to multiple collinear singularities that involve simultaneous vanishing of Mandelstam invariants in these collinear momenta and one of the two hard momenta

a or b. We can also generalize this to multiple collinear-soft or purely multiple soft singularities that arise from vanishing of additional Mandelstam invariants involving other hard momenta as well.

Note that the leading singularities in the additional Mandelstam invariants are already incorporated to the antenna function. Therefore, these singularities also capture the leading behavior in the multiple collinear-soft or multiple soft singularities. Indeed, the $h \to 0$ limit of the collinear splitting function must also describe the soft bremsstrahlung eikonal. As such, (4.100) describes the leading singularity behavior of L-loop leading-color scattering amplitudes in all singular limits involving the color-connected singular set of momenta $k_1, \cdots, k_m$.

One can generalize the factorization to multi-parton kinematics. The next level of factorization involves two unresolved parton kinematics. The factorization in doubly unresolved limit is given at L loops by

$$A_n^{(L)}(k_1, \cdots, k_n) \longrightarrow \sum_{\ell=0}^{L} \sum_{\lambda} \mathrm{Ant}^{(\ell)}(\hat{a}, \hat{b} \leftarrow a, 1, 2, b) \cdot A_{n-2}^{(\ell)}(k_1, \cdots, -k_{\hat{a}}, -k_{\hat{b}}, \cdots, k_n). \tag{4.101}$$

This antenna function have various channels, for instance, triple collinear, double collinear, collinear soft and double soft. Among them, we will focus on the first case that s_{a1}, s_{12}, t_{a12} goes to 0.

Much the way the splitting function or the eikonal function are universal, we expect the antenna function also have universal structures.

4.6.2 Lightlike Factorization of Wilson Loop

One expects that the lightlike polygon Wilson loops provides another class of processes that exhibit IR divergences and factorizations thereof. Indeed shape or geometry of the lightlike contour C_n exhibits two types of move that can be viewed as the soft and the collinear limits. The soft bremsstrahlung limit takes place when two adjacent vertex points coalesce. The collinear limit takes place when two adjacent edges coalesce, equivalently, when three consecutive vertices become lightlike arrayed.

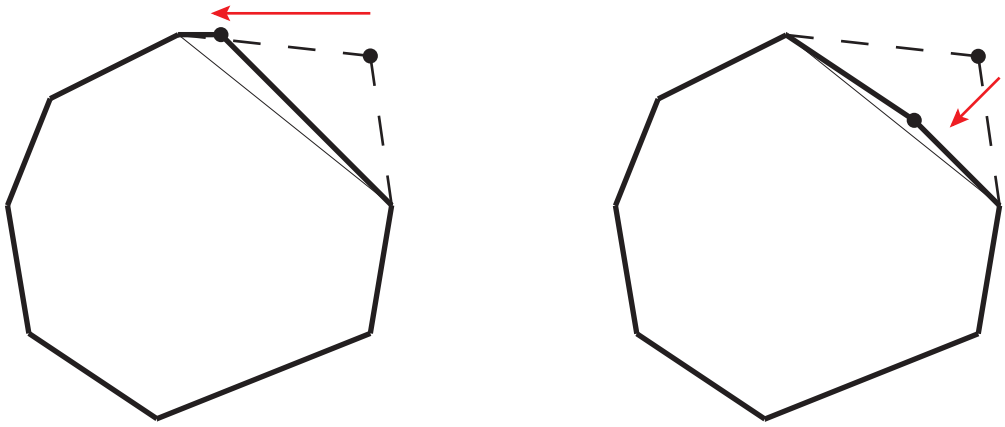

Figure 2 : *Infrared singularities of lightlike polygon. There are two limits a contour C_n is reduced to C_{n-1}. The left figure describes the soft bremsstrahlung limit. The vertex x_{i+1} coalesces to the adjacent vertex x_i, equivalently, the edge vector y_i approaches to 0. The right figure describes the collinear limit. The vertex x_i approaches the lightlike segment connecting the vertices, x_{i-1} and x_{i+1}, equivalently, two adjacent edge vectors y_{i-1} and y_i coalesce to a new lightlike vector. Although resulting topologies of are the same, the two limits needs to be distinguished. By analyticity, this is possible only if the limits are singular.*

The significance of these two processes is evident from geometric considerations among the vertex points $x_1, \cdots, x_n$. Generically, two non-adjacent vertex points are not lightlike separated. From either configurations, if we take succession of the above two processes for either vertex vectors or edge vectors within a lightlike polygon, we see that two non-adjacent cusp points of the polygon can be made lightlike separated. The limiting configuration is a lightlike polygon split to two lightlike polygons. Hereafter, this kinematic limit will be referred as *lightlike factorization*. The classification is purely geomeric, so it must hold for observables defined for general quantum field theories of arbitrary spacetime dimensions.

In applying the above infrared factorizations of lightlike contour to ABJM Wilson loops, there is one further issue to be considered. We have shown in the last section that the lightlike ABJM Wilson loop cannot be defined on a polygon of odd numbers of edges since it does not permit Euclidean configuration [4]. Whereas infrared factorization of the $(3+1)$-dimensional $\mathcal{N}=4$ SYM theory requires a single parton to fuse to other hard partons, infrared factorization of the $(2+1)$-dimensional ABJM theory requires two partons to fuse to other hard partons.

[4] Recall also that this parallels to the fact that the ABJM scattering amplitudes involve even number of partons, though reasons are entirely different.

Thus, in the ABJM theory, we need to define an antenna function for double parton emissions. [5].

Intuitively, the above discussion makes it clear that the lightlike factorization is *universal* — the factorization should be independent of geometric details of spectator vertices or edges in the rest of the polygon. In the ABJM theory, we explained in the previous section that the Euclidean condition of the Mandelstam variables and the closedness condition of the edge vectors restricted the contour to even number of vertices, equivalently, even number of edges. Consistency with these conditions require that the infrared singularity must involve odd numbers of consecutive edges fusing to a single edge and consecutive vertices pairing up to dimerized configuration. Therefore, the basic building block of the lightlike factorization of a polygon Wilson loop is the collinear-soft-collinear limit among 4 consecutive vertices, equivalently, 3 consecutive edges. We shall introduce the ABJM *antenna function* that describes in a unified way all leading singularities of such processes.

Incidentally, we do not consider the limit where three consecutive edges are purely collinear. This is because the corresponding edge vectors in general violate the Euclidean condition. We will further discuss this restriction below. We also do not consider the limit where two consecutive edges are purely soft. Although kinematically permitted, this limit requires to take several Mandelstam invariants to zero simultaneously. Numerically, such a limit is technically involved and difficult to handle. In this paper, we will not study this corner of the moduli space and simply contend that the universal antenna function we derive below be reduced to the correct double eikonal function of such processes once relevant factorization is taken judicially.

Our next goal is to explicitly check the universality of the antenna function for the lightlike Wilson loop. By definition, the Wilson loop operator is color-ordered. Therefore, we can describe its collinear factorization in a manner similar to the color-ordered scattering amplitudes in QCD exhibits the factorization with respect to the collinear divergences [**?**]. So, take the collinear limit that three adjacent edge vectors y_i, y_{i+1} and y_{i+2} become lightlike parallel and coalesce to a new lightlike edge vector y_P. This situation is described by what we call 'doubly unresolved limit' of $C_n \to C_{n-2}$:

$$y_i \to (1-h_1-h_2)y_P, \qquad y_{i+1} \to h_1 y_P, \quad y_{i+2} \to h_2 y_P \qquad \text{where} \qquad y_P^2 = 0. \tag{4.102}$$

[5] Antenna function was studied for scattering amplitudes in QCD and other gauge theories. We are adopting the same terminology to lightlike Wilson loop expectation values. In $(3+1)$-dimensional $\mathcal{N}=4$ SYM theory, the scattering amplitude - Wilson loop duality relates the universal splitting function for collinear limit in scattering amplitudes to the universal factorization for lightlike limit of Wilson loop expectation values.

In the doubly unresolved limit, we expect the lightlike polygon Wilson loop expectation value at L-loop factorizes universally as

$$\left\langle W_{\square}[C_n]\right\rangle^{(L)} \longrightarrow \sum_{\ell=0}^{L} \mathrm{Ant}^{(\ell)}(h_1,h_2;y_i,y_{i+1},y_{i+2})\left\langle W_{\square}[C_{n-2}]\right\rangle^{(L-\ell)}. \tag{4.103}$$

We will abbreviate the antenna function that arises from factorization of the polygon C_n Wilson loop as $\mathrm{Ant}[C_n]$. In the kinematics Eq.(4.102), the antenna function is closely related to the Wilson loop expectation value for the collapsing tetragon made of the edges $y_i, y_{i+1}, y_{i+2}, -y_P$. Our goal is to show that this antenna function is actually independent of the number of edges n of the contour C_n and hence universal. Note that the tree-level factorization for $L, \ell = 0$:

$$\left\langle W_{\square}[C_n]\right\rangle^{(0)} \quad \longrightarrow \quad \mathrm{Ant}^{(0)}[C_n]\cdot\left\langle W_{\square}[C_{n-2}]\right\rangle^{(0)} \tag{4.104}$$

is actually a trivial statement since, in our normalization, all the quantities involved are 1.

At two-loop order, the doubly-unresolved configuration leads to the factorization:

$$\begin{aligned}\left\langle W_{\square}[C_n]\right\rangle^{(2)} \quad \longrightarrow \quad & \mathrm{Ant}^{(2)}[C_4]\cdot\left\langle W_{\square}[C_{n-2}]\right\rangle^{(0)} + \mathrm{Ant}^{(0)}[C_4]\cdot\left\langle W_{\square}[C_n]\right\rangle^{(2)} \\ & = \left\langle W_{\square}[C_{n-2}]\right\rangle^{(2)} + \mathrm{Ant}^{(2)}[C_4].\end{aligned} \tag{4.105}$$

The antenna function $\mathrm{Ant}[C_4]$ is local in color-ordered contour geometry, so it is independent of n and universal:

$$\boxed{\mathrm{Ant}^{(2)}[C_4] = \left\langle W_{\square}[C_n]\right\rangle^{(2)} - \left\langle W_{\square}[C_{n-2}]\right\rangle^{(2)} \quad \text{for all } n.} \tag{4.106}$$

4.7 Antenna Function for the ABJM Wilson Loops

Built upon the idea of the previous section, we now construct the antenna function for the lightlike polygon Wilson loops in the ABJM theory. From (4.106), the antenna function is obtained by subtracting $\left\langle W_{\square}[C_{n-2}]\right\rangle^{(2)}$ from $\left\langle W_{\square}[C_n]\right\rangle^{(2)}$. At first sight, it appears imperative to calculate $\left\langle W_{\square}[C_{n-2}]\right\rangle^{(2)}$ and $\left\langle W_{\square}[C_n]\right\rangle^{(2)}$. This turns out not the case, as most of the Feynman diagrams cancel each other. Eventually, only a small subset of Feynman diagrams contributes to the antenna function. In fact, the number of these diagrams are fixed regardless of n, which again is an indicative of the universality of the antenna function.

4.7.1 Moduli Space of Lightlike Polygon Factorization

In section 2, we already learned that anomalous conformal Ward identity offers hints on the analytic structure of the Wilson loop expectation value, separately for matter contribution and gauge boson contribution. As such, we shall consider the factorization limit for each contribution. In this subsection, we focus on lightlike factorization of matter contribution.

triple collinear and soft-collinear kinematics

As alluded above, we will need to deal with doubly-unresolved configuration involving four consecutive vertices, say, x_2, x_3, x_4, x_5 on a polygon C_n. The lightlike factorization takes place when x_2 and x_5 are lightlike separated. To reach this configuration, take two step. First, take x_2 and x_5 lightlike seperated. This does not yet put the edge vectors y_2, y_3, y_4 parallel, nor the contour C_n factorized into two parts. Next, take x_{24}^2 and x_{35}^2 to 0. This gives the triple collinear / soft collinear limit of the edge vectors y_2, y_3, y_4. Upon taking these limits, the upper tetragon flattened, reducing C_n to C_{n-2}. Note that this limit still leaves the vertices x_3 and x_4 as unrestricted moduli parameters. A corner of this moduli space where the 3 Mandelstam variables $x_{24}^2, x_{35}^2, x_{25}^2$ go to zero. There are two ways to approach this corner:

- **triple-collinear limit**

$$y_2 \parallel y_3 \parallel y_4 \tag{4.107}$$

- **soft-collinear limit**

$$y_3 = 0, \quad y_2 \parallel y_4 \tag{4.108}$$

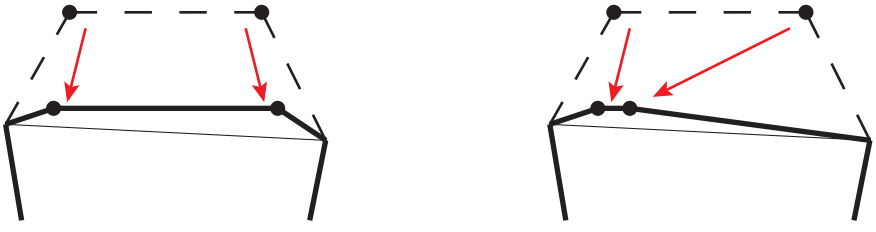

Figure 3 : *There are two different special limits in doubly unresolved kinematics. Left figure describes the triple collinear limit. Two cusps x_{i+1} and x_{i+2} approaches to a point on lightlike segment connecting x_i and x_{i+3}. Right figure describes the soft-collinear limit. The cusps x_{i+1}, x_{i+2} come close each other and the segment vectors y_{i-1} and y_{i+1} became parallel.*

The triple-collinear limit is described by the contour geometry

$$y_2 \equiv h_1 y_C, \quad y_3 \equiv h_2 y_C, \quad y_4 = h_3 y_C \quad \text{where} \quad h_1, h_2, h_3 \geq 0, \quad h_1 + h_2 + h_3 = 1, \quad y_C^2 = 0. \tag{4.109}$$

where the 'parton fraction' h_1, h_2, h_2 spans the local chart of the moduli space. Naively, the dimension of this moduli space is $[0,1] \times [0,1]$. The actual moduli space turns out $[0,1]$, as we now explain. The kinematics describes the limit that three consecutive segment vectors are parallel one another. The corresponding Mandelstam invariants are

$$x_{13}^2 = x_{14}^2 = h_1 x_{15}^2, \quad x_{46}^2 = x_{36}^2 = h_3 x_{26}^2 \quad x_{24}^2 = (1-h_3)^2 y_C^2, \quad x_{35}^2 = (1-h_1)^2 y_C^2, \quad x_{25}^2 = y_C^2 \to 0. \tag{4.110}$$

So we see that, as the three edge vectors y_2, y_3, y_4 become parallel one another, the three Mandelstam invariants $x_{25}^2, x_{24}^2, x_{35}^2$ goes to 0. Their ratios are fixed with respect to the parton fractions h_1, h_2, h_3. We then recall that the Mandelstam invariants of physical configuration must satisfy the Gram sub-determinant conditions. For the above triple-collinear configuration, the Gram sub-determinant condition requires $h_2^2 x_{15}^2 x_{26}^2 = 0$ and is solved by $h_2 \to 0$. Therefore, for all n, we must set $h_2 = 0$. This then leads to the moduli space of the triple-collinear limit to be the domain of $h_1 = -h_3$, viz. $[0,1]$.

The soft-collinear limit is described by the contour geometry

$$y_2 \equiv h_1 y_C, \quad y_3 \equiv y_S, \quad y_4 = h_3 y_C \quad \text{where} \quad h_1, h_3 \geq 0, \quad h_1 + h_3 = 1, \quad y_C^2 = 0, \quad y_S \simeq 0. \tag{4.111}$$

The moduli space of this configuration is given by the domain of $h_1 = -h_3$, viz. $[0,1]$. This can be checked straightforwardly. The contour geometry describes the limit that a diminishing edge vector is squeezed between two collinear edge vectors. The corresponding Mandelstam invariants are

$$x_{13}^2 = x_{14}^2 = h_1 x_{15}^2, \quad x_{46}^2 = x_{36}^2 = h_3 x_{26}^2, \quad x_{24}^2 = h_1 x_{25}^2, \quad x_{35}^2 = h_3 x_{25}^2, \quad x_{25}^2 = 2 y_C \cdot y_S \tag{4.112}$$

It is straightforward to check that this kinematics automatically satisfy the Gram sub-determinant conditions provided $y_C^2 = 0$ and $y_S \to 0$. The four Mandelstam invariants x_{13}^2, x_{14}^2, x_{46}^2 and x_{36}^2 coincides with the triple-collinear limit invariants if h_2 is taken to 0. However, the ratios among $x_{25}^2, x_{24}^2, x_{35}^2$ are different from the triple-collinear limit, so should be considered separately.

Factorization and Euclidean Condition

When computing the antenna function in perturbation theory, we need to impose two conditions to the moduli parameters of the polygon C_n: the Gram sub-determinant condition and the Euclidean condition. We identified that the Gram sub-determinant conditions is satisfied by both the triple collinear geometry on the subspace $h_2 = 0$ and the soft-collinear geometry. What about the Euclidean condition? Here, we show that the soft-collinear geometry of the polygon is uniquely singled out as the configuration that satisfy the Euclidean condition.

The triple collinear geometry is inconsistent with the Euclidean condition. To see this, start from

$$y_2 = h_1 y_C, \quad y_3 = h_2 y_C, \quad y_4 = h_3 y_C \quad \text{with} \quad h_1, h_2, h_3 \geq 0, \quad h_1 + h_2 + h_3 = 1, \quad y_C^2 = 0.$$

For a given lightlike vector y_C, the time-component of the y_2, y_3, y_4 vectors have the same sign since h_1, h_2, h_3 are all positive. On the other hand, the Euclidean condition requires alternating sign flip of the time-component. As such, the triple-collinear geometry contradicts this condition. We discard the triple collinear limit hereafter.

On the other hand, the soft-collinear geometry turns out to satisfy the Euclidean condition. To illustrate this, take the hexagon and consider the following parametrization of the edge vectors

$$y_2 = h_1(\sqrt{2}, 1, 1), \qquad y_3 = a(-\sqrt{2}, 1, 1), \qquad y_4 = h_3(\sqrt{2}, 1, 1) \tag{4.113}$$

We introduced a small parameter $a \simeq 0$ to render the vector y_3 soft. Fusion of these three edge vectors result in a new lightlike edge vector $y_C = (\sqrt{2}, 1, 1)$. The other edge vectors y_5, y_6 and y_1 are set to

$$y_5 = (-\sqrt{f^2 + g^2}, f, g), \qquad y_6 = (\sqrt{r^2 + s^2}, r, s), \qquad y_1 = (-\sqrt{b^2 + d^2}, b, d), \tag{4.114}$$

where g, r, s are free parameters while other three parameters b, d, f will be fixed by the closedness condition. The Mandelstam variables x_{ij}^2 can then be read from these edge vectors from the identities $-2y_i \cdot y_j = x_{i+1,j}^2 + x_{i,j+1}^2 - x_{i,j}^2 - x_{i+1,j+1}^2$. This configuration satisfies the Euclidean condition.

4.7.2 Matter Contribution to Antenna Function

Let's begin with the ABJM matter contribution to the antenna function. By (4.106), this contribution to the antenna function is extracted from

$$\mathrm{Ant}^{(2)}_{\mathrm{matter}}[C_4] = \left\langle \widetilde{W}_{\square}[C_n] \right\rangle^{(2)}_{\mathrm{matter}} - \left\langle \widetilde{W}_{\square}[C_{n-2}] \right\rangle^{(2)}_{\mathrm{matter}}. \tag{4.115}$$

Here, $\left\langle \widetilde{W}_{\square}[C_n] \right\rangle^{(2)}_{\mathrm{matter}}$ refers to Wilson loop expectation value for the polygon C_n of soft-collinear geometry.

After the soft-collinear limit is taken, the reduced polygon C_{n-2} consists of $(n-2)$ edge vectors $y_1, y_C, y_4, \cdots y_n$. Again, the new set of Mandelstam invariants x^2_{ij} are obtained by inner product of these edge vectors. The Wilson loop expectation value $\left\langle \widetilde{W}_{\square}[C_{n-2}] \right\rangle^{(2)}_{\mathrm{matter}}$ is obtained by inserting this new Mandelstam invariants to $\left\langle W_{\square}[C_{n-2}] \right\rangle^{(2)}_{\mathrm{matter}}$.

In case the three edge vectors $y_2,\ y_3,\ y_4$ coalesce in the soft-collinear limit, we shall call the vectors y_1, y_2, y_3, y_4, y_5 as 'relevant edges'. We can then classify the matter-dependent 2-loop diagrams according to the locations the one-loop gauge propagator is attached:

Group A	:	Neither end is attached to the relevant edges
Group B	:	One end is attached to the relevant edges while the other end is attached elsewhere
Group C	:	Both ends are attached to the relevant edges

We claim that Feynman diagrams belonging to Group A and Group B do not contribute to the antenna function. In other words,

$$\begin{aligned} \left\langle \widetilde{W}_{\square}[C_n] \right\rangle^{(2)}_{\mathrm{matter}}\Big|_{\text{Group A}} &= \left\langle \widetilde{W}_{\square}[C_{n-2}] \right\rangle^{(2)}_{\mathrm{matter}}\Big|_{\text{Group A}} \\ \left\langle \widetilde{W}_{\square}[C_n] \right\rangle^{(2)}_{\mathrm{matter}}\Big|_{\text{Group B}} &= \left\langle \widetilde{W}_{\square}[C_{n-2}] \right\rangle^{(2)}_{\mathrm{matter}}\Big|_{\text{Group B}} \end{aligned} \tag{4.116}$$

Nontrivial contributions to the antenna function stem entirely from 9 Feynman diagrams belonging to the Group C.

We found that, for any n, there are always 9 types of diagram that contribute to the antenna function:

$$\text{Group C} = \Big\{ I_{21},\ I_{32},\ I_{43},\ I_{54},\ I_{31},\ I_{41},\ I_{52},\ I_{53},\ I_{42} \Big\} \tag{4.117}$$

In other words, all nontrivial contributions to the antenna function are from 'local moves' around the three edge vectors fusing one another. This features a heuristic and intuitive explanation for the universality.

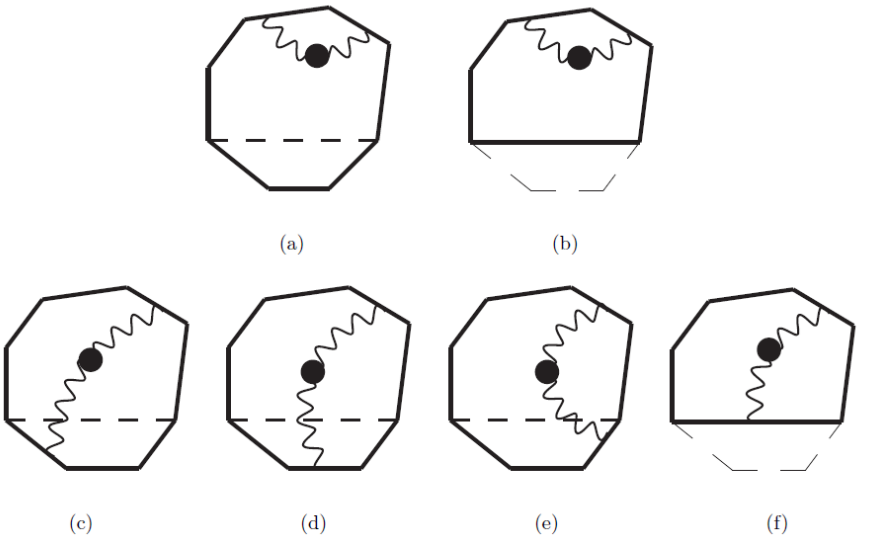

Figure 12: *Feynman diagrams in Group A and Group B. Upper diagrams belong to Group A. (a) is equivalent to (b) when collinear limit taken. Second line diagrams belong to Group B. (c)+(d)+(e) is equivalent to (f) after collinear limit. They are cancelled, therefore do not contribute to Antenna function.*

We calculated these 9 diagrams and computed the antenna function. From the known analytic results of these diagrams, we took the soft-collinear limit and subtracted the relevant C_{n-2} diagrams. Up to $O(\varepsilon^0)$, we found the result as

$$\begin{aligned}\mathrm{Ant}^{(2)}_{\mathrm{matter}} = &\frac{1}{4\varepsilon^2}+\frac{1}{4\varepsilon}\big(\mathrm{Log}h_1+\mathrm{Log}h_3+\mathrm{Log}(x_{24}^2+\mathrm{Log}(x_{35}^2)\big)\\ &+\frac{1}{2}\mathrm{Log}h_1\mathrm{Log}(x_{24}^2)+\frac{1}{2}\mathrm{Log}h_3\mathrm{Log}(x_{35}^2)+\frac{1}{2}\mathrm{Log}(x_{35}^2)\mathrm{Log}(x_{24}^2)-\frac{1}{2}\mathrm{Log}h_1\mathrm{Log}h_3\\ &-\frac{\pi^2}{6}.\end{aligned} \tag{4.118}$$

In obtaining this result, we used the Abel's identity for the dilogarithms :

$$\mathrm{Li}_2(u)+\mathrm{Li}_2(v)-\mathrm{Li}_2(uv)=\mathrm{Li}_2\Big(\frac{u-uv}{1-uv}\Big)+\mathrm{Li}_2\Big(\frac{v-uv}{1-uv}\Big)-\log\Big(\frac{1-u}{1-uv}\Big)\log\Big(\frac{1-v}{1-uv}\Big) \tag{4.119}$$

and the Landen's identity:

$$\mathrm{Li}_2(x)+\mathrm{Li}_2(\frac{1}{x})=\frac{\pi^2}{3}-\frac{1}{2}\mathrm{Log}^2(x)-i\pi\mathrm{Log}(x). \tag{4.120}$$

4.7.3 Chern-Simons Contribution to Antenna function

We now turn to the contribution of the pure Chern-Simons sector to the antenna function. Again, we expect that

$$\mathrm{Ant}^{(2)}_{\mathrm{CS}}[C_4] = \langle \widetilde{W}_{\square}[C_n]\rangle^{(2)}_{\mathrm{CS}} - \langle \widetilde{W}_{\square}[C_{n-2}]\rangle^{(2)}_{\mathrm{CS}} \tag{4.121}$$

Here, the Wilson loops $\langle \widetilde{W}_{\square}[C_n]\rangle^{(2)}_{CS}$ and $\langle \widetilde{W}_{\square}[C_{n-2}]\rangle^{(2)}_{CS}$ are defined the same way as we defined for the matter contributions.

As explained in the previous section, the pure Chern-Simons contribution consists of the ladder diagrams and the triple-vertex diagrams. We found that the ladder diagrams does not give rise to infrared divergences, so they do not contribute to the antenna function.

We thus focus on the triple-vertex diagrams. We can again classify the relevant Feynman diagrams according to the combinatorics the triple gauge bosons are attached to the polygon C_n. As for the matter contributions, we showed in the last subsection that only 'local moves' to the relevant edges contribute to the leading IR singularities. This turns out also the case for the Chern-Simons part: the contribution is completely determined by the triple-vertex diagrams whose gauge bosons are all attached to the relevant edges, y_1, y_2, y_3, y_4, y_5.

There are also IR divergences arising from 'semi-local moves'. For instance, I_{654} in C_6 is divergent. However, this divergence is cancelled by the diagram I_{65P} in C_4 and $y_2 \parallel y_3 \parallel y_4$ when we compute the antenna function as the difference between the Wilson loop of C_n and the Wilson loop of C_{n-2}. One readily notes that nontrivial contributions to the antenna function come from (1) the process that is divergent in C_n but finite in C_{n-2} and (2) the process that is finite in C_n but divergent in C_{n-2}. These two processes are completely captured by the local moves to the relevant edges.

Recall the pure Chern-Simons result of the lightlike Wilson loop expectation value for hexagon and tetragon:

$$\begin{aligned}
\langle W_{\square}[C_6]\rangle^{(2)}_{\mathrm{CS}} &= -\Big[\frac{\mathrm{Log}(2)}{2}\frac{\sum_{i=1}^{6}(x^2_{i,i+2}\pi e^{\gamma_E}\mu^2)^{2\varepsilon}}{2\varepsilon} - \frac{17}{16}\zeta_2 + \frac{3}{4}\mathrm{Log}^2(2)\Big] \\
\langle W_{\square}[C_4]\rangle^{(2)}_{\mathrm{CS}} &= -\Big[\frac{\mathrm{Log}(2)}{2}\frac{\sum_{i=1}^{4}(x^2_{i,i+2}\pi e^{\gamma_E}\mu^2)^{2\varepsilon}}{2\varepsilon} - \frac{5}{8}\zeta_2 + \frac{1}{2}\mathrm{Log}^2(2)\Big].
\end{aligned} \tag{4.122}$$

Then, $\langle \widetilde{W}_{\square}[C_6]\rangle^{(2)}_{\mathrm{CS}}$ is obtained by taking the soft-collinear geometry (4.112) to $\langle W_{\square}[C_6]\rangle^{(2)}_{\mathrm{CS}}$. For $\langle \widetilde{W}_{\square}[C_4]\rangle^{(2)}_{\mathrm{CS}}$, we replace x^2_{13} and x^2_{24} in (4.122) by x^2_{15} and x^2_{26}. The contribution to the

antenna function is then obtained from the difference

$$\begin{aligned}\mathrm{Ant}^{(2)}_{\mathrm{CS}}[C_6] &= \langle \widetilde{W}_{\square}[C_6]\rangle^{(2)}_{\mathrm{CS}} - \langle \widetilde{W}_{\square}[C_4]\rangle^{(2)}_{\mathrm{CS}} \\ &= \Big[\frac{\mathrm{Log}(2)}{2\varepsilon} + \frac{1}{2}\mathrm{Log}(2)\ \mathrm{Log}(h_1) + \frac{1}{2}\mathrm{Log}(2)\ \mathrm{Log}(h_3) + \frac{1}{2}\mathrm{Log}(2)\ \mathrm{Log}(x_{24}^2) \\ &+ \frac{1}{2}\mathrm{Log}(2)\ \mathrm{Log}(x_{35}^2) + \mathrm{Ant}^{(2)}[C_6]\Big|_{\mathrm{finite}}\Big]. \end{aligned} \tag{4.123}$$

Here,

$$\mathrm{Ant}^{(2)}[C_6]\Big|_{\mathrm{finite}} = -\frac{7}{4}\zeta_2 + \mathrm{Log}^2(2). \tag{4.124}$$

It turned out we need to numerically evaluate the Chern-Simons contribution to the antenna function. Hereafter, we shall explicitly compute the contribution from the soft-collinear factorization of hexagon C_6 and octagon C_8 contours.

hexagon $\longrightarrow$ tetragon

For computational simplicity, let's first consider the soft-collinear factorization of hexagon C_6 to tetragon C_4. We computed contribution of the Chern-Simions contribution to the antenna function $\mathrm{Ant}^{(2)}_{\mathrm{CS}}[C_6]$. Earlier, we alluded that the gauge boson ladder diagrams do not contribute to the antenna function, though they do exhibit leading IR singularities. We can classify the ladder diagrams into three groups:

$$\begin{aligned}&\text{Group A}: \quad \{I_{3366},\ I_{6634},\ I_{6623},\ I_{6624},\ I_{4466},\ I_{6622}\} \\ &\text{Group B}: \quad \{I_{5511}\} \\ &\text{Group C}: \quad \text{all other diagrams}\end{aligned}$$

We found numerically that diagrams belonging to Group C vanishes in the soft-collinear limit. We also checked numerically that the following identity holds:

$$\begin{aligned}\langle \widetilde{W}_{\square}[C_n]\rangle^{(2)}_{\mathrm{ladder}}\Big|_A - \langle \widetilde{W}_{\square}[C_{n-2}]\rangle^{(2)}_{\mathrm{ladder}}\Big|_A = 0 \\ \langle \widetilde{W}_{\square}[C_n]\rangle^{(2)}_{\mathrm{ladder}}\Big|_B - \langle \widetilde{W}_{\square}[C_{n-2}]\rangle^{(2)}_{\mathrm{ladder}}\Big|_B = 0.\end{aligned}$$

We conclude that the ladder diagrams do not contribute to the antenna function.

This brings us to the contribution of the triple-vertex diagrams. We found that only the following 10 diagrams give rise to leading IR singularities and hence can contribute to the

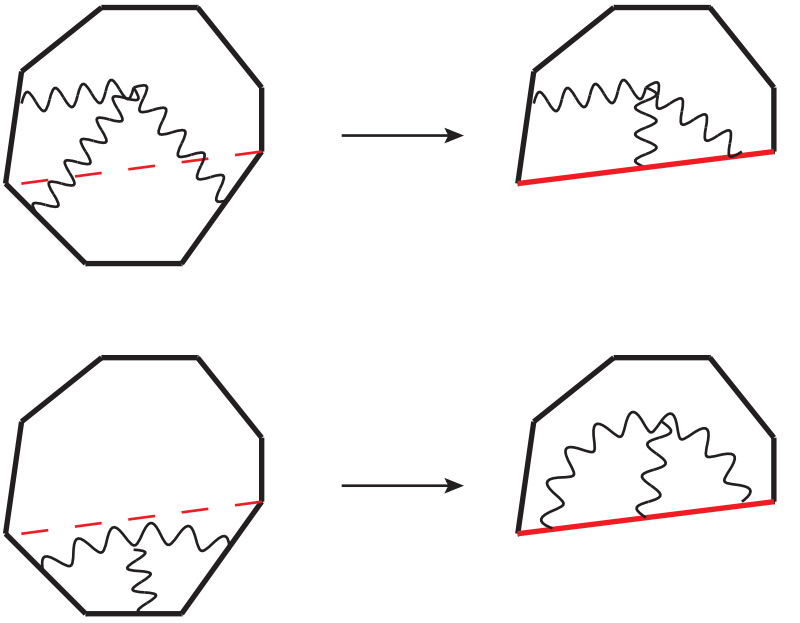

Figure 13: *Examples of 2-loop Feynman diagrams that belong to the set TV. These diagrams are "local" and hence yields nontrivial contribution to the antenna function. The red edge denotes the segment vector y_C resulting from taking the soft-collinear limit.*

antenna function:

$$TV = \{I_{321},\ I_{432},\ I_{543},\ I_{421},\ I_{532},\ I_{431},\ I_{542},\ I_{521},\ I_{531},\ I_{541}\} \tag{4.125}$$

We computed these diagrams numerically using the Mathematica package `FIESTA`. Following Table summarizes inputs and numerical results of the IR finite part of the antenna function derived from the hexagon Wilson loop.

	x_{13}^2	x_{24}^2	x_{35}^2	x_{46}^2	x_{15}^2	x_{26}^2	x_{14}^2	x_{25}^2	x_{36}^2	$\langle W \rangle_{\text{finite}}$	$\text{Ant}_{\text{finite}}$
(1)	-1.95797	-0.0005	-0.0005	-2.13973	-3.91357	-4.28024	-1.95511	-0.00100	-2.14001	-3.47673	-2.38762
(2)	-5.02424	-0.00100	-0.00100	-5.09307	-10.048	-10.188	-5.02275	-0.00200	-5.09389	-3.47701	-2.38886
(3)	-8.83791	-0.00100	-0.00100	-13.6207	-17.6764	-27.2428	-8.83749	-0.00200	-13.6211	-3.47126	-2.39603
(4)	-11.4515	-0.00199	-0.00100	-5.23415	-22.9042	-10.4691	-11.4517	-0.00200	-5.23392	-3.4768	-2.39128

Table 8: Table : *Numerical result for the IR finite part of the lightlike hexagon Wilson loop expectation value and the antenna function. Notice that, for different configurations of the Mandelstam invariants, the results suggest that the IR finite part of the antenna function maintains a constant value.*

There is an alternative method for calculating the antenna function. As in the two-parameter configuration of the hexagon, we can reduce the number of terms in the denominator of the Mellin-Barnes integrals by taking the soft-collinear configuration. Moreover, we take a hint from the previous numerical results that the IR finite part of the antenna function is independent of the polygon geometry. This allows us to take the asymptotic limits for 3 of the Mandelstam invariants $x_{25}^2, x_{15}^2, x_{26}^2$ and also for the the parton fractions $h_1 \to 0, h_3 \to 1$. Taking these limits, we succeeded in reducing to maximally 2-dimensional complex integrals. Evaluating these integrals numerically, we find that

$$\begin{aligned}\text{Ant}_{\text{CS}}^{(2)} = &\frac{0.346574}{\varepsilon} \\ &+\frac{1}{2}\text{Log}(2)\ \text{Log}(z_1)+\frac{1}{2}\text{Log}(2)\ \text{Log}(z_3)+\frac{1}{2}\text{Log}(2)\ \text{Log}(x_{24}^2)+\frac{1}{2}\text{Log}(2)\ \text{Log}(x_{35}^2) \\ &-2.398181603.\end{aligned} \tag{4.126}$$

This result fits to what we expect from (4.123). The numerical constant in (4.126) can be identified with

$$-2.398181603 := -\frac{7}{4}\zeta_2 + \text{Log}^2(2) = -2.398181603066195$$

within the precision of $O(10^{-7})$. This result reassures our intuitive picture that only those Feynman diagrams that are local move to the soft-collinear fusion contribute to the antenna function.

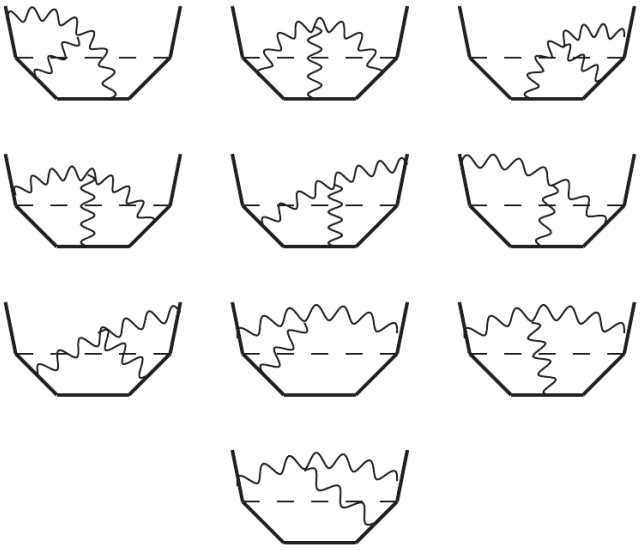

Figure 14: *Elements of TV. Regardless of n, there are always 5 relevant segment vectors for the soft-collinear kinematics. These 10 diagrams are expected to contribute to the leading IR singularities and hence to the antenna function.*

octagon $\longrightarrow$ hexagon

To convince that the antenna function we derived is universal for all n, we also computed the Chern-Simons part of the antenna function $\mathrm{Ant}^{(2)}_{\mathrm{CS}}[C_8]$ for the factorization of octagon C_8 to hexagon C_6. Again, the set of Feynman diagrams that contribute to the antenna function comes only from the triple-vertex diagrams and consists of the 10 diagrams TV. This is because there are 5 relevant edge vectors for the soft-collinear kinematics. In fact, upon careful diagrammatic considerations, we confirmed that this argument holds for arbitrary n.

Fortuitously, the 7 Feynman diagrams $\{I_{321},\, I_{432},\, I_{543},\, I_{421},\, I_{532},\, I_{431},\, I_{542}\}$ for the octagon C_8 are exactly the same as those for the hexagon C_6. The remaining three diagrams $\{I_{521},\, I_{541},\, I_{531}\}$ depend on the invariant $y_1 \cdot y_5$. We also need to modify this invariant according to the substitution

$$-2y_1\cdot y_5 = x_{25}^2 - x_{15}^2 - x_{26}^2 \quad \text{(Hexagon)} \quad \longrightarrow \quad -2y_1\cdot y_5 = x_{16}^2 + x_{25}^2 - x_{15}^2 - x_{26}^2 \quad \text{(Octagon)}, \tag{4.127}$$

from which we see that it generates an additional Mandelstam invariant x_{16}^2.

Such change of the Mandelstam invariant is an exception for the hexagon to octagon and

are not needed for the polygon with $n \geq 8$. That is, the sum of diagrams in the set TV yields the same result for all $n \geq 8$. Therefore, we expect the Chern-Simons contribution to the antenna function is the same for all $n \geq 8$. Of course, this is the feature we expect from the universality of the antenna function.

To evaluate the 10 diagrams belonging to the set TV, we start with the soft-collinear geometry of the octagon C_8:

$$y_2 \equiv h_1 y_C, \quad y_3 \equiv y_S, \quad y_4 = h_3 y_C, \quad h_1, h_3 \geq 0, \quad h_1 + h_3 = 1, \quad y_C^2 = 0 \quad y_S \simeq 0.$$

In this limit, the Mandelstam invariants scale as

$$x_{13}^2 = x_{14}^2 = h_1 x_{15}^2, \quad x_{46}^2 = x_{36}^2 = h_3 x_{26}^2, \quad x_{24}^2 = h_1 x_{25}^2, \quad x_{35}^2 = h_3 x_{25}^2, \quad x_{25}^2 = 2 y_C \cdot y_S$$

$$x_{47}^2 = h_3 x_{27}^2 + h_1 x_{57}^2, \quad x_{38}^2 = h_1 x_{58}^2 + h_3 x_{28}^2, \quad x_{37}^2 = h_1 x_{57}^2 + h_3 x_{27}^2, \quad x_{48}^2 = h_3 x_{28}^2 + h_1 x_{58}^2. \tag{4.128}$$

Algorithmically, we can generate this configuration starting from the hexagon by adding two edge vectors y_7 and y_8 and then imposing the Euclidean condition. The results of our numerical computation are summarized in Table 6. The results suggest that the finite part of the antenna function is independent of the choice of input Mandelstam invariants and that its numerical value is consistent with the numerical value extracted from the hexagon counterpart $\text{Ant}^{(2)}_{\text{CS, finite}}$.

From the numerical results based on the hexagon and octagon Wilson loops, we find that the Chern-Simons contribution to the two-loop antenna function is given by

$$\begin{aligned}\text{Ant}^{(2)}_{\text{CS}}[C_n] = &\frac{\text{Log}(2)}{2\varepsilon} \\ &+ \frac{1}{2}\text{Log}(2)\,\text{Log}(z_1) + \frac{1}{2}\text{Log}(2)\,\text{Log}(h_3) + \frac{1}{2}\text{Log}(2)\,\text{Log}(x_{24}^2) + \frac{1}{2}\text{Log}(2)\,\text{Log}(x_{35}^2) \\ &- \frac{7}{4}\zeta(2) + \text{Log}^2(2).\end{aligned} \tag{4.129}$$

4.7.4 ABJM Antenna Function

The two-loop antenna function of the ABJM theory is then obtained by adding the matter-dependent contribution $\text{Ant}^{(2)}_{\text{matter}}[C_n]$ and the pure Chern-Simons contribution $\text{Ant}^{(2)}_{\text{CS}}[C_n]$ and

	$\{x_{13}^2, x_{24}^2, x_{35}^2, x_{46}^2, x_{57}^2, x_{68}^2, x_{17}^2, x_{28}^2, x_{14}^2, x_{25}^2, x_{36}^2, x_{47}^2, x_{58}^2,$ $x_{16}^2, x_{27}^2, x_{38}^2, x_{15}^2, x_{26}^2, x_{37}^2, x_{48}^2\}$	$\mathrm{Ant}_{\mathrm{CS}}[C_8]_{\mathrm{finite}}$
(1)	{-0.53645, -0.00010, -0.00010, -0.47705, -0.25192, -11.3322 -2.27493, -7.89600, -0.53633, -0.00020, -0.47688, -0.53960, -0.87527, -2.00140, -0.82752, -4.38564, -1.07288, -0.95403, -0.53974, -4.38553 }	-2.39734
(2)	{-2.35947, -0.00020, -0.00020, -3.04945, -12.433, -4.83899 -15.7136, -14.7954, -2.35936, -0.00040, -3.04955, -15.0670, -8.89897, -0.450812, -17.7019, -11.8471, -4.71903, -6.09920, -15.0677, -11.8471 }	-2.39495
(3)	{-1.25316, -0.00020, -0.00020, -2.83305, -25.2163, -5.38963 -40.8014, -13.3704, -1.25260, -0.00040, -2.83315, -27.9871, -5.72270, -1.94647, -30.7599, -9.54667, -2.50596, -5.66640, -27.9889, -9.5462 }	-2.39414
(4)	{-2.04042, -0.00020, -0.00020, -2.85248, -25.2976, -0.636597, -47.2655, -8.46627, -2.04047, -0.00040, -2.85243, -28.1002, -2.39373, -0.349137, -30.9049, -5.42984, -4.08109,-5.70511, -28.1021, -5.42996 }	-2.39518
(5)	{-2.28437, -0.00010, -0.00010, -6.81235, -63.2938, -9.61232, -91.7177, -14.8614, -2.28411, -0.00020, -6.81221, -69.9258, -0.960108, -11.3101, -76.5589, -7.91075, -4.56858, -13.6247, -69.9268, -7.91066 }	-2.39859
(6)	{-0.654001, -0.00006, -0.00034, -5.93175, -30.7878, -3.90942, -60.0102, -8.71534, -0.653408, -0.00040, -5.93188, -36.6137, -0.131069, -7.86413, -37.6436, -7.42770, -4.35975, -6.97872, -36.6154, -7.42736 }	-2.38945

Table 9: *Numerical result for the Chern-Simons contribution to the two-loop antenna function* $Ant_{\mathrm{CS}}^{(2)}[C_8]_{\mathrm{finite}}$. *In numerical computation, we took* $x_{25}^2 \simeq 0$ *as a small quantity but not exactly zero. As we decrease* x_{25}^2, *we observed that* $Ant_{\mathrm{CS}}^{(2)}[C_8]_{\mathrm{finite}}$ *approaches to -2.39818.*

suitably rescaling the regulator energy scale. The result reads

$$
\begin{aligned}
&\mathrm{Ant}_{\mathrm{ABJM}}^{(2)} \\
&= \frac{1}{4\varepsilon^2} + \frac{1}{4\varepsilon}\left(\mathrm{Log}(z_1) + \mathrm{Log}(z_3) + \mathrm{Log}(x_{24}^2\hat{\mu}^2) + \mathrm{Log}(x_{35}^2\hat{\mu}^2)\right) \\
&+ \frac{1}{2}\mathrm{Log}(z_1)\mathrm{Log}(x_{24}^2\hat{\mu}^2) + \frac{1}{2}\mathrm{Log}(h_3)\mathrm{Log}(x_{35}^2\hat{\mu}^2) + \frac{1}{2}\mathrm{Log}(x_{35}^2\hat{\mu}^2)\mathrm{Log}(x_{24}^2\hat{\mu}^2) - \frac{1}{2}\mathrm{Log}(z_1)\mathrm{Log}(z_3) \\
&+ \frac{1}{2}\mathrm{Log}^2(2) - \frac{11}{4}\zeta(2). \qquad (4.130)
\end{aligned}
$$

Here, $\hat{\mu}^2 = 2\mu^2$ is the rescaled regularization scale. The result is independent of n, confirming our intuition that the IR factorization is a local move and hence the antenna function should be a universal quantity.

4.8 Recursion Relations and ABJM Wilson Loop Expecation Value

Having obtained the universal antenna function, in this section, we shall obtain the Wilson loop expectation value for arbitrary polygon with $n \geq 8$. The strategy is to utilize the lightlike factorization and derive recursion relations between Wilson loops for polygon contours C_n of

different n. Let's start with the Chern-Simons contribution. The two-loop antenna function takes the form

$$\mathrm{Ant}^{(2)}_{\mathrm{CS}}[C_n] = \mathrm{Ant}^{(2)}_{CS}[C_n]\Big|_{\mathrm{div}} + \mathrm{Ant}^{(2)}_{\mathrm{CS}}[C_n]\Big|_{\mathrm{finite}} \tag{4.131}$$

Here, $\mathrm{Ant}^{(2)}_{\mathrm{CS}}[C_n]\Big|_{\mathrm{div}}$ and $\mathrm{Ant}^{(2)}_{\mathrm{CS}}[C_n]\Big|_{\mathrm{finite}}$ are IR divergent, respectively, IR finite parts:

$$\begin{aligned}
\mathrm{Ant}^{(2)}_{\mathrm{CS}}[C_n]\Big|_{\mathrm{div}} &= \frac{\mathrm{Log}(2)}{2\varepsilon} + \frac{1}{2}\mathrm{Log}(2)\left[\mathrm{Log}(h_1) + \mathrm{Log}(h_3) + \mathrm{Log}(x_{24}^2) + \mathrm{Log}(x_{35}^2)\right] \\
\mathrm{Ant}^{(2)}_{\mathrm{CS}}[C_n]\Big|_{\mathrm{finite}} &= -\frac{7}{4}\zeta(2) + \mathrm{Log}^2(2).
\end{aligned} \tag{4.132}$$

In deriving the Wilson loop expectation value, we are primarily interested in the analytic structure of the remainder function $\mathrm{Rem}^{(2)}_{n,\mathrm{CS}}$. Therefore, it suffices to concentrate on the finite part, $\mathrm{Ant}^{(2)}_{\mathrm{CS}}[C_n]\Big|_{\mathrm{finite}}$.

Intuitively, we can guess for the IR finite part of the remainder function, $\mathrm{Rem}^{(2)}_{n,\mathrm{CS}} - \frac{n}{2}\mathrm{Log}(2)$. As a first step, consider $n = 8$ octagon. Before imposing the Gram sub-determinant conditions, there are twelve conformal cross-ratios for the octagon. The remainder function for the octagon is a function of these cross-ratios:

$$\mathrm{Rem}^{(2)}_{8,\mathrm{CS}} = \mathrm{Rem}^{(2)}_{8,\mathrm{CS}}\left(u_{14}, u_{25}, u_{36}, u_{47}, u_{58}, u_{16}, u_{27}, u_{38}, u_{15}, u_{26}, u_{37}, u_{48}\right) \tag{4.133}$$

In the soft-collinear limit, $y_2 \parallel y_4$ and $y_3 \sim 0$, these cross-ratios are restricted accordingly:

$$u_{14} = u_{25} = u_{36} = u_{38} = u_{37} = 1, \quad u_{15} = 0$$

$$u_{47} = \frac{1-u_{26}}{u_{48}}, \quad u_{27} = \frac{1-u_{48}}{u_{26}}. \tag{4.134}$$

On the other hands, in the soft-collinear limit, the octagon C_8 is reduced to the hexagon C_6, for which the following nine Mandelstam invariants are relevant:

$$x_{16}^2,\ x_{15}^2,\ x_{26}^2,\ x_{17}^2,\ x_{27}^2,\ x_{28}^2,\ x_{57}^2,\ x_{58}^2,\ x_{68}^2. \tag{4.135}$$

From these invariants, we can form the following three conformal cross-ratios:

$$u_{58} = \frac{x_{15}^2 x_{68}^2}{x_{58}^2 x_{16}^2}, \qquad u_{16} = \frac{x_{17}^2 x_{26}^2}{x_{16}^2 x_{27}^2}, \qquad u_{27}u_{37}u_{47} = \frac{x_{28}^2 x_{57}^2}{x_{27}^2 x_{58}^2} \tag{4.136}$$

Therefore, by the lightlike factorization, the finite part of the antenna function $\mathrm{Ant}^{(2)}_{\mathrm{CS}}[C_8]\Big|_{\mathrm{finite}}$ must be reduced to

$$\begin{aligned}
&\mathrm{Rem}^{(2)}_{8,\mathrm{CS}}\big(1,1,1,(1-u_{26})/u_{48},u_{58},u_{16},(1-u_{48})/u_{26},1,0,u_{26},1,u_{48}\big)-4\mathrm{Log}(2)\\
&=\mathrm{Rem}^{(2)}_{6,\mathrm{CS}}\big(u_{58},u_{16},u_{27}u_{37}u_{47}\big)-3\mathrm{Log}(2)+\mathrm{Ant}^{(2)}_{\mathrm{CS}}[C_8]\Big|_{\mathrm{finite}}\\
&=\mathrm{Rem}^{(2)}_{6,\mathrm{CS}}\big(u_{58},u_{16},u_{27}u_{37}u_{47}\big)-3\mathrm{Log}(2)-\frac{7}{4}\zeta(2)+\mathrm{Log}^2(2)\\
&=-6\zeta(2)+4\mathrm{Log}^2(2).
\end{aligned}\tag{4.137}$$

In the last expression, we used the numerical result that $\mathrm{Rem}^{(2)}_{6,\mathrm{CS}}\big(u_{58},u_{16},u_{27}u_{37}u_{47}\big)$ is a constant, independent of the input values of the conformal cross-ratios.

With such restricted information, it is impossible to determine general structure of the remainder function $\mathrm{Rem}^{(2)}_{8,\mathrm{CS}}(u_{14},u_{25},u_{36},\cdots,u_{48})$. However, for a given analytic structure of the remainder function, its soft-collinear limit should be controlled by the universal antenna function. This enables us to draw a conjecture that is consistent with the soft-collinear geometry to be

$$\mathrm{Rem}^{(2)}_{8,\mathrm{CS}}=-6\zeta(2)+4\mathrm{Log}^2(2)+4\mathrm{Log}(2).\tag{4.138}$$

In other words, our conjecture is that the remainder function is independent of the twelve conformal cross-ratios. Moreover, utilizing numerical evidence that $\mathrm{Rem}^{(2)}_{n,\mathrm{CS}}$ is constant-valued for arbitrary n, we find that the remainder function obeys the recursion relation

$$\boxed{\mathrm{Rem}^{(2)}_{n,\mathrm{CS}}-\frac{n}{2}\mathrm{Log}(2)=\mathrm{Rem}^{(2)}_{n-2,\mathrm{CS}}-\frac{n-2}{2}\mathrm{Log}(2)+\mathrm{Ant}^{(2)}_{\mathrm{CS}}[C_n]\Big|_{\mathrm{finite}}.}\tag{4.139}$$

We can now iteratively solve this recursion relation along with our conjecture as the input:

$$\begin{aligned}
\mathrm{Rem}^{(2)}_{n,\mathrm{CS}}-\frac{n}{2}\mathrm{Log}(2)&=\mathrm{Rem}^{(2)}_{n-2,\mathrm{CS}}-\frac{n-2}{2}\mathrm{Log}(2)+\mathrm{Ant}^{(2)}_{\mathrm{CS}}[C_n]\Big|_{\mathrm{finite}}\\
&=\mathrm{Rem}^{(2)}_{n-2,\mathrm{CS}}-\frac{n-2}{2}\mathrm{Log}(2)-\frac{7}{4}\zeta(2)+\mathrm{Log}^2(2)\\
&=\cdots\\
&=\mathrm{Rem}^{(2)}_{6,\mathrm{CS}}-3\mathrm{Log}(2)+\frac{n-6}{2}\big(-\frac{7}{4}\zeta(2)+\mathrm{Log}^2(2)\big)\\
&=\big[\frac{1}{2}\mathrm{Log}^2(2)-\frac{7\pi^2}{48}\big]n+\frac{\pi^2}{6}.
\end{aligned}\tag{4.140}$$

Our conjecture is further supported by numerical estimation of $\mathrm{Rem}^{(2)}_{n,\mathrm{CS}}$ for $n=8,10,12,\cdots,20$ [50].

Putting together, we now have the analytic result for the Chern-Simons contribution to the lightlike polygon Wilson loop expectation value as

$$\left\langle W_{\square}[C_n]\right\rangle^{(2)}_{\rm CS} = -\frac{\mathrm{Log}(2)}{2}\sum_{i=1}^{n}\frac{(x^2_{i,i+2}\pi e^{\gamma_E}\mu^2)^{2\varepsilon}}{2\varepsilon} + n\left(\frac{7\pi^2}{48} - \frac{1}{2}\mathrm{Log}^2(2)\right) - \frac{\pi^2}{6}. \qquad (4.141)$$

Combining with the matter contribution (4.42), we finally arrives at the central result of this paper:

$$\boxed{\left\langle W_{\square}[C_n]\right\rangle^{(2)}_{\rm ABJM} = -\frac{1}{2}\sum_{i=1}^{n}\frac{(x^2_{i,i+2}8\pi e^{\gamma_E}\mu^2)^{2\varepsilon}}{(2\varepsilon)^2} + \mathrm{BDS}^{(2)}_n + n\left(\frac{\pi^2}{12} + \frac{3}{4}\mathrm{Log}^2(2)\right) - \frac{\pi^2}{6}.} \qquad (4.142)$$

4.9 Circular Wilson Loop

In this section, we shall study the $n \to \infty$ limit of our result. In Euclidean geometry, a circle (more generally an ellipse) can be obtained from a polygon C_n by inscribing its cusps to touch the circle and taking the continuum limit $n \to \infty$. In Lorentzian geometry, a spacelike circle (more generally an ellipse) can be obtained from a lightlike polygon C_n by inscribing its edges to cross the circle and taking the continuum limit $n \to \infty$. It should therefore be possible to obtain the spacelike circular Wilson loop expectation value from the continuum limit of the lightlike polygon Wilson loop expectation value. [31]

Evidently, the biggest differnce between spacelike circular Wilson loop and lightlike polygon Wilson loop is the existence of cusps. Associated with these cusps are the UV divergences. The divergent parts are essentially abelian and they get exponentiated and factor out. The remaining finite part should then correspond to the spacelike circular Wilson loop expectation value.

To obtain the circular Wilson loop, we shall set location of the n cusps [64] as

$$x_{2k} = (2\sin\frac{\pi}{2n}, \quad \cos\frac{(2k+1)\pi}{n}, \quad \sin\frac{(2k+1)\pi}{n}), \qquad x_{2k+1} = (0, \quad \cos\frac{2k\pi}{n}, \quad \sin\frac{2k\pi}{n}) \qquad (4.143)$$

This kinematics yields a polygon whose contour is sandwiched between two spacelike cir-

cles. Mandelstam invariants of the polygon are given by

$$x_{2k,2j}^2 = -4\sin^2\frac{(k-j)\pi}{n} \tag{4.144}$$

$$x_{2k+1,2j+1}^2 = x_{2k,2j}^2 \tag{4.145}$$

$$x_{2k,2j+1}^2 = 4\left(\sin^2\frac{\pi}{2n} - \sin^2\frac{(k-j-\frac{1}{2})\pi}{n}\right) \tag{4.146}$$

Evidently, the polygon satisfy Euclidean condition and the closedness condition. Also, $(x_{2k+1} - x_{2k})^2 = 0$ holds.

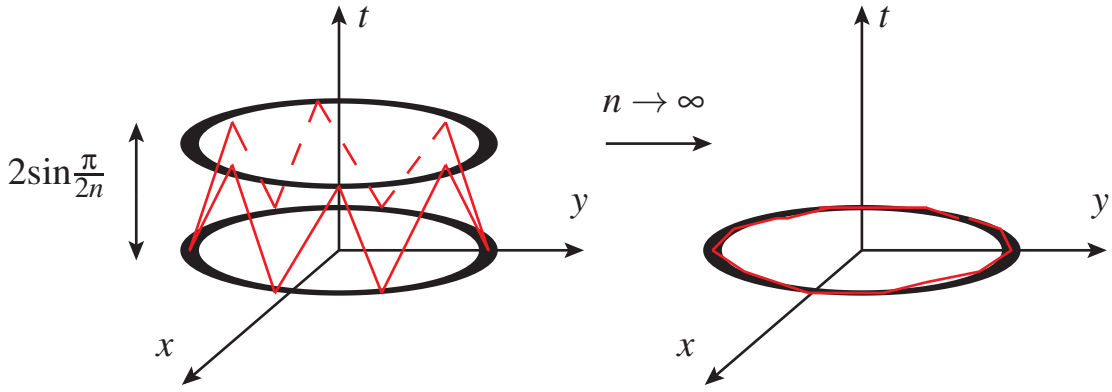

Yet, as we mentioned in Section 3, this $(1+1)$-dimensional kinematics do not satisfy the Gram sub-determinant conditions. While this is true for finite n, we now argue that the conditions are met in the $n \to \infty$ limit.

First focus on the pure Chern-Simons contribution. As we calculated, our expectation is

$$\langle W_\square[C_n]\rangle_{\rm CS}^{(2)} = -\frac{\mathrm{Log}(2)}{2}\sum_{i=1}^{n}\frac{(x_{i,i+2}^2\pi e^{\gamma_E}\mu^2)^{2\varepsilon}}{2\varepsilon} + n\left(\frac{7\pi^2}{48} - \frac{1}{2}\mathrm{Log}^2(2)\right) - \frac{\pi^2}{6}. \tag{4.147}$$

when configuration saatisfies Gram sub-determinant conditions. Note that $(k\times k)$ Gram sub-determinant conditions consist of k-th power of $\sin^2\frac{\pi}{n}$, because of all the Mandelstam invariants (4.146) accompanied with the factor of $\sin^2\frac{\pi}{n}$. For finite n, we see that these invariants do not satisfy the Gram sub-determinant conditions. Therefore, the structure (4.147) is not valid for finite n. However, for large n, all the Gram sub-determinant goes to zero, therefore Eq.(4.147) will be valid. Geometrically, distance between the two enveloping circles $2\sin\frac{\pi}{2n}$ goes to 0, and the polygon collapses to a spacelike circle. This explained in Figure 4.9.

Dropping off the UV divergent parts,

$$\left\langle W_{\square}[C_n]\right\rangle^{(2)}_{\rm CS}\Big|_{\rm finite} = n\left(\frac{7\pi^2}{48}-\frac{1}{2}{\rm Log}^2(2)\right)-\frac{\pi^2}{6}. \tag{4.148}$$

We note that the result is independent of the kinematics of C_n (the shape of the polygon). This fits well with the expectation that the pure Chern-Simons theory is topological. The continuum limit $n\to\infty$ gives rise to a linear divergence proportional to the perimeter $n:=2\pi R/a$ for a circle of radius R and short-distance measure a. It would be very interesting to understand this from the viewpoint of polygon regularization of the topological link invariants.

For the matter-dependent part, the lightlike polygon Wilson loop expectation value was

$$\left\langle W_{\square}[C_n]\right\rangle^{(2)}_{\rm matter} = \quad -\frac{1}{2}\sum_{i=1}^{n}\frac{1}{(2\varepsilon)^2}(x^2_{i,i+2}4\pi e^{\gamma_E}\mu^2)^{2\varepsilon}+{\rm BDS}^{(2)}_n-\frac{1}{16}n\pi^2+O(\varepsilon). \tag{4.149}$$

Dropping off the UV divergent part,

$$\left\langle W_{\square}[C_n]\right\rangle^{(2)}_{\rm matter}\Big|_{\rm finite} = -{\rm Li}_2(1-as)-{\rm Li}_2(1-at)+{\rm Li}_2(1-aP^2)+{\rm Li}_2(1-aQ^2)-\frac{1}{16}n\pi^2. \tag{4.150}$$

We recall the parameters were defined by

$$a=\frac{s+t-P^2-Q^2}{st-P^2Q^2},\quad P^2=x^2_{i,j+2},\quad Q^2=x^2_{i+1,j},\quad s=x^2_{i,j},\quad t=x^2_{i+1,j+1}. \tag{4.151}$$

Unlike the pure Chern-Simons part, the matter-dependent part is sensitive to the kinematics of C_n (the shape of the polygon) The next step is to consider a suitable kinematics so that the lightlike polygon C_n asymptotes to the spacelike circle C. This regular polygon kinematics is given in (4.144), (4.145) and (4.146). We took this kinematics to $\left\langle W_{\square}[C_n]\right\rangle^{(2)}_{\rm matter}\Big|_{\rm finite}$ and evaluated its value numerically with respect to n.

Geometric property of regular polygon implies $x^2_{i,j}=x^2_{i+1,j+1}=\cdots=x^2_{i-1,j-1}$. This leads,

$$I_{i,j}=I_{i+1,j+1}=\cdots=I_{i-1,j-1} \tag{4.152}$$

Also, let define $F(n)$ and $f(n)$ by

$$F(n) \equiv \sum_{\substack{i>j \\ i\neq j+1}} I_{i,j} = \sum_{\substack{\text{permutation} \\ \text{of j*}}} \sum_{i=j*+2}^{n+j*-2} I_{i,j=j*}$$
$$f(n) \equiv \sum_{i=j*+2}^{n+j*-2} I_{i,j=j*} \tag{4.153}$$

Here $j*$ is some fixed number. By definition, $F(n)$ is related to $\left\langle W_{\square}[C_n]\right\rangle^{(2)}_{\text{matter}}|_{\text{finite}}$. Also, (4.152) gaurantees that $F(n) = nf(n)$.

We make a fitting funtion for $f(n)$ by $f(n) = \frac{a}{n^2} + \frac{b}{n} + c$. As we seen in Figure (15), this fitting function works well. Each coefficients a, b, c are estimated by

$$a = -21.1513(\pm 0.005399), \quad b = 9.85953(\pm 0.001135), \quad c = -0.573233(\pm 2.458e-005) \tag{4.154}$$

Among them, value of b is closed to $\pi^2 = 9.869604401$.

From this observation, we expect

$$\left\langle W_{\square}[C_n]\right\rangle^{(2)}_{\text{matter}}|_{\text{finite}} = F(n) = \frac{a}{n} + \pi^2 + cn \tag{4.155}$$

First term will be decays at $n \to \infty$ limit.

Eventually, we expect UV finite part of regular polygon Wilson loop expectation value at large n limit by

$$\begin{aligned}\left\langle W_{\square}[C^{\text{regular}}_n]\right\rangle^{(2)}_{\text{ABJM}}|_{\text{finite}} &= \left\langle W_{\square}C^{\text{regular}}_n]\right\rangle^{(2)}_{\text{matter}}|_{\text{finite}} + \left\langle W_{\square}[C^{\text{regular}}_n]\right\rangle^{(2)}_{\text{CS}}|_{\text{finite}} \\ &= \rho n + \left(\pi^2 - \frac{\pi^2}{6}\right)\end{aligned} \tag{4.156}$$

In n-independent constant, π^2 came from above numerical fitting and $-\frac{\pi^2}{6}$ inherited from constant in $\left\langle W_{\square}[C_n]\right\rangle^{(2)}_{\text{CS}}|_{\text{finite}}$. In [40], circular (space-like)Wilson loop expectation value in ABJM theory calculated and result was given by,

$$\left\langle W_{\square}[\bigcirc]\right\rangle_{\text{ABJM}} = 1 + \lambda^2\left(\pi^2 - \frac{\pi^2}{6}\right) + \cdots \tag{4.157}$$

Also, matrix model computation for $\frac{1}{6}$ BPS Wilson loop result was [67],

$$\left\langle W_{\square}[\bigcirc]\right\rangle_{\text{ABJM}} = 1 + \frac{5\pi^2}{6}\lambda^2 + O(\lambda^3) \tag{4.158}$$

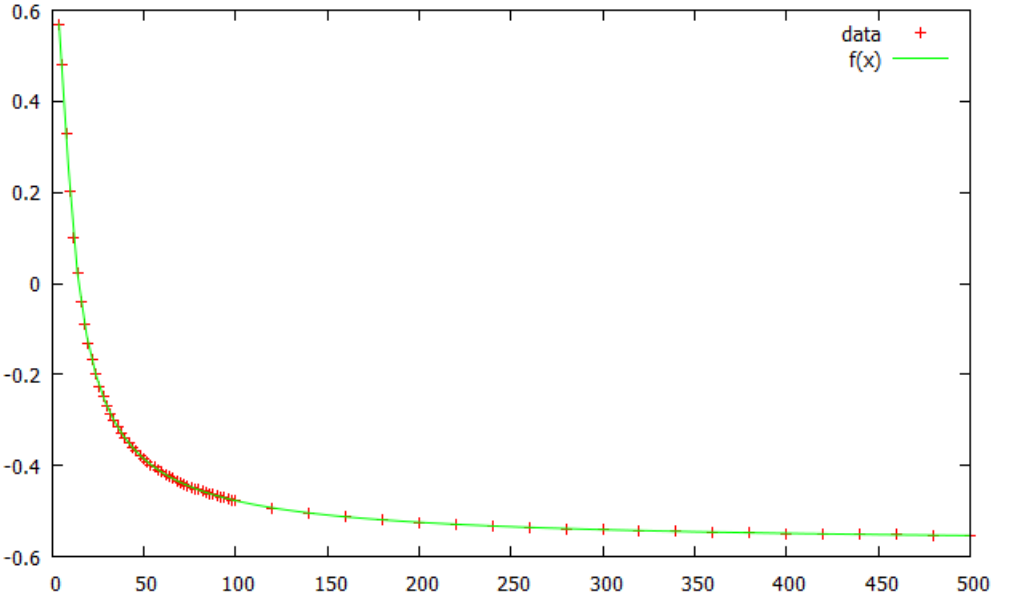

Figure 15: Figure 7 *Large n behavior of the lightlike regular polygon Wilson loop expectation value*

Our result in large n limit (4.156) exibits same result.

Chapter 5

Outro

The several nonperturbative approaches in conformal field theory was mainly focused in this thesis. Especially, we considered two specific observables defined in conformal field theory : 4-point correlation function and polygonal Wilson loop expectation value. Since conformal symmetry is sufficiently powerful, part of structure of them can be fixed. For instance, we discussed about conformal Casimir equation for correlation function and anomalous conformal Ward identity for polygonal Wilson loop expectation value.

The conformal bootstrap method is intrinsically non-perturbative method. Already this method succesfully obtained numerical value of critical exponent, without any perturbative computation. Not only 3-dimensional IR fixed point, but also 5-dimensional UV fixed point is also specified by conformal bootstrap.

One of the remarkable progress of recent is mixed correlation bootstrap. The semi-definite program enables analyzing mixed 4-point correlation function. In this work, they assumed only two fields σ and ϵ are relevant operators. When all possible mixed 4-point correlation function which respects $\mathbb{Z}_2$ symmetry is considered, surprisingly allowed region localized on isolated area near Ising theory. This may suggests that the only unitary theory which consistent with crossing symmetry in 3-dimensional field theory is Ising class.

When we made a conjecture on structure of 2-loop Wilson loop expectation value for arbitrary n, we utilized soft/collinear limit. To be consistent with Gram determinant constraint, we observed only soft-collinear limit is available for Wilson loop defined in ABJM theory.

Recently, this kind of unresolved limit was highlighted again. Especially, soft behavior of scattering amplitude defined in gravity or gauge theory is quiet interesting. The old Weinberg's theorem or Low theorem predicted the universal factorization under soft limit. Strominger et.al showed this universal behavior can be understood as Ward identity of new hidden symmetry, that is BMS supertranslation symmetry. Likewise, they also insisted that the Low theorem can be interpreted by 2D Kac-Moody algebra. Also, higher-order correction of soft theorem is obtained by utilizing BCFW recursion relation.

However, as we observed throughout polygonal Wilson loop, collinear kinematics also shows universal factorization. In the case of gravity theory, it was already showed that collinear divergence suitably canceled, and the only IR divergence contributes to inclusive

amplitude is soft limt. But for the gauge theory, no such restrict exist and we can consider both soft and collinear kinematics. Does collinear factorization also related to some hidden symmetry? It would be interesting to investigate behavior of observables under specific kinematics.

The idea of renormalization group flow(RG flow) is often used in various theoretical physics. Often they utilized to analyze theory at IR limit. For example, we can consider $\mathcal{N} = (2,2)$ gauge linear sigma model defined in 2-dimension. The localization technique enables computing partition function of this system, and the result is independent from coupling constant. This means that we can use this partition function to extract some information of IR limit. Indeed, this theory expected to be flow into non-linear sigma model at IR fixed point. One of the non-trivial object in this limit is the Gromov-Witten invariant, which counts instantons defined on world sheet. The partition function of GLSM can be utilized to extract this Gromov-Witten invariant at least for genus 0 case.

So far we discussed only very specific case of RG flow. In this thesis, we mainly focused special class of RG flow that has starting UV fixed point and ending IR fixed point. Manifestly this is not all the case. For the case of the QED, when we flow into IR area, the massive electron fields are integrated out and only massless photons are remains. By the way, if we considering pure Yang-Mills theory, it is known that is has massive spectrum(glueball) at IR limit, due to dimensional transmutation. This kind of class often called by mass-gap theory. These kind of non-trivial IR physics is not easy to understand since most of these physics requires non-perturbative analysis. Moreover, the degree of freedom of IR physics is often not well matched with DOF of UV physics. The typical example is QCD. In this theory, the fundametal object is quark. However, confinement arose at IR limit and effective action of it is decribed by meson field rather than quark itself. The another example is chiral symmetry breaking $G = SU(N_F)_L \times SU(N_F)_R$ to $H = SU(N_F)_D$. As a result, one of the effective field in IR limit is pion. This pion field can be understood as Goldstone boson of quotient group G/H.

Therefore, in generic case, understanding IR physics is non-trivial problem. We don't know what is good degree of freedom, or what is interaction of them. For specific case like IR theory is scale invariant or supersymmetric case(like Seiberg-Witten description) maybe we can partially answer about IR physics. The lesson of these case study would guide us to the way of understanding non-perturbative IR physics.

Bibliography

[1] S. Coleman and J. Mandula, "All Possible Symmetries of the S Matrix", Phys. Rev. 159, 1251(1967).

[2] J.A.Lipa, D.R.Swanson, J.A.Nissen, T.C.P.Chul and U.E.Israelsson, "Heat Capacity and Thermal Relaxation of Bulk Helium very near the Lambda Point", Phys. Rev. Lett. 76, 944(1996).

[3] G. Veneziano, "Construction of a Crossing-Symmetric Regge-Behaved Amplitude for Linearly Rising REgge Trajectories", Nuovo Cim. 57A, 190(1968).

[4] L. Fei, S. Giombi and I. Klebanov, "Critical $O(N)$ Models in $6-\varepsilon$ Dimensions", arXiv:1404.1094 [hep-th].

[5] L. Fei, S. Giombi, I. Klebanov and G. Tarnopolsky, "Three Loop Analysis of the Critical $O(N)$ Models in $6-\varepsilon$ Dimensions", arXiv:1411.1099 [hep-th].

[6] F. Kos, D. Poland and D. Simmons-Duffin, "Bootstrapping the $O(N)$ Models", arXiv:1307.6856 [hep-th].

[7] F. A. Dolan and H. Osborn, "Conformal Four Point Functions ans the Operator Product Expansion", arXiv:0011040 [hep-th].

[8] F. A. Dolan and H. Osborn, "Conformal Partial Waves : Futher Mathematical Results", arXiv:1108.6194 [hep-th].

[9] S. Ferrara, R. Gatto and A. F. Grillo, "Conformal Invariance on the Light cone and Canonincal Dimensions", Nucl. Phys. B34(1971), p.349.

[10] G. Mack, "Convergence of Operator Product Expansions on the Vacuum in Conformal Invariant Quantum Field Theory", Commun. math. Phys53, 155-184(1977).

[11] S. El-Showk, M. F. Paulos, D. Poland, S. Rychkov, D. Simmons-Duffin and A. Vichi, "Solving the 3D Ising Model with the Conformal Bootstrap", arXiv:1203.6064 [hep-th].

[12] R. Guida and J. Zinn-Justin, "Critical exponents of the N vector model", arXiv:9803240 [cond-mat].

[13] Y. Deng and H. W. J. Blote, "Simultaneous analysis of several models in the three dimensional ising universality class", Phys. Rev. E 68(2003).

[14] S. El-Showk, M. F. Paulos, D. Poland, S. Rychkov, D. Simmons-Duffin and A. Vichi, "Solving the 3D Ising Model with the Conformal Bootstrap II", arXiv:1403.4545 [hep-th].

[15] A. M. Polyakov, "Non-Hamiltonian approach to conformal quantum field theory", Zh. Eksp. Teor. Fiz. 66, 23-42(1974).

[16] R. Rattazzi, S. Rychkov, E. Tonni and A. Vichi, "Bounding scalar operator dimensions in 4D CFT", arXiv:0807.0004 [hep-th].

[17] D. Poland, D. Simmons-Duffin and A. Vichi, "Carving Out the Space of 4D CFTs", arXiv:1109.5176 [hep-th].

[18] M. Hogervorst and S. Rychkov, "Radial Coordinates for Conformal Blocks", arXiv:1303.1111 [hep-th].

[19] Y. Nakayama and T. Ohtsuki, "Five dimensional $O(N)$-symetruc CFTs from conformal bootstrap", arXiv:1404.5201 [hep-th].

[20] F. Gliozzi and A. Rago, "Critical exponents of the 3d Ising and related models from Conformal Bootstrap", arXiv:1403.6003 [hep-th].

[21] X. Bekaert, E. Joung and J. Mourad, "Comments on higher-spin holography", arXiv:1202.0543 [hep-th].

[22] I. Klebanov and A. M. Polyakov, "AdS dual of the critical $O(N)$ vector model", arXiv:0210114 [hep-th].

[23] A. Vichi, "Improved bounds for CFT's with global symmetries", arXiv:1106.4037 [hep-th].

[24] D. J. Broadhurst and A .V. Kotikov, "Compact anayltical form for non-zeta terms in critical exponents at order $\frac{1}{N^3}$", arXiv:1106.4037 [hep-th].

[25] O. Aharony, O. Bergman, D. L. Jafferis, J. Maldacena "*N=6 superconformal Chern-Simons-matter theories, M2-branes and their gravity duals*," arXiv:0806.1218 [hep-th].

[26] J. M. Drummond, J. Henn, G. P. Korchemsky, E. Sokatchev "*On planar gluon amplitude/Wilson loops duality*," arXiv:0709.2368 [hep-th].

[27] J. M. Drummond, J. Henn, G. P. Korchemsky, E. Sokatchev "*Conformal Ward identities for Wilson loops and a test of the duality with gluon amplitudes*," arXiv:0712.1223 [hep-th].

[28] Z. Bern, L. Dixon, V. A. Smirnov "*Iteration of Planar Amplitudes in Maximally Supersymmetric Yang-Mills Theory at Three Loops and Beyond*," arXiv:0505205 [hep-th]

[29] J. M. Drummond, J. Henn, G. P. Korchemsky, E. Sokatchev "*The hexagon Wilson loop and the BDS anstaz for the six-gluon amplitude*," arXiv:0712.4138 [hep-th].

[30] Z. Bern, L. Dixon, D. Kosower, R. Roiban, M. Spradlin, C.Vergu, A. Volovich "*The two-loop Six-Gluon MHV Amplitude in Maximally Supersymmetric Yang-Mills Theory*," arXiv:0803.1465 [hep-th]

[31] L. F. Alday, J. Maldacena "*Gluon scattering amplitudes at strong coupling*," arXiv:0705.0303 [hep-th].

[32] L. F. Alday, J. Maldacena "*Null polygonal Wilson loops and minimal surfaced in Anti-de-Sitter space*," arXiv:0904.0663 [hep-th].

[33] C. Anastasiou, A. Brandhuber, P. Heslop, V. V. Khoze, B. Spence, G. Travaglini "*Two-Loop Polygon Wilson Loops in N=4 SYM*," arXiv:0902.2245 [hep-th].

[34] J. M. Drummond, J. Henn, G. P. Korchemsky, E. Sokatchev "*Dual superconformal symmetry of scattering amplitude in N=4 super-Yang-Mills theory*," arXiv:0807.1095 [hep-th].

[35] V. D. Duca, C. Duhr, V. A. Smirnov "*The Two-Loop Hexagon Wilson Loop in N=4 SYM*," arXiv:1003.1702 [hep-th].

[36] A. B. Goncharov, M. Spradlin, C. Vergu, A. Volovich "*Classical Polylogarithms for Amplitudes and Wilson Loops*," arXiv:1006.5703 [hep-th].

[37] P. Heslop, V. V. Khoze "*Wilson Loops @ 3-Loops in Special Kinematics*," arXiv:1109.0058 [hep-th].

[38] L .J .Dixon, J. M. Drummond, J. M. Henn "*Bootstrapping the three-loop hexagon*," arXiv:1108.4461 [hep-th].

[39] L .J .Dixon, J. M. Drummond, J. M. Henn "*Analytic result for the two-loop six-point NMHV amplitude in N=4 super Yang-Mills theory*," arXiv:1111.1704 [hep-th].

[40] S. -J Rey, T. Suyama, S. Yamaguchi "*Wilson Loops in Superconformal Chern-Simons Theory and Fundamental Strings in Anti-de Sitter Supergravity Dual*," arXiv:0809.3786 [hep-th].

[41] N. Drukker, J. Plefka, D. Young "*Wilson loops in 3-dimensional N=6 supersymmetric Chern-Simons Theory and their string theory duals*," arXiv:0809.2787 [hep-th].

[42] J. M. Henn, J. Plefka, K. Wiegandt "*Light-like polygonal Wilson loops in 3d Chern-Simons and ABJM theory*," arXiv:1004.0226 [hep-th].

[43] W. Chen, Y. Huang "*Dualities for Loop Amplitudes of N=6 Chern-Simons Matter theory*," arXiv:1107.2710 [hep-th].

[44] M. S. Bianchi, M. Leoni, A. Mauri, S. Penati, A. Santambogio "*Scattering Amplitudes/Wilson Loop Duality in ABJM Theory*," arXiv:1107.3139 [hep-th].

[45] M. S. Bianchi, M. Leoni, S. Penati "*An all order identity between ABJM and N=4 SYM four-point amplitudes*," arXiv:1112.3649 [hep-th].

[46] T. Bargheer, N. Beisert, F. Loebbert, T. McLoughlin "*Conformal Anomaly for Amplitudes in N=6 Superconformal Chern-Simons Theory*," arXiv:1204.4406 [hep-th].

[47] M. Bianchi, M. Leoni, A. Mauri, S, Penati, A. Santambrogio "*One Loop Amplitudes in ABJM*," arXiv:1204.4407 [hep-th].

[48] A. Brandhuber, G. Travaglini, C. Wen "*All one-loop amplitudes in N=6 superconformal Chern-Simons theory*," arXiv:1207.6908 [hep-th].

[49] Y. Huang, S. Caron-Huot "*The two-loop six-point amplitude in ABJM theory*," arXiv:1210.4226 [hep-th].

[50] K. Wiegandt "*Equivalence of Wilson Loops in ABJM and N=4 SYM Theory*," arXiv:1110.1373 [hep-th].

[51] E. Guadagnini, M. Martellini, M. Mintchev "*Wilson lines in Chern-Simons theory and link invariants*," Nuclear Physics B330(1990) 575-607.

[52] A. Brandhuber, P. Heslop, G. Travaglini "*MHV Amplitude in N=4 Super Yang-Mills and Wilson Loops*," arXiv:0707.1153 [hep-th].

[53] M. Czakon "*Automatized analytic continuation of Mellin-Barnes integrals*," arXiv:0511200 [hep-ph].

[54] A. V. Smirnov, V. A. Smirnov, M. Tentyokov "FIESTA 2 *:parallelizeable multiloop numerical calculations*," arXiv:0912.0158 [hep-ph].

[55] A. V. Smirnov, V. A. Smirnov "*On the Resolution of Singularities of Multiple Mellin-Barnes Integrals*," arXiv:0901.0386 [hep-ph].

[56] D. A. Kosower "barnesroutines," http://projects.hepforge.org/mbtools/.

[57] D. A. Kosower "*Multiple Singular Emission in Gauge Theories* ," arXiv:0212097 [hep-ph].

[58] F.A. Berends and W.T. Giele "*Recursive calculations for processes with n gluons*," Nucl. Phys. B306 (1988) 759.

[59] M. Czakon "MBasymptotics," http://projects.hepforge.org/mbtools/.

[60] Z. Bern, V. D. Duca, W. B. Kilgore, C. R. Schmidt "*The Infrared Behavior of One-Loop QCD Amplitudes at Next-to-Next-to-Leading Order*," arXiv:9903516 [hep-ph].

[61] Z. Kormagodski "*On collinear factorization of Wilson loops and MHV amplitude in N=4 SYM*," arXiv:0801.3274 [hep-th].

[62] Z. Bern, L. J. Dixon, D. A. Kosower, R. Roiban, M. Spradlin, C. Vergu, A. Volovich "*The Two-Loop Six Gluon MHV Amplitude in Maximally Supersymmetric Yang-Mills Theory*," arXiv:0803.1465 [hep-th].

[63] D. A. Kosower "*All-Order Collinear Behavior in Gauge Theories*," arXiv:9901201 [hep-ph].

[64] A. Brandhuber, P. Heslop, V. V. Khoze, G. Travaglini "*Simplicity of Polygon Wilson Loops in N=4 SYM*," arXiv:0910.4898 [hep-th].

[65] S. -J. Rey, J. T. Yee "*Macroscopic strings as heavy quarks in large N gauge theory and anti de-Sitter supergravity*," arXiv:9803001 [hep-th].

[66] J. Maldacena "*Wilson loops in large N field theories*," arXiv:9803002 [hep-th].

[67] M. Marino, P. Putrov "*Exact results in ABJM theory from topological strings*," arXiv:0912.3074 [hep-th].

[68] M. Bianchi, G. Giribet, M. Leoni, S. Penati "*Light-like Wilson loops in ABJM and maximal transcendentality*," arXiv:1304.6085 [hep-th].

Appendices

Chapter A

Appendix A : Notation, Convention and Feynman Rules

In this section, we present our notations for calculation.

• $\mathbb{R}^{1,2}$ metric:

$$g_{mn} = \text{diag}(-,+,+) \quad \text{with} \quad m,n = 0,1,2$$
$$\varepsilon^{\mu\nu\rho}\varepsilon_{\alpha\beta\gamma} = -\det\begin{pmatrix} \delta^{\mu}_{\alpha} & \delta^{\mu}_{\beta} & \delta^{\mu}_{\gamma} \\ \delta^{\nu}_{\alpha} & \delta^{\nu}_{\beta} & \delta^{\nu}_{\gamma} \\ \delta^{\rho}_{\alpha} & \delta^{\rho}_{\alpha} & \delta^{\rho}_{\alpha} \end{pmatrix} \tag{A.1}$$

• Gauge and global symmetries of ABJM theory

$$\begin{aligned} &\text{Gauge symmetry : U(N)} \times \overline{\text{U(N)}} \\ &\text{Global symmetry : SU(4)} \end{aligned} \tag{A.2}$$

We denote trace over U(N) and $\overline{\text{U(N)}}$ as Tr and $\overline{\text{Tr}}$, respectively. We also denote generators for U(N) and $\overline{\text{U(N)}}$ gauge groups by the same notation T^a,$(a = 0,1,\cdots,N^2-1)$. They are Hermitian and normalized to

$$\text{Tr}(T^a T^b) = \frac{1}{2}\delta^{ab} \tag{A.3}$$

• Chern-Simons part of ABJM action is :

$$S_{CS} = \frac{k}{4\pi}\int d^d x \varepsilon^{\mu\nu\rho}\text{Tr}\Big(A_\mu \partial_\nu A_\rho - \frac{2i}{3}A_\mu A_\nu A_\rho\Big) \tag{A.4}$$
$$\overline{S}_{CS} = -\frac{k}{4\pi}\int d^d x \varepsilon^{\mu\nu\rho}\overline{\text{Tr}}\Big(\overline{A}_\mu \partial_\nu \overline{A}_\rho - \frac{2i}{3}\overline{A}_\mu \overline{A}_\nu \overline{A}_\rho\Big) \tag{A.5}$$
$$S_{\text{gauge fixing}} = \frac{k}{4\pi}\int d^d x\Big[\frac{1}{\xi}\text{Tr}(\partial_\mu A^\mu)^2 + \text{Tr}(\partial_\mu c^* D_\mu c)\Big] \tag{A.6}$$
$$\overline{S}_{\text{gauge fixing}} = -\frac{k}{4\pi}\int d^d x\Big[\frac{1}{\xi}\overline{\text{Tr}}(\partial_\mu \overline{A}^\mu)^2 + \overline{\text{Tr}}(\partial_\mu \overline{c}^* D_\mu \overline{c})\Big] \tag{A.7}$$

Here A_μ is in adjoint representation of U(N) while $\overline{A_\mu}$ is in adjoint representation of $\overline{\text{U(N)}}$. $S_{\text{gauge fixing}}$ and $\overline{S}_{\text{gauge fixing}}$ are obtained by Fadeev-Popov method. $c, \overline{c}$ are pair of Fadeev-Popov ghosts while star means their conjugate. In here, covariant derivative $D_\mu c$ defined by $\partial_\mu c + i[A_\mu, c]$.

Note that (A.4) is invariant under below gauge transformation.

$$A \to gAg^{-1} - i(\partial_\mu g)g^{-1} \tag{A.8}$$

Here $g(x)$ is element of gauge group. Under this transformation,

$$S_{CS} \to S_{CS} - \frac{k}{12\pi} g^{-1}(\partial_\mu g)g^{-1}(\partial_\nu g)g^{-1}(\partial_\rho g) + i\frac{k}{4\pi}\partial_\mu(g^{-1}(\partial_\nu g)A_\rho) \tag{A.9}$$

Second term is related to will-known winding number density. Winding number density is:

$$w(g) = \frac{1}{24\pi^2}\varepsilon^{\mu\nu\rho} g^{-1}(\partial_\mu g)g^{-1}(\partial_\nu g)g^{-1}(\partial_\rho g) \tag{A.10}$$

Hence second term in (A.9) is equivalent to $-2\pi k w(g)$. For $e^{iS_{CS}}$, this part do not appeared since $w(g)$ has only integer numbers. Third term in (A.9) is just total derivative term, it will be vanished with appropriate boundary condition.

• Wilson loop operator of supersymmetric theory defined in [65, 66]:

$$W_N[C] = \frac{1}{N}\text{Tr}\mathcal{P}\text{exp}\Big[i\oint_C d\tau\Big(A_m\dot{x}^m(\tau) + |\dot{x}|M_I^J Y^I Y_J^\dagger\Big)\Big] \tag{A.11}$$

This operator is invariant under transformation (A.8). Also, under specific choice of matrix M_I^J, (4.13) preserves $\frac{1}{6}$ supersymmetry of $\mathcal{N} = 6$ supersymmetry in ABJM theory. When contour is given by time-like line, this fact was explicitly proved with transformation rules of various field contents in ABJM theory. [40, 41]. Since we concentrated on light-like contour, matter contributed term(later term) in (A.11) would be dropped. Therefore, Wilson loop operator of $\overline{\text{U(N)}}$ part (denoted by $\overline{W}_N[C]$) at light-like contour is given by,

$$\overline{W}_N[C] = \frac{1}{N}\overline{\text{Tr}}\mathcal{P}\text{exp}\Big[i\oint_C d\tau\Big(\overline{A}_m\dot{x}^m(\tau)\Big)\Big] \tag{A.12}$$

Hence, suitable Wilson loop operator of ABJM theory is defined by

$$\mathcal{W}_N[C] := \frac{1}{2}\big(W_N[C] + \overline{W}_N[C]\big) \tag{A.13}$$

• Feynman rules for gauge field

We can read Feynman rules explicitly from ABJM action (A.4)-(A.7):

$$\text{U(N) gauge propagator}: \quad \Delta_{\mu\nu} = \frac{2\pi}{k}\Big(\frac{\varepsilon_{\mu\nu\rho}p^{\rho}}{p^2} + \xi\frac{p_\mu p_\nu}{p^4}\Big) \tag{A.14}$$

$$\overline{\text{U(N)}} \text{ gauge propagator}: \quad \overline{\Delta}_{\mu\nu} = -\frac{2\pi}{k}\Big(\frac{\varepsilon_{\mu\nu\rho}p^{\rho}}{p^2} + \xi\frac{p_\mu p_\nu}{p^4}\Big) \tag{A.15}$$

In this document, we choose Landau gauge i.e $\xi = 0$. A Feynman rules in position space could be obtained by Fourier transformation. For convenience, we consider propagator between x and y.

$$\Delta_{\mu\nu}(x,y) = \frac{2\pi}{k}\int \frac{d^d p}{(2\pi)^d}\frac{\varepsilon_{\mu\nu\rho}p^{\rho}}{p^2}e^{-ip\cdot(x-y)} \tag{A.16}$$

Due to BDS divergent part, we should expand up to ε^2 order to obtain finite piece. This requires formula of arbitrary dimension. For d-dimension there are $d-1$ angle variables in spherical coordinate system. These can be integrated out first. After some calculation we obtain,

$$\Delta_{\mu\nu}(x,y) = \frac{2\pi}{k}\frac{1}{(2\pi)^d}\varepsilon_{\mu\nu\rho}\partial^{\rho}|x-y|^{2-d}\int_0^\infty dt\; t^{\frac{d}{2}-2}\, J_{\frac{d}{2}-1}(t) \tag{A.17}$$

where $J_\nu(t)$ is Bessel function and $|x-y| = ((x-y)^2)^{\frac{1}{2}}$. After doing integration over t and differentiation over x_ρ, finally we obtain propagator in position space.

$$\Delta_{\mu\nu}(x,y) = \frac{\Gamma(\frac{d}{2})}{k\,\pi^{(\frac{d}{2}-1)}}\frac{\varepsilon_{\mu\nu\rho}(x-y)^{\rho}}{((x-y)^2)^{\frac{d}{2}}} \tag{A.18}$$

• Coordinates setting of light-like polygon

In this document, we used following notation.

$$x_{ij}^{\mu} = x_i^{\mu} - x_j^{\mu} \tag{A.19}$$

To parametrizing location on light-like polygon, we defined x_i^{μ} for indicate position of i-th cusp point. Then,

$$z_i^{\mu} = x_i^{\mu} + \tau\, p_i^{\mu} \quad \text{where} \quad \tau \in [0,1] \tag{A.20}$$

above z_i^{μ} parametrize some point between x_i^{μ} and x_{i+1}^{μ}. From this parametrization, we can convert vector integration $\int dz^{\mu}$ to scalar parameter integration like $\int_0^1 d\tau\, p^{\mu}$.

After some algebra we can relate momentum to Mandelstam variables by use above definitions.

$$2p_i\cdot p_j = x_{i,j+1}^2 + x_{i+1,j}^2 - x_{i,j}^2 - x_{i+1,j+1}^2 \tag{A.21}$$

• Path ordering of Wilson loop operator

As we seen in Feynman rules for gauge field, $\langle A_\mu A_\nu \rangle$ and $\langle A_\nu A_\mu \rangle$ will give a different sign due to epsilon tensor. Hence, we need to define suitable definition of path ordering for correct calculation. We choose path ordering as

$$\begin{aligned} \mathcal{P}(A_\mu(z(\tau))A_\nu(z(\tau'))) &= \langle A_\mu(z(\tau))A_\nu(z(\tau')) \rangle \quad \text{for} \quad \tau > \tau' \\ \mathcal{P}(A_\mu(z(\tau))A_\nu(z(\tau'))) &= \langle A_\nu(z(\tau'))A_\mu(z(\tau)) \rangle \quad \text{for} \quad \tau < \tau' \end{aligned} \tag{A.22}$$

τ, τ' are parameters running from 0 to 1.

It is well known that Wilson loop operator along contour C is expanded as following.

$$\begin{aligned} W_N[C] = \frac{1}{N}\mathrm{Tr}\mathcal{P}\Big[\mathbb{I} + i\oint_C dx^\mu A_\mu(x) - \oint_C dx^\mu \int^x dy^\nu A_\mu(x)A_\nu(y) \\ - i\oint_C dx^\mu \int^x dy^\nu \int^y dz^\rho A_\mu(x)A_\nu(y)A_\rho(z) \\ + \oint_C dx^\mu \int^x dy^\nu \int^y dz^\rho \int^z dw^\sigma A_\mu(x)A_\nu(y)A_\rho(z)A_\sigma(w) + \cdots \Big] \end{aligned} \tag{A.23}$$

Chapter B

Appendix B : Self energy of gauge field

One of important trick in Wilson loop calculation is treatment of matter contributed part. This part could be considered as effectively one-loop propagator in $\mathcal{N}=4$ SYM theory. This is cornerstone of similarity of Wilson loop at $\mathcal{N}=4$ SYM and ABJM theory. In here, we briefly present calculation of self energy correction up to two loop order. To do this, we need matter part of ABJM action.

• ABJM action for matter:

$$S_{ABJM} \supset \int d^dx \Big[\frac{1}{2}\overline{\mathrm{Tr}}\Big(-(D_mY)^\dagger_I D^m Y^I + i\Psi^{\dagger I}\not{D}\Psi_I\Big) + \frac{1}{2}\mathrm{Tr}\Big(-D_mY^I(D^mY)^\dagger_I + i\Psi_I\not{D}\Psi^{\dagger I}\Big) - V_{\mathrm{F}} - V_{\mathrm{B}}\Big] \tag{B.1}$$

Complexified Hermitian scalars and Majorana spinors in this action are($I=1,2,3,4$):

$$\begin{aligned}
Y^I &= (X^1+iX^5, X^2+iX^6, X^3-iX^7, X^4-iX^8): && (\mathbf{N},\overline{\mathbf{N}};\mathbf{4})\\
Y^\dagger_I &= (X^1-iX^5, X^2-iX^6, X^3+iX^7, X^4+iX^8): && (\overline{\mathbf{N}},\mathbf{N};\overline{\mathbf{4}})\\
\Psi_I &= (\psi^2+i\chi^2, -\psi^1-i\chi^1, \psi_4-i\chi_4, -\psi_3+i\chi_3): && (\mathbf{N},\overline{\mathbf{N}};\overline{\mathbf{4}})\\
\Psi^{\dagger I} &= (\psi_2-i\chi_2, -\psi_1+i\chi^1, \psi^4+i\chi^4, -\psi^3-i\chi^3): && (\overline{\mathbf{N}},\mathbf{N};\mathbf{4})
\end{aligned} \tag{B.2}$$

Here, covariant derivatives are defined as

$$D_mY^I = \partial_mY^I + iA_mY^I - iY^I\overline{A}_m\,, \quad D_mY^\dagger_I = \partial_mY^\dagger_I + i\overline{A}_mY^\dagger_I - iY^\dagger_IA_m \tag{B.3}$$

and similarly for fermions $\Psi_I, \Psi^{\dagger I}$. V_{F} and V_{B} are interaction terms, it contains sextet bosonic interaction and Yukawa interaction.

• $\mathbb{R}^{1,2}$ Majorana spinor and Dirac matrices:

$$\begin{aligned}
&\Psi \equiv \text{two-component Majorana spinor} \\
&\Psi^{\alpha} = \varepsilon^{\alpha\beta}\Psi_{\beta}, \quad \Psi_{\alpha} = \varepsilon_{\alpha\beta}\Psi^{\beta} \quad \text{where} \quad \varepsilon^{\alpha\beta} = -\varepsilon_{\alpha\beta} = i\sigma^2 \\
&\gamma^{n\beta}_{\alpha} = (i\sigma^2, \sigma^3, \sigma^1), \quad (\gamma^m)_{\alpha\beta} = (-\mathbb{I}, \sigma^1, -\sigma^3) \quad \text{obeying} \quad \gamma^m\gamma^n = g^{mn}\,\mathbb{I}_{2\times 2} - \varepsilon^{mnp}\gamma_p. \\
&\text{Hence,} \quad \mathrm{Tr}(\gamma^m\gamma^n) = 2g^{mn}
\end{aligned} \tag{B.4}$$

• Feynman rules for bosons, fermions and ghosts are explicitly readable from ABJM action:

$$\begin{aligned}
\text{boson propagator}: \quad & D_I{}^J(p) = \delta^J_I \frac{-i}{p^2 - i\varepsilon} \\
\text{fermion propagator}: \quad & S^I{}_J(p) = \delta^I_J \frac{i\not{p}}{p^2 - i\varepsilon} \\
\text{ghost propagator}: \quad & K(p) = \frac{-i}{p^2 - i\varepsilon}
\end{aligned} \tag{B.5}$$

• Self energy correction came from Boson and Fermion

There are four possible interactions contributes to self energy correction of gauge field. For convenience, we divided them into two groups. We consider correction came from boson and fermion firstly. This one-loop level corrected gauge field propagator will be attached to light-like polygon and this procedure yields two-loop order Wilson loop matter contributed diagram. Hence,

$$i\Delta_{\alpha\beta} = \frac{\varepsilon_{\alpha\mu\tau}k^{\tau}}{k^2} i\Pi_{\mu\nu} \frac{\varepsilon_{\nu\beta\kappa}k^{\kappa}}{k^2} \tag{B.6}$$

Here, $i\Pi_{\mu\nu} = i\Pi^b_{\mu\nu} + i\Pi^f_{\mu\nu}$ is self correction of gauge field due to boson and fermion, respectively.

Boson contribution is:

$$\begin{aligned}
i\Pi^b_{\mu\nu} &= 4\int \frac{d^dl}{(2\pi)^d} \frac{i}{(k+l)^2} i(2l+k)_{\mu} \frac{i}{l^2} i(2l+k)_{\nu} \\
&= 4\int \frac{d^dl}{(2\pi)^d} \frac{(2l+k)_{\mu}(2l+k)_{\nu}}{l^2(k+l)^2}
\end{aligned} \tag{B.7}$$

Fermion contribution is:

$$i\Pi^f_{\mu\nu} = (-1)^{\text{FD}} 4\text{Tr}\Big[\int \frac{d^d l}{(2\pi)^d}\gamma_\nu \frac{\not{l}}{l^2}\gamma_\mu \frac{(\not{k}+\not{l})}{(k+l)^2}\Big] \tag{B.8}$$

In both case, extra factor 4 came from 4 complex scalars/complex fundamental fermions coupled to gauge field. Numerator can be simplified by applying (B.4). It gives $\text{Tr}[\gamma_\mu\gamma_\rho\gamma_\nu\gamma_\sigma] = 2g_{\mu\rho}g_{\nu\sigma} + 2g_{\rho\nu}g_{\mu\sigma} - 2g_{\mu\nu}g_{\rho\sigma}$. Hence,

$$i\Pi^f_{\mu\nu} = -8\int \frac{d^d l}{(2\pi)^d}\frac{l_\mu(l+k)_\nu + (l+k)_\nu l_\mu - g_{\mu\nu} l\cdot(l+k)}{l^2(k+l)^2} \tag{B.9}$$

and,

$$i\Pi^b_{\mu\nu} + i\Pi^f_{\mu\nu} = \int \frac{d^d l}{(2\pi)^d}\frac{4k_\mu k_\nu + 8g_{\mu\nu} l\cdot(l+k)}{l^2(k+l)^2} \tag{B.10}$$

$k_\mu k_\nu$ term will be vanished due to epsilon tensors in (B.6). After Wick rotation, this integration can be converted to Euclidean d dimensional integration. Then, we used Feynman parameter and following formula for integration.

$$\int \frac{d^d\bar{l}}{(2\pi)^d}\frac{(\bar{l}^2)^a}{(\bar{l}^2+D)^b} = \frac{\Gamma(b-a-\frac{1}{2}d)\Gamma(a+\frac{d}{2})}{(4\pi)^{\frac{d}{2}}\Gamma(b)\Gamma(\frac{d}{2})}D^{-(b-a-\frac{d}{2})} \tag{B.11}$$

After all, we arrives to

$$i\Pi^b_{\mu\nu} + i\Pi^f_{\mu\nu} = -8ig_{\mu\nu}\frac{1}{(4\pi)^{\frac{d}{2}}}\Gamma\Big(1-\frac{d}{2}\Big)\frac{\Gamma(\frac{d}{2})\Gamma(\frac{d}{2})}{\Gamma(d)}(k^2)^{(\frac{d}{2}-1)} \tag{B.12}$$

Return to (B.6), self energy corrected gauge field propagation becomes

$$i\Delta_{\alpha\beta} = -8i\frac{\Gamma(1-\frac{d}{2})}{(4\pi)^{\frac{d}{2}}}\frac{\big(\Gamma(\frac{d}{2})\big)^2}{\Gamma(d-1)}\frac{1}{(k^2)^{3-\frac{d}{2}}}(g_{\alpha\beta}k^2 - k_\alpha k_\beta) \tag{B.13}$$

To apply our calculation on position space, we again use Fourier transformation procedure to here like (A.16). Note that latter term of (B.13) which is double derivative after transformation do not did anything for our case. Hence it is enough that consider transformation of first term in (B.13).

$$i\Delta_{\alpha\beta} = \frac{i}{2\pi^d}\frac{\Gamma(1-\frac{d}{2})\Gamma(\frac{d}{2})\Gamma(\frac{d}{2})}{\Gamma(d-1)}\frac{\Gamma(d-2)}{\Gamma(2-\frac{d}{2})}\frac{g_{\alpha\beta}}{(x^2)^{d-2}} \tag{B.14}$$

When we calculating matter diagram, we considered additional factor $\left(\frac{2\pi}{k}\right)^2$ to here.

• Self energy correction came from gauge field and ghost

Another possible self energy correction came from triple gauge field interaction and ghost contributed interaction.

From triple gauge field interaction,

$$\begin{aligned} i\Pi_{\nu\gamma}^{\text{gauge}} &= 3\times 3\int \frac{d^dl}{(2\pi)^d}\frac{2\pi}{k}\frac{\varepsilon_{\alpha\mu q}l^q}{l^2}\left(i\frac{k}{4\pi}\frac{2}{3}\right)\varepsilon_{\mu\nu\rho}\frac{2\pi}{k}\frac{\varepsilon_{\rho\beta r}(l+k)^r}{(l+k)^2}\left(i\frac{k}{4\pi}\frac{2}{3}\right)\varepsilon_{\alpha\beta\gamma} \\ &= -\int \frac{d^dl}{(2\pi)^d}\frac{l^\nu(l+k)^\gamma+(l+k)^\nu l^\gamma}{l^2(l+k)^2} \end{aligned} \tag{B.15}$$

Two factor 3 are came from vertex interaction term.

From ghost contributed loop,

$$i\Pi_{\nu\gamma}^{\text{ghost}} = (-1)^{\text{FD}}\int \frac{d^dl}{(2\pi)^d}\frac{(l+k)^\nu l^\gamma+(l+k)^\gamma l^\nu}{l^2(l+k)^2} \tag{B.16}$$

Above two corrections exactly cancels each other.

Chapter C

Appendix C : Mellin-Barnes transformation

The Mellin-Barnes transformation is frequently used tool for Feynman diagram calculation. Basic transformation rule is following:

$$\frac{1}{(X+Y)^{\lambda}} = \frac{1}{\Gamma(\lambda)} \int_{-i\infty}^{i\infty} \frac{dz}{2\pi i} \Gamma(-z)\Gamma(\lambda+z) \frac{Y^z}{X^{(\lambda+z)}} \tag{C.1}$$

It replaces power of summation to complex integration of array of Gamma functions. For more complex structure, number of Mellin-Barnes parameter z_i's are increased. For example,

$$\frac{1}{(X+Y+Z)^{\lambda}} = \frac{1}{\Gamma(\lambda)} \int_{-i\infty}^{i\infty} \frac{dz_1}{2\pi i} \int_{-i\infty}^{i\infty} \frac{dz_2}{2\pi i} \Gamma(-z_1)\Gamma(-z_2)\Gamma(\lambda+z_1+z_2) \frac{Z^{z_1} Y^{z_2}}{X^{(\lambda+z_1+z_2)}} \tag{C.2}$$

and so on. The integral contour is chosen that poles from Gamma functions like $\Gamma(\cdots + z)$ lie on left side of contour and poles from Gamma functions like $\Gamma(\cdots - z)$ lie on right side of contour. This Mellin-Barnes transformation has benefit not only numerical evaluation, but also asymptotic expansion in various kinematics.

Some integrations could be exactly calculated by Barnes lemma. At least Barnes lemma enable us to reduce our complex integration. The first Barnes lemma is:

$$\int_{-i\infty}^{i\infty} \frac{dz}{2\pi i} \Gamma(\lambda_1+z)\Gamma(\lambda_2+z)\Gamma(\lambda_3-z)\Gamma(\lambda_4-z) = \frac{\Gamma(\lambda_1+\lambda_3)\Gamma(\lambda_1+\lambda_4)\Gamma(\lambda_2+\lambda_3)\Gamma(\lambda_2+\lambda_4)}{\Gamma(\lambda_1+\lambda_2+\lambda_3+\lambda_4)} \tag{C.3}$$

And the second Barnes lemma is:

$$\begin{aligned} &\int_{-i\infty}^{i\infty} \frac{dz}{2\pi i} \frac{\Gamma(\lambda_1+z)\Gamma(\lambda_2+z)\Gamma(\lambda_3+z)\Gamma(\lambda_4-z)\Gamma(\lambda_5-z)}{\Gamma(\lambda_1+\lambda_2+\lambda_3+\lambda_4+\lambda_5+z)} \\ &\qquad = \frac{\Gamma(\lambda_1+\lambda_4)\Gamma(\lambda_1+\lambda_5)\Gamma(\lambda_2+\lambda_4)\Gamma(\lambda_2+\lambda_5)\Gamma(\lambda_3+\lambda_4)\Gamma(\lambda_3+\lambda_5)}{\Gamma(\lambda_1+\lambda_2+\lambda_4+\lambda_5)\Gamma(\lambda_1+\lambda_3+\lambda_4+\lambda_5)\Gamma(\lambda_2+\lambda_3+\lambda_4+\lambda_5)} \end{aligned} \tag{C.4}$$

These procedure are automized by `barnesroutines`.

Chapter D

Appendix D : Ladder Diagrams

◎ $I_{\text{Ladder}}^{\{4,4,1,1\}}$

This diagram could be obtained by just inserting $(4,4,1,1)$ to (i,j,k,l) in (4.44).

$$I_{\text{Ladder}}^{\{4,4,1,1\}} = \int_0^{\tau_j} d\tau_i \int_0^1 d\tau_j \int_0^{\tau_l} d\tau_k \int_0^1 d\tau_l \frac{\varepsilon(p_1,p_4,z_1-z_4)}{[(z_1-z_4)^2]^{\frac{d}{2}}} \frac{\varepsilon(p_1,p_4,z_1-z_4)}{[(z_1-z_4)^2]^{\frac{d}{2}}} \tag{D.1}$$

After little algebra, this becomes

$$I_{\text{Ladder}}^{\{4,4,1,1\}} = \frac{1}{4} \int_0^1 d\tau_i \int_0^1 d\tau_j \int_0^1 d\tau_k \int_0^1 d\tau_l \frac{\tau_l \tau_j N_{4411}}{\left(\Delta_1^{\{4,4,1,1\}}\right)^{\frac{d}{2}} \left(\Delta_2^{\{4,4,1,1\}}\right)^{\frac{d}{2}}} \tag{D.2}$$

where

$$\begin{aligned}
N_{4411} &= (x_{14}^2 - x_{15}^2 - x_{24}^2 + x_{25}^2)(-x_{15}^2 x_{24}^2 + x_{14}^2 x_{25}^2) \\
\Delta_1^{\{4,4,1,1\}} &= x_{14}^2 \bar{\tau}_i \bar{\tau}_l + x_{14}^2 \tau_i \bar{\tau}_j \bar{\tau}_l + x_{15}^2 \bar{\tau}_i \tau_l + x_{15}^2 \tau_i \bar{\tau}_j \tau_l + x_{24}^2 \tau_i \tau_j \bar{\tau}_l + x_{25}^2 \tau_i \tau_j \tau_l \\
\Delta_2^{\{4,4,1,1\}} &= x_{14}^2 \bar{\tau}_k \bar{\tau}_j + x_{14}^2 \tau_k \bar{\tau}_l \bar{\tau}_j + x_{15}^2 \tau_k \tau_l \bar{\tau}_j + x_{24}^2 \tau_j \bar{\tau}_k + x_{24}^2 \tau_j \tau_k \bar{\tau}_l + x_{25}^2 \tau_j \tau_k \tau_l
\end{aligned} \tag{D.3}$$

◎ $I_{\text{Ladder}}^{\{5,4,1,1\}}$

This diagram can be obtained by just inserting $(5,4,1,1)$ to (i,j,k,l) in (4.44).

$$I_{\text{Ladder}}^{\{5,4,1,1\}} = \int_0^{\tau_j} d\tau_i \int_0^1 d\tau_j \int_0^1 d\tau_k \int_0^1 d\tau_l \frac{\varepsilon(p_1,p_5,z_1-z_5)}{[(z_1-z_5)^2]^{\frac{d}{2}}} \frac{\varepsilon(p_1,p_4,z_1-z_4)}{[(z_1-z_4)^2]^{\frac{d}{2}}} \tag{D.4}$$

After little algebra, this becomes

$$I_{\text{Ladder}}^{\{5,4,1,1\}} = -\frac{1}{8} \int_0^1 d\tau_i \int_0^1 d\tau_j \int_0^1 d\tau_k \int_0^1 d\tau_l \frac{\tau_j N_{5411}}{\left(\Delta_1^{\{5,4,1,1\}}\right) \left(\Delta_2^{\{5,4,1,1\}}\right)} \tag{D.5}$$

where

$$
\begin{aligned}
N_{5411} &= (x_{15}^2)^2(x_{24}^2+x_{26}^2-x_{46}^2)-x_{15}^2(x_{24}^2x_{25}^2-2x_{24}^2x_{26}^2+x_{25}^2x_{26}^2+x_{14}^2(x_{25}^2+x_{26}^2)-2x_{25}^2x_{46}^2)\\
&\quad +x_{25}^2(x_{14}^2(x_{25}^2-x_{26}^2)-x_{25}^2x_{46}^2)\\
\Delta_1^{\{5,4,1,1\}} &= x_{15}^2\bar{\tau}_i\bar{\tau}_l+x_{15}^2\tau_i\bar{\tau}_j\bar{\tau}_l+x_{25}^2\tau_i\tau_j\bar{\tau}_l+x_{26}^2\tau_i\tau_j\tau_l\\
\Delta_2^{\{5,4,1,1\}} &= x_{14}^2\bar{\tau}_j\bar{\tau}_k+x_{15}^2\bar{\tau}_j\tau_k+x_{24}^2\tau_j\bar{\tau}_k+x_{25}^2\tau_j\tau_k
\end{aligned}
\tag{D.6}
$$

$\circledcirc\ I_{\text{Ladder}}^{\{4,3,1,1\}}$

This diagram can be obtained by just inserting $(4,3,1,1)$ to (i,j,k,l) in (4.44).

$$
I_{\text{Ladder}}^{\{4,3,1,1\}} = \int_0^{\tau_j} d\tau_i \int_0^1 d\tau_j \int_0^1 d\tau_k \int_0^1 d\tau_l \frac{\varepsilon(p_1,p_4,z_1-z_4)}{[(z_1-z_4)^2]^{\frac{d}{2}}}\frac{\varepsilon(p_1,p_3,z_1-z_3)}{[(z_1-z_3)^2]^{\frac{d}{2}}} \tag{D.7}
$$

After little algebra, this becomes

$$
I_{\text{Ladder}}^{\{4,3,1,1\}} = -\frac{1}{8}\int_0^1 d\tau_i \int_0^1 d\tau_j \int_0^1 d\tau_k \int_0^1 d\tau_l \frac{\tau_j N_{4311}}{\left(\Delta_1^{\{4,3,1,1\}}\right)^{\frac{d}{2}}\left(\Delta_2^{\{4,3,1,1\}}\right)^{\frac{d}{2}}} \tag{D.8}
$$

where

$$
\begin{aligned}
N_{4311} &= x_{13}^2x_{24}^2(-x_{14}^2+2x_{15}^2+x_{24}^2)-x_{13}^2(x_{14}^2+x_{24}^2)x_{25}^2\\
&\quad +(x_{14}^2-x_{24}^2)(-x_{15}^2x_{24}^2+x_{14}^2x_{25}^2-x_{14}^2x_{35}^2+x_{24}^2x_{35}^2)\\
\Delta_1^{\{4,3,1,1\}} &= x_{14}^2\bar{\tau}_i\bar{\tau}_l+x_{14}^2\tau_i\bar{\tau}_j\bar{\tau}_l+x_{15}^2\bar{\tau}_i\tau_l+x_{15}^2\tau_i\bar{\tau}_j\tau_l+x_{24}^2\tau_i\tau_j\bar{\tau}_l+x_{25}^2\tau_i\tau_j\tau_l\\
\Delta_2^{\{4,3,1,1\}} &= x_{13}^2\bar{\tau}_j\bar{\tau}_k+x_{14}^2\bar{\tau}_j\tau_k+x_{24}^2\tau_j\tau_k
\end{aligned}
\tag{D.9}
$$

$\circledcirc\ I_{\text{Ladder}}^{\{5,3,1,1\}}$

This diagram can be obtained by just inserting $(5,3,1,1)$ to (i,j,k,l) in (4.44).

$$
I_{\text{Ladder}}^{\{5,3,1,1\}} = \int_0^{\tau_j} d\tau_i \int_0^1 d\tau_j \int_0^1 d\tau_k \int_0^1 d\tau_l \frac{\varepsilon(p_1,p_5,z_1-z_5)}{[(z_1-z_5)^2]^{\frac{d}{2}}}\frac{\varepsilon(p_1,p_3,z_1-z_3)}{[(z_1-z_3)^2]^{\frac{d}{2}}} \tag{D.10}
$$

After little algebra, this becomes

$$-\frac{1}{8}\int_0^1 d\tau_i\int_0^1 d\tau_j\int_0^1 d\tau_k\int_0^1 d\tau_l\frac{\tau_j N_{5311}}{\left(\Delta_1^{\{5,3,1,1\}}\right)^{\frac{d}{2}}\left(\Delta_2^{\{5,3,1,1\}}\right)^{\frac{d}{2}}} \tag{D.11}$$

where

$$\begin{aligned}
N_{5311} &= (x_{14}^2-x_{24}^2)(-x_{26}^2x_{35}^2+x_{15}^2(x_{26}^2-x_{36}^2)+x_{25}^2x_{36}^2)\\
&\quad -x_{13}^2(-x_{24}^2x_{25}^2+x_{24}^2x_{26}^2+x_{15}^2(x_{24}^2+x_{26}^2-x_{46}^2)+x_{25}^2x_{46}^2)\\
\Delta_1^{\{5,3,1,1\}} &= x_{15}^2\bar{\tau}_i\bar{\tau}_l+x_{15}^2\tau_i\bar{\tau}_j\bar{\tau}_l+x_{25}^2\tau_i\tau_j\bar{\tau}_l+x_{26}^2\tau_i\tau_j\tau_l\\
\Delta_2^{\{5,3,1,1\}} &= x_{13}^2\bar{\tau}_j\bar{\tau}_k+x_{14}^2\bar{\tau}_j\tau_k+x_{24}^2\tau_j\tau_k
\end{aligned} \tag{D.12}$$

$\circledcirc\ I_{\text{Ladder}}^{\{3,3,1,1\}}$

This diagram can be obtained by just inserting $(3,3,1,1)$ to (i,j,k,l) in (4.44).

$$I_{\text{Ladder}}^{\{3,3,1,1\}} = \int_0^{\tau_j} d\tau_i\int_0^1 d\tau_j\int_0^{\tau_l} d\tau_k\int_0^1 d\tau_l\frac{\varepsilon(p_1,p_3,z_1-z_3)}{[(z_1-z_3)^2]^{\frac{d}{2}}}\frac{\varepsilon(p_1,p_3,z_1-z_3)}{[(z_1-z_3)^2]^{\frac{d}{2}}} \tag{D.13}$$

After little algebra, this becomes

$$I_{\text{Ladder}}^{\{3,3,1,1\}} = \frac{1}{4}\int_0^1 d\tau_i\int_0^1 d\tau_j\int_0^1 d\tau_k\int_0^1 d\tau_l\frac{\tau_l\tau_j N_{3311}}{\left(\Delta_1^{\{3,3,1,1\}}\right)^{\frac{d}{2}}\left(\Delta_2^{\{3,3,1,1\}}\right)^{\frac{d}{2}}} \tag{D.14}$$

where

$$\begin{aligned}
N_{3311} &= x_{13}^2x_{24}^2(x_{13}^2-x_{14}^2+x_{24}^2)\\
\Delta_1^{\{3,3,1,1\}} &= x_{13}^2\bar{\tau}_i\bar{\tau}_l+x_{13}^2\tau_i\bar{\tau}_j\bar{\tau}_l+x_{14}^2\bar{\tau}_i\tau_l+x_{14}^2\tau_i\bar{\tau}_j\tau_l+x_{24}^2\tau_i\tau_j\tau_l\\
\Delta_2^{\{3,3,1,1\}} &= x_{13}^2\bar{\tau}_j\bar{\tau}_k+x_{13}^2\bar{\tau}_j\tau_k\bar{\tau}_l+x_{14}^2\bar{\tau}_j\tau_k\tau_l+x_{24}^2\tau_j\tau_k\tau_l
\end{aligned} \tag{D.15}$$

$\circledcirc\ I_{\text{Ladder}}^{\{5,4,2,1\}}$

This diagram can be obtained by just inserting $(5,4,2,1)$ to (i,j,k,l) in (4.44).

$$I_{\text{Ladder}}^{\{5,4,2,1\}} = \int_0^1 d\tau_i\int_0^1 d\tau_j\int_0^1 d\tau_k\int_0^1 d\tau_l\frac{\varepsilon(p_1,p_5,z_1-z_5)}{[(z_1-z_5)^2]^{\frac{d}{2}}}\frac{\varepsilon(p_2,p_4,z_2-z_4)}{[(z_2-z_4)^2]^{\frac{d}{2}}} \tag{D.16}$$

After little algebra, this becomes

$$-\frac{1}{8}\int_0^1 d\tau_i \int_0^1 d\tau_j \int_0^1 d\tau_k \int_0^1 d\tau_l \frac{N_{5421}}{[x_{15}^2\bar{\tau}_i\bar{\tau}_l + x_{25}^2\tau_i\bar{\tau}_l + x_{26}^2\tau_i\tau_l]^{\frac{d}{2}}[x_{24}^2\bar{\tau}_j\bar{\tau}_k + x_{25}^2\bar{\tau}_j\tau_k + x_{35}^2\tau_j\tau_k]^{\frac{d}{2}}} \tag{D.17}$$

where

$$\begin{aligned} N_{5421} = & -x_{14}^2(x_{25}^2)^2 - x_{13}^2(x_{24}^2 - x_{25}^2)(x_{25}^2 - x_{26}^2) + x_{14}^2x_{25}^2x_{26}^2 + x_{14}^2x_{25}^2x_{35}^2 + x_{14}^2x_{26}^2x_{35}^2 \\ & - x_{24}^2x_{26}^2x_{35}^2 - 2x_{14}^2x_{25}^2x_{36}^2 + x_{24}^2x_{25}^2x_{36}^2 - (x_{25}^2)^2x_{36}^2 + 2x_{13}^2x_{25}^2x_{46}^2 + x_{25}^2(x_{25}^2 - x_{35}^2)x_{46}^2 \\ & + x_{15}^2(-x_{26}^2x_{35}^2 + x_{25}^2x_{36}^2 + x_{24}^2(x_{25}^2 - x_{26}^2 - x_{35}^2 + x_{36}^2) - x_{25}^2x_{46}^2 + x_{35}^2x_{46}^2) \end{aligned} \tag{D.18}$$

At last step in every ladder diagram, we converted to multi-dimensional integration with domain $[0,1]$. This is because to use numerical multidimensional integral package and to apply Mellin-Barnes transformation.

Chapter E

Appendix E : Dimensional Redection Scheme

In Wilson loop calculation(3 dimension), there is an ambiguous issue on choice of scheme. [1] This problem originated from existence of epsilon tensor. We already know that (momentum, position, etc) vector should be living in $D = 3 - 2\varepsilon$ dimension to resolve UV divergence appearing at cusp of Wilson loop. However, for epsilon tensor, it seems that there are two possible choice.

$$\begin{aligned} \varepsilon^{\mu\nu\rho}\varepsilon_{\mu\sigma\tau} &= (\delta_{\nu\tau}\delta_{\rho\sigma} - \delta_{\nu\sigma}\delta_{\rho\tau})\Gamma(D-1) \quad \text{(D dimension case)} \\ \varepsilon^{\mu\nu\rho}\varepsilon_{\mu\sigma\tau} &= (\delta_{\nu\tau}\delta_{\rho\sigma} - \delta_{\nu\sigma}\delta_{\rho\tau}) \qquad\quad \text{(3 dimension case)} \end{aligned} \tag{E.1}$$

Semenoff et al. showed in their paper that first choice do not consistent with gauge invariance, that is Ward-Takahashi-Slavnov-Taylor identity. Hence, we should consider spinorial object(including gamma function)and epsilon tensor living in exact 3 dimension while other physical vectors living in D dimension. This scheme also works well on calculation of half-BPS circular Wilson loop in ABJM theory, whose result matched to localization computation.

However, there appears another ambiguity in Wilson loop calculation. For instance, expression of vertex diagrams are consist of tensor integrals. Basic strategy for these tensor integrals is taking derivatives on scalar integrals. During this derivative procedure, there appears $\tilde{\eta}_{\mu\nu}$ which perfectly isolated from epsilon tensor contraction. The problem is this : $\eta_{\mu\nu}\tilde{\eta}^{\mu\nu} = 3$? or $\eta_{\mu\nu}\tilde{\eta}^{\mu\nu} = 3 - 2\varepsilon$?

Unfortunately, we cannot decide one of them from S-T identity calculation. Even if we distinguish $\tilde{\eta}^{\mu\nu}$ to $\eta^{\mu\nu}$, two loop renormalization factor does not changed in pure Chern-Simons part : it is still gives 1 as far as epsilon tensor lives in exact 3-dimension. Neverthless, we want to argue that $\eta_{\mu\nu}\tilde{\eta}^{\mu\nu} = 3 - 2\varepsilon$ is more suitable choice.

We can decompose exact 3-dimensional metric $\eta^{\mu\nu}$. That is,

$$\eta_{\mu\nu} = \hat{\eta}_{\mu\nu} + \hat{\tilde{\eta}}_{\mu\nu} \tag{E.2}$$

[1] Recently, this was indicated in [68].

where $\hat{\eta}_{\mu\nu}$ is $3-2\varepsilon$ dimensional object while $\hat{\hat{\eta}}_{\mu\nu}$ is 2ε dimensional. In some sense, this is kind of block diagonalization for continuous dimension. That is, we can consider $\eta^{\mu\nu}p_\nu$ as following.

$$\left(\begin{array}{c|c} \hat{\eta}_{\hat{a}\hat{b}} & \\ \hline & \hat{\hat{\eta}}_{\hat{\alpha}\hat{\beta}} \end{array}\right)\left(\begin{array}{c} p^{\hat{b}} \\ \hline p^{\hat{\hat{b}}} \end{array}\right)$$

Decomposed things are mutually orthogonal, contraction among themselves working like following.

$$\begin{aligned} \hat{\eta}_{\hat{\mu}\hat{\nu}}\hat{\eta}^{\hat{\mu}\hat{\nu}} = 3-2\varepsilon, \qquad \hat{\hat{\eta}}_{\hat{\hat{\mu}}\hat{\hat{\nu}}}\hat{\hat{\eta}}^{\hat{\hat{\mu}}\hat{\hat{\nu}}} = 2\varepsilon, \qquad \hat{\eta}_{\hat{\mu}\hat{\nu}}\hat{\hat{\eta}}^{\hat{\hat{\mu}}\hat{\hat{\nu}}} = 0 \\ \hat{\eta}_{\hat{\mu}\hat{\nu}}p^{\hat{\nu}} = p_{\hat{\mu}}, \qquad \hat{\hat{\eta}}_{\hat{\hat{\mu}}\hat{\hat{\nu}}}p^{\hat{\nu}} = 0 \end{aligned} \tag{E.3}$$

From now on, our p^μ means $p^{\hat{\mu}}$ since there is no appearance of $p^{\hat{\hat{\mu}}}$ in our calculation.

When $\eta_{\mu\nu}$ or $\hat{\eta}_{\hat{\mu}\hat{\nu}}$ acts on p^ν, we can consider them as equivalent object since $\eta_{\mu\nu}p^\nu = (\hat{\eta}_{\hat{\mu}\hat{\nu}} + \hat{\hat{\eta}}_{\hat{\hat{\mu}}\hat{\hat{\nu}}})p^\nu = (\hat{\eta}_{\hat{\mu}\hat{\nu}})p^\nu$. Similarly, $\eta^{\mu\nu}\hat{\eta}_{\hat{\nu}\hat{\rho}} = (\hat{\eta}^{\hat{\mu}\hat{\nu}} + \hat{\hat{\eta}}^{\hat{\hat{\mu}}\hat{\hat{\nu}}})\hat{\eta}_{\hat{\nu}\hat{\rho}} = \hat{\eta}^{\hat{\mu}}_{\hat{\rho}}$. However, $\eta_{\mu\nu}\eta^{\mu\nu}$ and $\eta_{\mu\nu}\hat{\eta}^{\hat{\mu}\hat{\nu}}$ gives manifestly different number : 3 and $3-2\varepsilon$ respectively. For instance, let examine this to following term that appeared in I_{321}.

$$\varepsilon^{\alpha\beta\gamma}\varepsilon^{\mu\nu\rho}\hat{\eta}_{\hat{\gamma}\hat{\rho}}p_{1,\alpha}p_{2,\beta}p_{3,\mu}p_{2,\nu} \tag{E.4}$$

$\eta^{\gamma\rho}$ will be appeared from contraction of epsilon tensor, and this will be contracted to $\hat{\eta}_{\hat{\gamma}\hat{\rho}}$. This gives $3-2\varepsilon$, not 3.

Chapter F

Appendix F : Expressions for vertex diagrams

F.0.1 $I_{\text{Vertex}}^{\{3,2,1\}}$

To calculate this diagram, we insert $\{3,2,1\}$ to (4.49). In this subsection, we used absolute value notation for convenience. That is, $|x-y|$ means $\left((x-y)^2\right)^{\frac{1}{2}}$.

$$I_{\text{vertex}}^{\{3,2,1\}} = \int dz_3^{\mu} dz_2^{\nu} dz_1^{\rho} \varepsilon^{\alpha\beta\gamma} \varepsilon_{\mu\alpha\sigma} \varepsilon_{\nu\beta\lambda} \varepsilon_{\rho\gamma\tau} \int d^d w \frac{(w-z_3)^{\sigma}(w-z_2)^{\lambda}(w-z_1)^{\tau}}{|w-z_3|^d |w-z_2|^d |w-z_1|^d} \tag{F.1}$$

This equals to

$$\int ds_3 ds_2 ds_1 p_3^{\mu} p_2^{\nu} p_1^{\rho} (-\varepsilon_{\nu\mu\lambda}\varepsilon_{\rho\sigma\tau} + \varepsilon_{\nu\sigma\lambda}\varepsilon_{\rho\mu\tau}) \int d^d w \frac{(w-z_{32})^{\sigma}(w)^{\lambda}(w-z_{12})^{\tau}}{|w-z_{32}|^d |w|^d |w-z_{12}|^d} \tag{F.2}$$

Here, we transformed $w-z_2$ to w. After some algebra on numerator, we can obtain following result.

$$I_{\text{vertex}}^{\{3,2,1\}} = \int d\tau_3 d\tau_2 d\tau_1 \int d^d w \frac{-\varepsilon(p_1,p_2,w)\varepsilon(p_3,p_2,w)}{|w|^d |w-z_{32}|^d |w-z_{12}|^d} \tag{F.3}$$

Here we use small trick. We can replace w by differential operator.

$$I_{\text{vertex}}^{\{3,2,1\}} = \frac{1}{(d-2)^2} \int d\tau_3 d\tau_2 d\tau_1 \int d^d w \frac{-\varepsilon(p_1,p_2,\partial_{z_1})\varepsilon(p_3,p_2,\partial_{z_3})}{|w|^d |w-z_{12}|^{d-2} |w-z_{32}|^{d-2}} \tag{F.4}$$

Introducing Feynman parameter β_1,β_2,β_3 as standard way $I_{\text{vertex}}^{\{3,2,1\}}$ is,

$$\begin{aligned}
&\int d\{\tau_i, w, \beta_j\} \frac{\delta(\sum \beta_i - 1)}{(d-2)^2} \frac{-\varepsilon(p_1,p_2,\partial_{z_1})\varepsilon(p_3,p_2,\partial_{z_3})(\beta_1\beta_2\beta_3)^{\frac{d-2}{2}-1}\beta_2}{[\beta_1(w-z_{12})^2 + \beta_2 w^2 + \beta_3(w-z_{32})^2]^{\frac{3d-4}{2}}} \frac{\Gamma(\frac{3d}{2}-2)}{\Gamma(\frac{d}{2})\Gamma(\frac{d}{2}-1)^2} \\
&= \int d\{\tau_i, l, \beta_j\} \frac{\delta(\sum \beta_i - 1)}{(d-2)^2} \frac{-\varepsilon(p_1,p_2,\partial_{z_1})\varepsilon(p_3,p_2,\partial_{z_3})(\beta_1\beta_2\beta_3)^{\frac{d}{2}-2}\beta_2}{[l^2+\Delta]^{\frac{3d-4}{2}}} \frac{\Gamma(\frac{3d}{2}-2)}{\Gamma(\frac{d}{2})\Gamma(\frac{d}{2}-1)^2} \\
&= -\frac{i\pi^{\frac{d}{2}}}{(d-2)^2} \frac{\Gamma(d-2)}{\Gamma(\frac{d}{2})\Gamma(\frac{d}{2}-1)^2} \int d\{\tau_i, \beta_j\} \delta(\sum \beta_i - 1)(\beta_1\beta_2\beta_3)^{\frac{d}{2}-2}\beta_2 \\
&\qquad \times \varepsilon(p_1,p_2,\partial_{z_1})\varepsilon(p_3,p_2,\partial_{z_3})\Delta^{2-d}
\end{aligned}$$

$$= -\frac{i\pi^{\frac{d}{2}}\Gamma(d-2)}{4\Gamma(\frac{d}{2})^3}\int d\{\tau_i,\beta_j\}\delta(\sum\beta_i-1)(\beta_1\beta_2\beta_3)^{\frac{d}{2}-2}\beta_2\varepsilon(p_1,p_2,\partial_{z_1})\varepsilon(p_3,p_2,\partial_{z_3})\Delta^{2-d} \tag{F.5}$$

Here is our notation on Δ, and β_i,

$$\begin{aligned}\Delta &= \beta_1\bar{\beta}_1 z_{12}^2+\beta_3\bar{\beta}_3 z_{32}^2-2\beta_1\beta_3 z_{12}\cdot z_{32}\\ &= \bar{\tau}_1 xys(\bar{\tau}_3\bar{y}+\tau_2\bar{x}y)+\tau_3 y\bar{y}t(\bar{\tau}_2\bar{x}+\tau_1 x)+\bar{\tau}_1\tau_3 uxy\bar{y} \qquad \text{(F.6)}\\ \beta_1 = xy \quad \beta_2 = (1-x)y \quad \beta_3 = (1-y) \quad x_{13}^2 = s \quad x_{14}^2 = u \quad x_{24}^2 &= t \qquad \text{(F.7)}\end{aligned}$$

To proceed calculation, we should know expression of differentiate operator on Δ.

$$\begin{aligned}\frac{\partial}{\partial z_1^\gamma}\Delta^{2-d} &= (2-d)\Delta^{1-d}[2\beta_1\bar{\beta}_1 z_{12,\gamma}-2\beta_1\beta_3 z_{32,\gamma}]\\ \frac{\partial}{\partial z_3^\rho}\frac{\partial}{\partial z_1^\gamma}\Delta^{2-d} &= (2-d)(1-d)\Delta^{-d}[2\beta_3\bar{\beta}_3 z_{32,\rho}-2\beta_1\beta_3 z_{12,\rho}][2\beta_1\bar{\beta}_1 z_{12,\gamma}-2\beta_1\beta_3 z_{32,\gamma}]\\ &\quad -(2-d)\Delta^{1-d}2\beta_1\beta_3\hat{\delta}_{\rho\gamma} \qquad \text{(F.8)}\end{aligned}$$

Numerator could be simplified by suitable manipulation. Considering previous dimensional reduction scheme carefully, the result is,

$$\begin{aligned}I_{\text{vertex}}^{\{3,2,1\}} &= \frac{i\pi^{\frac{d}{2}}\Gamma(d-2)}{8\Gamma(\frac{d}{2})^3}(2-d)\\ &\quad\times\int d\tau_{1,2,3}dxdyy(x\bar{x}y^2\bar{y})^{\frac{d}{2}-2}\bar{x}y\Big[\frac{2(1-d)}{\Delta^d}(\bar{\tau}_1\tau_3 st(s-u+t)x^2y^2\bar{y}^2)-(d-2)\frac{xy\bar{y}}{\Delta^{d-1}}st\Big]\\ &= \kappa st\int d\tau_{1,2,3}dxdy(x\bar{x}\bar{y})^{\frac{d}{2}-1}\Big[\frac{(d-2)}{\Delta_y^{d-1}}+\frac{2(d-1)}{\Delta_y^d}x\bar{y}\bar{\tau}_1\tau_3(s-u+t)\Big] \qquad \text{(F.9)}\end{aligned}$$

where coefficient κ is given by

$$\kappa = \frac{i\pi^{\frac{d}{2}}\Gamma(d-1)}{8\Gamma(\frac{d}{2})^3} \tag{F.10}$$

and Δ_y means divide Δ by y. That is,

$$\Delta_y = \bar{\tau}_1 xs(\bar{\tau}_3\bar{y}+\tau_2\bar{x}y)+\tau_3\bar{y}t(\bar{\tau}_2\bar{x}+\tau_1 x)+\bar{\tau}_1\tau_3 ux\bar{y} \tag{F.11}$$

To prevent spurious pole, we only consider the case of Mandelstam variables live on Euclidean region. In other words, All Mandelstam variables considered as negative-definite.

F.0.2 $I_{\text{Vertex}}^{\{4,2,1\}}$

We again inserted $\{4,2,1\}$ into (4.49).

$$I_{\text{vertex}}^{\{4,2,1\}} = \int dz_4^{\mu} dz_2^{\nu} dz_1^{\rho} \varepsilon^{\alpha\beta\gamma} \varepsilon_{\mu\alpha\sigma} \varepsilon_{\nu\beta\lambda} \varepsilon_{\rho\gamma\tau} \int d^d w \frac{(w-z_4)^{\sigma}(w-z_2)^{\lambda}(w-z_1)^{\tau}}{|w-z_4|^d |w-z_2|^d |w-z_1|^d} \tag{F.12}$$

This becomes

$$\int ds_4 ds_2 ds_1 p_4^{\mu} p_2^{\nu} p_1^{\rho} (-\varepsilon_{\nu\mu\lambda}\varepsilon_{\rho\sigma\tau} + \varepsilon_{\nu\sigma\lambda}\varepsilon_{\rho\mu\tau}) \int d^d w \frac{(w-z_{42})^{\sigma}(w)^{\lambda}(w-z_{12})^{\tau}}{|w-z_{42}|^d |w|^d |w-z_{12}|^d} \tag{F.13}$$

Little algebra for $I_{\text{vertex}}^{\{4,2,1\}}$ gives

$$\begin{aligned}
&-\tilde{\kappa} \int d\beta_1 d\beta_2 d\beta_3 \beta_1^{\frac{d}{2}-1} \beta_2^{\frac{d}{2}-2} \beta_3^{\frac{d}{2}-2} \delta(\textstyle\sum \beta_i - 1) \Delta^{-d} \\
&\qquad \Big[-\varepsilon(p_4, p_2, \beta_2\beta_3 z_{12} - \beta_3\bar{\beta}_3 z_{42}) \varepsilon(p_1, p_2, \beta_2\beta_3 z_{42} - \beta_2\bar{\beta}_2 z_{12}) \\
&\qquad -\varepsilon(p_4, p_2, \beta_2\beta_3 z_{12} - \beta_3\bar{\beta}_3 z_{42}) \varepsilon(p_1, p_3, \beta_2\beta_3 z_{42} - \beta_2\bar{\beta}_2 z_{12}) \\
&\qquad +\varepsilon(p_3, p_2, \beta_2\beta_3 z_{12} - \beta_3\bar{\beta}_3 z_{42}) \varepsilon(p_1, p_4, \beta_2\beta_3 z_{42} - \beta_2\bar{\beta}_2 z_{12}) \Big] \\
&-\tilde{\kappa} \int d\beta_1 d\beta_2 d\beta_3 \beta_1^{\frac{d}{2}-1} \beta_2^{\frac{d}{2}-2} \beta_3^{\frac{d}{2}-1} \delta(\textstyle\sum \beta_i - 1) \Delta^{-d} \\
&\qquad \Big[\varepsilon(p_4, p_2, p_3) \varepsilon(p_1, p_2, \beta_2\beta_3 z_{42} - \beta_2\bar{\beta}_2 z_{12}) \\
&\qquad +\varepsilon(p_4, p_2, p_3) \varepsilon(p_1, p_3, \beta_2\beta_3 z_{42} - \beta_2\bar{\beta}_2 z_{12}) \\
&\qquad +s_4 \varepsilon(p_4, p_2, p_3) \varepsilon(p_1, p_4, \beta_2\beta_3 z_{42} - \beta_2\bar{\beta}_2 z_{12}) \Big] \\
&+\frac{1}{2(1-d)} \tilde{\kappa} \int d\beta_1 d\beta_2 d\beta_3 (\beta_1\beta_2\beta_3)^{\frac{d}{2}-1} \delta(\textstyle\sum \beta_i - 1) \Delta^{1-d} \\
&\qquad \Big[(p_4 \cdot p_2)(p_1 \cdot p_2) - (p_1 \cdot p_4)(p_2 \cdot p_3) + (p_3 \cdot p_1)(p_2 \cdot p_4) \Big]
\end{aligned} \tag{F.14}$$

where $\tilde{\kappa}$ is

$$\tilde{\kappa} = i\pi^{\frac{d}{2}} (1-d) \frac{\Gamma(d-1)}{\Gamma(\frac{d}{2})^3} \tag{F.15}$$

Terms in (F.14) could be converted into a function of Mandelstam variables. There appears long expression for this numerator piece. To eliminate delta function, we reparametrize β_i by two parameter x, y.

$$\beta_1 = xy, \quad \beta_2 = \bar{x}y, \quad \beta_3 = \bar{y} \tag{F.16}$$

Finally,

$$I_{\text{vertex}}^{\{4,2,1\}} = \tilde{\kappa}\int ds_{1,2,4}\int dxdy(x\bar{x}\bar{y})^{\frac{d}{2}-1}\frac{1}{\Delta_y^d}F_{B,421}(x_{i,j}^2) + \frac{1}{2(1-d)}\tilde{\kappa}\int ds_{1,2,4}\int dxdy(x\bar{x}\bar{y})^{\frac{d}{2}-1}\frac{(d-2)}{\Delta_y^{d-1}}F_{A,421}(x_{i,j}^2) \tag{F.17}$$

Here $F_{A,421}(x_{i,j}^2)$ and $F_{B,421}(x_{i,j}^2)$ are function of Mandelstam variables obtained from expanding (F.14). Denominator Δ_y obtained by dividing Δ by y.

$$\Delta_y = x_{13}^2\tau_2 xy\bar{\tau}_1\bar{x} + x_{14}^2\bar{\tau}_1\bar{\tau}_4\bar{x}\bar{y} + x_{15}^2\bar{\tau}_1\tau_4\bar{x}\bar{y} + x_{24}^2\bar{\tau}_4\bar{y}(\tau_1\bar{x}+\bar{\tau}_2 x) + x_{25}^2\tau_4\bar{y}(\tau_1\bar{x}+\bar{\tau}_2 x) + x_{35}^2\tau_2\tau_4 x\bar{y} \tag{F.18}$$

This expression do not give $\frac{1}{\varepsilon}$ divergence. In other words, this diagrams contributes only to IR finite part.

F.0.3 $I_{\text{Vertex}}^{\{4,3,1\}}$

This evaluation is very parallel to previous vertex diagrams. We again inserted $\{4,3,1\}$ into (4.49).

$$I_{\text{vertex}}^{\{4,3,1\}} = \int dz_4^{\mu} dz_3^{\nu} dz_1^{\rho} \varepsilon^{\alpha\beta\gamma} \varepsilon_{\mu\alpha\sigma} \varepsilon_{\nu\beta\lambda} \varepsilon_{\rho\gamma\tau} \int d^d w \frac{(w-z_4)^{\sigma}(w-z_3)^{\lambda}(w-z_1)^{\tau}}{|w-z_4|^d |w-z_3|^d |w-z_1|^d} \tag{F.19}$$

Little algebra for $I_{\text{vertex}}^{\{4,3,1\}}$ gives

$$\begin{aligned}
&-\tilde{\kappa} \int d\beta_1 d\beta_2 d\beta_3 \beta_1^{\frac{d}{2}-2} \beta_2^{\frac{d}{2}-1} \beta_3^{\frac{d}{2}-2} \delta(\textstyle\sum \beta_i - 1) \Delta^{-d} \\
&\qquad \Big[-\varepsilon(p_3, p_1, \beta_1\beta_3 z_{43} - \beta_1\bar{\beta}_1 z_{13}) \varepsilon(p_4, p_2, \beta_1\beta_3 z_{13} - \beta_3\bar{\beta}_3 z_{43}) \\
&\qquad -\varepsilon(p_3, p_1, \beta_1\beta_3 z_{43} - \beta_1\bar{\beta}_1 z_{13}) \varepsilon(p_4, p_3, \beta_1\beta_3 z_{13} - \beta_3\bar{\beta}_3 z_{43}) \\
&\qquad +\varepsilon(p_3, p_2, \beta_1\beta_3 z_{43} - \beta_1\bar{\beta}_1 z_{13}) \varepsilon(p_4, p_1, \beta_1\beta_3 z_{13} - \beta_3\bar{\beta}_3 z_{43}) \Big] \\
&-\tilde{\kappa} \int d\beta_1 d\beta_2 d\beta_3 \beta_1^{\frac{d}{2}-1} \beta_2^{\frac{d}{2}-1} \beta_3^{\frac{d}{2}-2} \delta(\textstyle\sum \beta_i - 1) \Delta^{-d} \\
&\qquad \Big[\varepsilon(p_3, p_1, p_2) \varepsilon(p_4, p_2, \beta_1\beta_3 z_{13} - \beta_3\bar{\beta}_3 z_{43}) \\
&\qquad +\varepsilon(p_3, p_1, p_2) \varepsilon(p_4, p_3, \beta_1\beta_3 z_{13} - \beta_3\bar{\beta}_3 z_{43}) \\
&\qquad +\bar{s_1} \varepsilon(p_3, p_1, p_2) \varepsilon(p_4, p_1, \beta_1\beta_3 z_{13} - \beta_3\bar{\beta}_3 z_{43}) \Big] \\
&+\frac{1}{2(1-d)} \tilde{\kappa} \int d\beta_1 d\beta_2 d\beta_3 (\beta_1\beta_2\beta_3)^{\frac{d}{2}-1} \delta(\textstyle\sum \beta_i - 1) \Delta^{1-d} \\
&\qquad \Big[(p_3 \cdot p_1)(p_4 \cdot p_3) - (p_1 \cdot p_4)(p_2 \cdot p_3) + (p_3 \cdot p_1)(p_2 \cdot p_4) \Big]
\end{aligned} \tag{F.20}$$

As before, $\tilde{\kappa}$ is defined by

$$\tilde{\kappa} = i\pi^{\frac{d}{2}} (1-d) \frac{\Gamma(d-1)}{\Gamma(\frac{d}{2})^3} \tag{F.21}$$

In numerical works, we translated (F.20) as a function of Mandelstam variables. As before, There appears long expression for this numerator piece. To eliminate delta function, we reparametrize β_i by two parameter x, y again.

$$\beta_1 = xy, \quad \beta_2 = \bar{x}y, \quad \beta_3 = \bar{y} \tag{F.22}$$

Finally,

$$I_{\text{vertex}}^{\{4,3,1\}} = \tilde{\kappa}\int ds_{1,3,4}\int dxdy(x\bar{x}\bar{y})^{\frac{d}{2}-1}\frac{1}{\Delta_y^d}F_{B,431}(x_{i,j}^2) + \frac{1}{2(1-d)}\tilde{\kappa}\int ds_{1,3,4}\int dxdy(x\bar{x}\bar{y})^{\frac{d}{2}-1}\frac{(d-2)}{\Delta_y^{d-1}}F_{A,431}(x_{i,j}^2) \tag{F.23}$$

Here $F_{A,431}(x_{i,j}^2)$ and $F_{B,431}(x_{i,j}^2)$ are function of Mandelstam variables obtained from expanding (F.20). Denominator Δ_y obtained by dividing Δ by y.

$$\Delta_y = -x_{13}^2 x\bar{x}y\bar{\tau}_1\bar{\tau}_3 - x_{14}^2 x\bar{\tau}_1(\bar{x}y\tau_3+\bar{y}\bar{\tau}_4) - x_{15}^2 x\bar{y}\bar{\tau}_1\tau_4 - x_{24}^2 x\tau_1(\bar{x}y\tau_3+\bar{y}\bar{\tau}_4) - x_{25}^2 x\bar{y}\tau_1\tau_4 - x_{35}^2\bar{x}\bar{y}\bar{\tau}_3\tau_4 \tag{F.24}$$

In case of configuration satisfy Gram determinant constraint, we observed that numerical value for I_{421} and I_{431} agrees. Unfortunately, it is hard to see directly from these expressions due to its complexity.

F.0.4 $I_{\text{Vertex}}^{\{5,3,1\}}$

This part has most complex structure among whole diagrams. Start from (4.49),

$$I_{\text{vertex}}^{\{5,3,1\}} = \int dz_5^\mu dz_3^\nu dz_1^\rho \varepsilon^{\alpha\beta\gamma}\varepsilon_{\mu\alpha\sigma}\varepsilon_{\nu\beta\lambda}\varepsilon_{\rho\gamma\tau}\int d^d w\frac{(w-z_5)^\sigma(w-z_3)^\lambda(w-z_1)^\tau}{|w-z_5|^d|w-z_3|^d|w-z_1|^d} \tag{F.25}$$

After straightforward algebra, we got

$$I_{\text{vertex}}^{\{5,3,1\}} = 4\frac{(1-d)}{2-d}\tau\int[d\beta_3]\int d\tau_{5,3,1}\frac{1}{\Delta^d}H_B(x_{i,j}^2) + 2\frac{1}{2-d}\tau\int[d\beta_3]\int d\tau_{5,3,1}\frac{1}{\Delta^{d-1}}H_A(x_{i,j}^2) + 2\frac{(1-d)}{2-d}\tilde{\tau}\int[d\tilde{\beta_3}]\int d\tau_{5,3,1}\frac{1}{\Delta^d}H_C(x_{i,j}^2) \tag{F.26}$$

Here,

$$\tau = -i\pi^{\frac{d}{2}}\frac{\Gamma(d-2)}{\Gamma(\frac{3d}{2}-2)}, \qquad \tilde{\tau} = -i\pi^{\frac{d}{2}}\frac{\Gamma(d-1)}{\Gamma(\frac{3d}{2}-1)} \tag{F.27}$$

and

$$\int[d\beta_3] = \int_0^1 d\beta_1 d\beta_2 d\beta_3(\beta_1\beta_2\beta_3)^{\frac{d}{2}-2}\beta_2\delta(\sum_i\beta_i-1)\frac{\Gamma(\frac{3d}{2}-2)}{\Gamma(\frac{d}{2})\Gamma(\frac{d}{2}-1)^2}$$
$$\int[d\tilde{\beta_3}] = \int_0^1 d\beta_1 d\beta_2 d\beta_3(\beta_1\beta_2\beta_3)^{\frac{d}{2}-2}\beta_1\beta_2\delta(\sum_i\beta_i-1)\frac{\Gamma(\frac{3d}{2}-1)}{\Gamma(\frac{d}{2})^2\Gamma(\frac{d}{2}-1)} \tag{F.28}$$

and denominator Δ_y is given by

$$\Delta_y = x_{13}^2 x\bar{x}y\bar{\tau}_1\bar{\tau}_3 + x_{14}^2 x\bar{x}y\bar{\tau}_1\tau_3 + x_{24}^2 x\bar{x}y\tau_1\tau_3 + x_{15}^2 x\bar{y}\bar{\tau}_1\bar{\tau}_5 + x_{25}^2 x\bar{y}\tau_1\bar{\tau}_5 + x_{26}^2 x\bar{y}\tau_1\tau_5 + x_{35}^2 \bar{x}\bar{y}\tau_3\bar{\tau}_5 + x_{36}^2 \bar{x}\bar{y}\tau_3\tau_5 + x_{46}^2 \bar{x}\bar{y}\tau_3\tau_5 \tag{F.29}$$

again Δ_y means divide Δ by y.

$H_A(x_{i,j}^2)$, $H_B(x_{i,j}^2)$ and $H_C(x_{i,j}^2)$ are quiet complex functions of Mandelstam variables. We can combine first and third term in (F.26),so finally got more compact following expression.

$$\alpha_1 \int_0^1 dxdy \int_0^1 d\tau_{5,3,1} \frac{1}{\Delta_y^d} (x\bar{x}\bar{y})^{\frac{d}{2}-1} F_{B,531}(x_{i,j}^2) \tag{F.30}$$

where

$$\alpha_1 = -i\pi^{\frac{d}{2}}(1-d)\frac{\Gamma(d-1)}{\Gamma(\frac{d}{2})^3} \tag{F.31}$$

which gives a value of $16i$ at three dimension.

For second term in (F.26),

$$\frac{\alpha_1}{2(1-d)} \int_0^1 dxdy \int_0^1 d\tau_{5,3,1} (x\bar{x}\bar{y})^{\frac{d}{2}-1} F_{A,531}(x_{i,j}^2) \frac{(d-2)}{\Delta_y^{d-1}} \tag{F.32}$$

We do not explicitly write down function $F_{A,ijk}$ and $F_{B,ijk}$ here.

Chapter G

Appendix G : Expressions for I_{521} and I_{541}

For the splitting function($n > 6$) we introduced new kind of vertex diagrams, I_{521} and I_{541}. Due to vanishment of x_{16}^2 in hexagon, these diagrams could be obtained from permutating I_{421} or I_{431} therein. However, these diagrams manifestly distinguished in case of octagon. We summarized there expression in here. Even in generel n-gon setup, expression of I_{521} and I_{541} are same with here since inner product formula $2p_i \cdot p_j = x_{i,j+1}^2 + x_{i+1,j}^2 - x_{i,j}^2 - x_{i+1,j+1}^2$ unchanged.

• Scalar integration I_{541}

Start from

$$I_{\text{vertex}}^{\{5,4,1\}} = \int dz_5^\mu dz_4^\nu dz_1^\rho \varepsilon^{\alpha\beta\gamma}\varepsilon_{\mu\alpha\sigma}\varepsilon_{\nu\beta\lambda}\varepsilon_{\rho\gamma\tau}\int d^d w \frac{(w-z_5)^\sigma (w-z_4)^\lambda (w-z_1)^\tau}{|w-z_5|^d |w-z_4|^d |w-z_1|^d} \tag{G.1}$$

This expression equivalent to

$$\begin{aligned} I_{541} = &\frac{1}{(d-2)^2}\int d^d w \frac{\varepsilon(p_4,p_5,\partial_{z_5})\varepsilon(p_1,p_2,\partial_{z_1})}{|w|^d |w-z_{54}|^{d-2}|w-z_{14}|^{d-2}} \\ &+ \frac{1}{(d-2)^2}\int d^d w \frac{\varepsilon(p_4,p_5,\partial_{z_5})\varepsilon(p_1,p_3,\partial_{z_1})}{|w|^d |w-z_{54}|^{d-2}|w-z_{14}|^{d-2}} \\ &+ \frac{1}{(d-2)^2}\int d^d w \frac{\varepsilon(p_4,p_5,\partial_{z_5})\varepsilon(p_1,p_4,\partial_{z_1})}{|w|^d |w-z_{54}|^{d-2}|w-z_{14}|^{d-2}} \end{aligned} \tag{G.2}$$

Feynman parameter $\beta_1, \beta_2, \beta_3$ and Δ are defined as

$$\begin{aligned} \beta_1 = xy, \quad \beta_2 = \overline{x}y, \quad \beta_3 = \overline{y} \\ \int [d\beta_3] = \int_0^1 d\beta_1 d\beta_2 d\beta_3 (\beta_1\beta_2\beta_3)^{\frac{d}{2}-2}\beta_1 \delta(\sum_i \beta_i - 1)\frac{\Gamma(\frac{3d}{2}-2)}{\Gamma(\frac{d}{2})\Gamma(\frac{d}{2}-1)^2} \\ \Delta = -2\beta_2\beta_3 z_{14}\cdot z_{54} + \beta_2\overline{\beta}_2 z_{14}^2 + \beta_3\overline{\beta}_3 z_{54}^2 \end{aligned} \tag{G.3}$$

Then, I_{541} became

$$
\begin{aligned}
&-\tilde{\tau}\int d\beta_1 d\beta_2 d\beta_3 \beta_1^{\frac{d}{2}-1}\beta_2^{\frac{d}{2}-2}\beta_3^{\frac{d}{2}-2}\delta(\sum\beta_i-1)\Delta^{-d} \\
&\qquad\Big[\varepsilon(p_4,p_5,\beta_2\beta_3 z_{14}-\beta_3\bar{\beta}_3 z_{54})\varepsilon(p_1,p_2,\beta_2\beta_3 z_{54}-\beta_2\bar{\beta}_2 z_{14}) \\
&\qquad+\varepsilon(p_4,p_5,\beta_2\beta_3 z_{14}-\beta_3\bar{\beta}_3 z_{54})\varepsilon(p_1,p_3,\beta_2\beta_3 z_{54}-\beta_2\bar{\beta}_2 z_{14}) \\
&\qquad+\varepsilon(p_4,p_5,\beta_2\beta_3 z_{14}-\beta_3\bar{\beta}_3 z_{54})\varepsilon(p_1,p_4,\beta_2\beta_3 z_{54}-\beta_2\bar{\beta}_2 z_{14})\Big] \\
&+\frac{1}{2(1-d)}\tilde{\tau}\int d\beta_1 d\beta_2 d\beta_3(\beta_1\beta_2\beta_3)^{\frac{d}{2}-1}\delta(\sum\beta_i-1)\Delta^{1-d} \\
&\qquad\Big[(p_4\cdot p_1)(p_5\cdot p_2)-(p_4\cdot p_2)(p_5\cdot p_1) \\
&\qquad+(p_4\cdot p_1)(p_5\cdot p_3)-(p_4\cdot p_3)(p_5\cdot p_1)+(p_4\cdot p_1)(p_5\cdot p_4)\Big]
\end{aligned}
\tag{G.4}
$$

where

$$
\tilde{\tau}=i\pi^{\frac{d}{2}}(1-d)\frac{\Gamma(d-1)}{\Gamma(\frac{d}{2})^3} \tag{G.5}
$$

• Scalar integration I_{521}

Methodlogically, computation ways identical to that of I_{541}. However, expression is more complex. Here we just briefly summarize result. We do not written here explicit full expression of numerator as a function of Mandelstam variables. Obtaining this expression is necessary procedure for calculation via FIESTA2, however they could be gained straighforwardly from below expression. I_{521} is,

$$
\begin{aligned}
I_{421}=&\frac{1}{(d-2)^2}\int d^dw\frac{\varepsilon(p_2,p_5,\partial_{z_5})\varepsilon(p_1,p_2,\partial_{z_1})}{|w|^d|w-z_{52}|^{d-2}|w-z_{12}|^{d-2}}+\frac{1}{(d-2)^2}\int d^dw\frac{\varepsilon(p_2,p_5,\partial_{z_5})\varepsilon(p_1,p_3,\partial_{z_1})}{|w|^d|w-z_{52}|^{d-2}|w-z_{12}|^{d-2}} \\
&+\frac{1}{(d-2)^2}\int d^dw\frac{\varepsilon(p_2,p_5,\partial_{z_5})\varepsilon(p_1,p_4,\partial_{z_1})}{|w|^d|w-z_{52}|^{d-2}|w-z_{12}|^{d-2}}-\frac{1}{(d-2)^2}\int d^dw\frac{\varepsilon(p_2,p_3,\partial_{z_5})\varepsilon(p_1,p_5,\partial_{z_1})}{|w|^d|w-z_{52}|^{d-2}|w-z_{12}|^{d-2}} \\
&-\frac{1}{(d-2)^2}\int d^dw\frac{\varepsilon(p_2,p_4,\partial_{z_5})\varepsilon(p_1,p_5,\partial_{z_1})}{|w|^d|w-z_{52}|^{d-2}|w-z_{12}|^{d-2}}-\frac{1}{d-2}\int d^dw\frac{\varepsilon(p_2,p_5,p_3)\varepsilon(p_1,p_2,\partial_{z_1})}{|w|^d|w-z_{12}|^{d-2}|w-z_{52}|^d} \\
&-\frac{1}{d-2}\int d^dw\frac{\varepsilon(p_2,p_5,p_4)\varepsilon(p_1,p_2,\partial_{z_1})}{|w|^d|w-z_{12}|^{d-2}|w-z_{52}|^d}-\frac{1}{d-2}\int d^dw\frac{\varepsilon(p_2,p_5,p_3)\varepsilon(p_1,p_3,\partial_{z_1})}{|w|^d|w-z_{12}|^{d-2}|w-z_{52}|^d}
\end{aligned}
\tag{G.6}
$$

$$
\begin{aligned}
&-\frac{1}{d-2}\int d^dw\frac{\varepsilon(p_2,p_5,p_4)\varepsilon(p_1,p_3,\partial_{z_1})}{|w|^d|w-z_{12}|^{d-2}|w-z_{52}|^d}-\frac{1}{d-2}\int d^dw\frac{\varepsilon(p_2,p_5,p_3)\varepsilon(p_1,p_4,\partial_{z_1})}{|w|^d|w-z_{12}|^{d-2}|w-z_{52}|^d}\\
&-\frac{1}{d-2}\int d^dw\frac{\varepsilon(p_2,p_5,p_4)\varepsilon(p_1,p_4,\partial_{z_1})}{|w|^d|w-z_{12}|^{d-2}|w-z_{52}|^d}+\frac{1}{d-2}\int d^dw\frac{s_5\varepsilon(p_2,p_3,p_5)\varepsilon(p_1,p_5,\partial_{z_1})}{|w|^d|w-z_{12}|^{d-2}|w-z_{52}|^d}\\
&+\frac{1}{d-2}\int d^dw\frac{s_5\varepsilon(p_2,p_4,p_5)\varepsilon(p_1,p_5,\partial_{z_1})}{|w|^d|w-z_{12}|^{d-2}|w-z_{52}|^d}
\end{aligned}
\tag{G.7}
$$

Note that latter 8 terms (proportional to $\frac{1}{(d-2)}$) are negligible in triple collinear limit since epsilon tensor contains two of p_2,p_3,p_4 that being parallel vectors in triple collinear limit. Although we considered their contribution in computation, here we just wrote down expressions for dominant part. β_1,β_2,β_3 are defined as before, but Δ is slightly different.

$$
\begin{aligned}
\beta_1=xy,\quad \beta_2=\overline{x}y,\quad \beta_3=\overline{y}\\
\int[d\beta_3]=\int_0^1 d\beta_1 d\beta_2 d\beta_3(\beta_1\beta_2\beta_3)^{\frac{d}{2}-2}\beta_1\delta(\sum_i\beta_i-1)\frac{\Gamma(\frac{3d}{2}-2)}{\Gamma(\frac{d}{2})\Gamma(\frac{d}{2}-1)^2}\\
\Delta=-2\beta_2\beta_3 z_{12}\cdot z_{52}+\beta_2\overline{\beta}_2 z_{12}^2+\beta_3\overline{\beta}_3 z_{52}^2
\end{aligned}
\tag{G.8}
$$

The dominant 5-terms can be summarized as follow.

$$
\begin{aligned}
&-\tilde{\tau}\int d\beta_1 d\beta_2 d\beta_3\beta_1^{\frac{d}{2}-1}\beta_2^{\frac{d}{2}-2}\beta_3^{\frac{d}{2}-2}\delta(\sum\beta_i-1)\Delta^{-d}\\
&\qquad\Big[\varepsilon(p_2,p_5,\beta_2\beta_3 z_{12}-\beta_3\bar{\beta}_3 z_{52})\varepsilon(p_1,p_2,\beta_2\beta_3 z_{52}-\beta_2\bar{\beta}_2 z_{12})\\
&\qquad+\varepsilon(p_2,p_5,\beta_2\beta_3 z_{12}-\beta_3\bar{\beta}_3 z_{52})\varepsilon(p_1,p_3,\beta_2\beta_3 z_{52}-\beta_2\bar{\beta}_2 z_{12})\\
&\qquad+\varepsilon(p_2,p_5,\beta_2\beta_3 z_{12}-\beta_3\bar{\beta}_3 z_{52})\varepsilon(p_1,p_4,\beta_2\beta_3 z_{52}-\beta_2\bar{\beta}_2 z_{12})\\
&\qquad-\varepsilon(p_2,p_3,\beta_2\beta_3 z_{12}-\beta_3\bar{\beta}_3 z_{52})\varepsilon(p_1,p_5,\beta_2\beta_3 z_{52}-\beta_2\bar{\beta}_2 z_{12})\\
&\qquad-\varepsilon(p_2,p_4,\beta_2\beta_3 z_{12}-\beta_3\bar{\beta}_3 z_{52})\varepsilon(p_1,p_5,\beta_2\beta_3 z_{52}-\beta_2\bar{\beta}_2 z_{12})\Big]\\
&+\frac{1}{2(1-d)}\tilde{\tau}\int d\beta_1 d\beta_2 d\beta_3(\beta_1\beta_2\beta_3)^{\frac{d}{2}-1}\delta(\sum\beta_i-1)\Delta^{1-d}\\
&\qquad\Big[(p_1\cdot p_2)(p_2\cdot p_5)-(p_2\cdot p_3)(p_5\cdot p_1)\\
&\qquad+(p_2\cdot p_1)(p_4\cdot p_5)-(p_2\cdot p_4)(p_5\cdot p_1)+(p_2\cdot p_5)(p_3\cdot p_1)\\
&\qquad-(p_2\cdot p_1)(p_5\cdot p_4)+(p_2\cdot p_5)(p_1\cdot p_4)\Big]
\end{aligned}
\tag{G.9}
$$

where

$$
\tilde{\tau}=i\pi^{\frac{d}{2}}(1-d)\frac{\Gamma(d-1)}{\Gamma(\frac{d}{2})^3}
\tag{G.10}
$$

Chapter H

Appendix H : Gram determinant constraint for conformal cross ratio

We can always consider vector living in $d+2$ dimension. For spacetime vector $x^\mu(\mu = 0,1,\cdots,d-1)$, let denotes this $d+2$ dimensional vector as $X^A = (X_{-1},X_0,X_1,X_2,\cdots,X_d)$ $\left(X^A = (X^\mu,X^+,X^-) \text{ in lightcone coordinate}\right)$ with metric $\eta^{AB} = (-1,-1,1,1,1,\cdots)$ with satisfies special constraints

$$-X_{-1}^2 - X_0^2 + X_1^2 + X_2^2 + \cdots + X_d^2 = X^\mu X_\mu - 2X^+X^- = 0 \quad (\mu = 0,1,2,\cdots,d-1) \tag{H.1}$$

For lightcone coordiates X^+,X^- these vectors are related to spacetime vector by following relation.

$$x^\mu = \frac{X^\mu}{X^+} \tag{H.2}$$

All possible group transformation of X^A which remains restricts $X^A X_A = 0$ are equivalent to conformal group trnasformation of spacetime vector x^μ. It is easy to see metric in X space and x space also related by $-2X_i^A X_{j,A} = X_i^+ X_j^+ x_{ij}^2$. Let introduce $n \times n$ matrix G_n which (i,j)th components are x_{ij}^2. Then due to the metric relation, G is Gram matrix with $d+2$ dimensional vectors X,Y. In 3-dimensional case, determinant of G_6 shoud be vanished since X and Y are 5-dimensional vector. This gives one constraint $\Delta = 0$ on conformal cross ratio.

$$|G_6| = \text{Det}\begin{pmatrix} 0 & 0 & x_{13}^2 & x_{14}^2 & x_{15}^2 & 0 \\ 0 & 0 & 0 & x_{24}^2 & x_{25}^2 & x_{26}^2 \\ x_{13}^2 & 0 & 0 & 0 & x_{35}^2 & x_{36}^2 \\ x_{14}^2 & x_{24}^2 & 0 & 0 & 0 & x_{46}^2 \\ x_{15}^2 & x_{25}^2 & x_{35}^2 & 0 & 0 & 0 \\ 0 & x_{26}^2 & x_{36}^2 & x_{46}^2 & 0 & 0 \end{pmatrix} = (x_{14}^2 x_{25}^2 x_{36}^2)\Delta \tag{H.3}$$

where

$$\Delta \equiv \left((1-u_1^2-u_2^2-u_3^2)^2 - 4u_1u_2u_3\right) \tag{H.4}$$

As we will see, our configurations are satisfy this condition so there are 2 independent cross ratios for hexagon, which expected from conformal counting.

초 록

이 논문에서는 등각장론에서 정의된 다양한 물리량들을 통해 섭동적 혹은 비섭동적인 등각장론의 성질을 규명한다. 첫째로, 5차원 등각장론에서 정의된 4점함수에 유니테리성질 및 교차 대칭성을 통한 제한조건을 분석하여 UV 고정점에 해당하는 등각장론이 존재함을 논의하였다. 다양한 차원에서 이 방법은 비섭동적인 상호작용하는 이론을 통해 규명할 수 있는 임계지수를 성공적으로 유도해낼 수 있음이 확인되었다.

둘째로, 초대칭을 가지는 3차원 ABJM 이론에서 경로가 첨점을 가지는 경우에 해당하는 윌슨고리를 조사함으로써 해당 이론의 성질을 규명하고자 하였다. 특히, 윌슨고리의 특정한 극한을 조사함으로써 6각형 윌슨고리의 결과로부터 n각형 윌슨고리의 결과를 얻어낼 수 있는 방법을 제시한다. 이 결과는 n이 무한대로 가는 극한에서 초대칭 국소화를 통해 얻어낸 비섭동적인 결과와 잘 일치한다는 것이 확인되었다.

주요어 : 끈이론, 등각장론
학번 : 2008-20435